SINGLE MOLECULE STUDIES OF ACIDITY IN HETEROGENEOUS CATALYSTS

by

XIAOJIAO SUN

B.A., Dalian University of Technology, 2009

AN ABSTRACT OF A DISSERTATION

submitted in partial fulfillment of the requirements for the degree

DOCTOR OF PHILOSOPHY

Department of Chemical Engineering
College of Engineering

KANSAS STATE UNIVERSITY
Manhattan, Kansas

2013

Abstract

Amorphous silica-alumina is widely used as a solid acid catalyst for various reactions in oil refining and the petrochemical industry. The strength and the number of the acid sites in the material are most often believed to arise from the alumina atoms inserted into the silica lattice. The existence of the acidity distribution across the framework is a result of the local composition or the short-range interactions on the silica-alumina surface. Conventional techniques used to characterize silica-alumina provide effective information on the average acidity, but may not reflect the heterogeneity of surface acidity within the material.

Recently, it is possible to study individual catalytic sites on solid catalysts by single molecule fluorescence microscopy with high time and space resolution. Fluorophores can be chosen that emit at different wavelengths depending on the properties of the local environment. By doping these fluorophores into a solid matrix at nanomolar concentrations, individual probe molecules can be imaged. Valuable information can be extracted by analyzing changes in the fluorescence spectrum of the guest molecules within a host matrix. In this research, silica-alumina thin films were studied with single molecule fluorescence microscopy. The samples were prepared by a sol-gel method and a wide-field fluorescence microscope was used to locate and characterize the fluorescent behaviors of pH sensitive probes. In mesoporous thin films, the ratio of the dye emission at two wavelengths provides an effective means to sense the effective pH of the microenvironment in which each molecule resides. The goal of this work was to develop methods to quantify the acidity of individual micro-environments in heterogeneous networks. Pure silica films treated with external phosphate solutions of different pH values were used to provide references of the fluorescence signals from individual dye molecules. SM emission data were obtained from mesoporous Al-Si films as a function of Al content in films ranging from 0% to 20% alumina. Histograms of the emission ratio revealed that films became more acidic with increasing Al content.

The acidity on interior surfaces in zeolite pores was also of interest in this work. A microfluidic device was built to isolate the interior surface from the exterior surface. Some preliminary results showed the potential of using SM fluorescence method to study the acidic properties inside the pores of zeolite crystals.

SINGLE MOLECULE STUDIES OF ACIDITY IN HETEROGENEOUS CATALYSTS

by

XIAOJIAO SUN

B.A., Dalian University of Technology, 2009

A DISSERTATION

submitted in partial fulfillment of the requirements for the degree

DOCTOR OF PHILOSOPHY

Department of Chemical Engineering
College of Engineering

KANSAS STATE UNIVERSITY
Manhattan, Kansas

2013

Approved by:

Major Professor
Keith L. Hohn

Abstract

Amorphous silica-alumina is widely used as a solid acid catalyst for various reactions in oil refining and the petrochemical industry. The strength and the number of the acid sites in the material are most often believed to arise from the alumina atoms inserted into the silica lattice. The existence of the acidity distribution across the framework is a result of the local composition or the short-range interactions on the silica-alumina surface. Conventional techniques used to characterize silica-alumina provide effective information on the average acidity, but may not reflect the heterogeneity of surface acidity within the material.

Recently, it is possible to study individual catalytic sites on solid catalysts by single molecule fluorescence microscopy with high time and space resolution. Fluorophores can be chosen that emit at different wavelengths depending on the properties of the local environment. By doping these fluorophores into a solid matrix at nanomolar concentrations, individual probe molecules can be imaged. Valuable information can be extracted by analyzing changes in the fluorescence spectrum of the guest molecules within a host matrix. In this research, silica-alumina thin films were studied with single molecule fluorescence microscopy. The samples were prepared by a sol-gel method and a wide-field fluorescence microscope was used to locate and characterize the fluorescent behaviors of pH sensitive probes. In mesoporous thin films, the ratio of the dye emission at two wavelengths provides an effective means to sense the effective pH of the microenvironment in which each molecule resides. The goal of this work was to develop methods to quantify the acidity of individual micro-environments in heterogeneous networks. Pure silica films treated with external phosphate solutions of different pH values were used to provide references of the fluorescence signals from individual dye molecules. SM emission data were obtained from mesoporous Al-Si films as a function of Al content in films ranging from 0% to 20% alumina. Histograms of the emission ratio revealed that films became more acidic with increasing Al content.

The acidity on interior surfaces in zeolite pores was also of interest in this work. A microfluidic device was built to isolate the interior surface from the exterior surface. Some preliminary results showed the potential of using SM fluorescence method to study the acidic properties inside the pores of zeolite crystals.

Table of Contents

List of Figures ix
List of Tables xiii
Acknowledgements xiv
Dedication xv
Chapter 1 - Introduction 1
1.1 Acid sites on Silica-alumina 1
1.1.1 Significance of Solid Acid Catalysts 1
Amorphous silica-alumina 2
Zeolite and zeolite-type catalysts 3
Metal oxides 5
Resins 5
Heteropolyacids 6
Other solid acid catalysts 7
1.1.2 Chemistry of Amorphous Silica-alumina 7
1.1.3 Characterization Methods for Studying Acidity in Solid Frameworks 11
Hammett Titration 11
Nuclear magnetic resonance 13
Infrared spectroscopy 15
Temperature programmed desorption 15
1.2 Single Molecule Fluorescence Microscopy 16
1.2.1 Principles of Fluorescence Microscopy 16
1.2.2 Fluorescence Techniques for the Observation of Single Molecules 18
Near-field Fluorescence Microscopy 19
Fluorescence correlation spectroscopy 21
Wide-field Methods 22
Confocal Methods 26
Fluorescence resonance energy transfer 28
1.2.3 Solid Catalysts Characterization with Single Molecule Methods 29

Activity mapping 30
Reaction kinetics 30
Molecular diffusion in the pores and on the surfaces 31
1.2.4 Single molecule fluorescence studies of acidity in solid catalysts 32
Acidity characterization by pH-sensitive dye molecules 32
Characterization by fluorogenic reactions 33
Reference 36
Chapter 2 - Sample Preparation and Experimental Setup 46
2.1 Preparation of C-SNARF-1 doped phosphate bulk solutions for conventional spectra study by a fluorimeter 46
2.2 Preparation of silica and amorphous silica-alumina thin films 46
2.2.1 As-synthesized Films 47
Pure silica samples 47
Silica-alumina samples 48
2.2.2 Calcined Films 48
2.2.4 Buffered Thin Films 49
2.3 Instrumentation 49
2.2.1 Single molecule setup 49
2.2.2 Fluorometer 50
2.3 Data analysis 51
Reference 52
Chapter 3 - Single Molecule Studies of Acidity Distributions in Mesoporous Silica-Alumina Thin Films 53
3.1 Introduction 53
3.2 Experimental section 55
3.2.1 Sample preparation 55
3.2.2 Instrumentation and method 56
3.3 Result and discussion 57
3.3.1 Bulk pH studies of C-SNARF-1 in aqueous solutions 57
3.3.2 C-SNARF-1 pH response in thin films at the single molecule level. 59

3.3.3 Acidity properties of mesoporous Si-Al composite films probed by single molecule fluorescent spectroscopic methods 62
3.3 Conclusion 66
Reference 68
Chapter 4 - Single molecule fluorescence studies of amorphous silica-alumina thin films by probing with Violamine R 73
4.1 Introduction 73
4.2 Experimental section 74
4.2.1 Dye purification 74
4.2.2 Sample preparation 74
4.2.3 Instrumentation and method 74
4.3 Result and discussion 75
4.3.1 Violamine R pH response in aqueous solutions 75
Reference 80
Chapter 5 - Single molecule fluorescence microscopic study of ordered porous materials 81
5.1 Introduction 81
5.2 Experiments 85
5.2.1 Photolithography of the photoresists 85
5.2.2 Fabrication of the microfluidic device 87
5.2.3 Calibration of the pH response of the dye molecules in the ordered zeolite porous systems 88
5.2.4 Acidity measurements inside the zeolite channels 91
5.3 Preliminary Result and discussion 92
5.3.1 Zeolite fixation on the glass surface 92
5.3.2 Stability of the microfluidic channel 94
5.4 Future work 95
Reference 97
Chapter 6 - Conclusion and future work 100
Conclusion 100
Future work 101
Appendix A - Structures of the dye molecules 102

Appendix B - Fabrication of the microfluidic device 104
Appendix C - PDMS slab preparation 106
Appendix D - $AlPO_4$-5 synthesis 107
Appendix E - SAPO-5 synthesis 109
Reference 111

List of Figures

Figure 1.1 Schematic drawings of different types of hydroxyl groups representing different types of acid sites in zeolite network. a) A bridging hydroxyl group connecting a tetrahedral silicon and an aluminum cation. b) A terminal surface silanol group on the external surface. c) A hydroxyl group on a surface aluminum atom. 4

Figure 1.2 Illustration for the valence distribution on silicon and aluminum atoms. a) The valence is satisfied for both silicon and oxygen atoms in absence of aluminum atoms. b) When a tetrahedral aluminum atom replaces one silicon atom in the framework, the valence of the oxygen atoms does not satisfy and a hydrogen ion is needed to associate with the oxygen atoms. And this hydrogen ion possesses Brønsted acidity. 9

Figure 1.3 Scheme of the reversible conversion of Brønsted and Lewis aid site upon water addition and removal in the amorphous silica-alumina. 11

Figure 1.4 Jablonski Diagram. A simplified and typical energy level scheme to describe the single molecule fluorescence process and other competing processes. S_0 represents the ground state, S_1 represents the first excited state, and T1 represents the lowest triplet state. There are several levels of vibrational states in each electronic state. Photons with a energy of hv can excite the transition from the ground state to excited states. Fluoresce, nonfluorescence or intersystem crossing processes are of different rates and all of them can bring back the excited molecule to the ground state. 17

Figure 1.5 A schematic drawing of a near-field scanning optical microscope. The spatial resolution of the technique is defined by the dimension of the aperture, d, which is smaller than the wavelength of the excitation light. The sample is very close to the aperture in order to get excited before the light can diffract. 20

Figure 1.6 A schematic drawing of a focal volume of an objective for FCS experiments. The red dots represent the dye molecules. They are doped in a solution at the single molecule level and move into and out of the focal volume. 21

Figure 1.7 A schematic drawing of an epifluorescence microscope. The excitation depth is infinite and the molecules from the out-of focal plan in the sample are excited, becoming a source of background noise. 23

Figure 1.8 Schematic drawings for two experimental configurations for TIRF experiments based on different excitation pathways. a) The configuration for the through-the-objective mode. The excitation light passes through the objective, overlapping with the fluorescence signal pathway for a short distance. b) The configuration for the prism-based mode. In both configurations, only a small volume of the sample can be excited by the light source, lowing the background from the out-of-focus fluorescence. 26
Figure 1.9 A schematic drawing of confocal microscopy. Only the molecules in the focal volume can be excited and emitted fluorescence signals to. This configuration decreases the background to a great extent for the small excitation volume. The signal is focused by a tube lens through an aperture and reject the out-of-focal plan fluorescence automatically. A point detector, such as an avalanche photo diodes (APD) is used to count the number of photons from individual fluorophores. 27
Figure 1.10 An illustration of a fluorescence resonance energy transfer process. A light source is used to excite the donor and the energy is transferred to the acceptor through a nonradiative process. The excited donor then can release the energy through radiative or nonradiative processes. The FRET process can only happen when there is an overlap of the spectra of the two fluorophores and when there is an appropriate distance between the two. 29
Figure 2.1 The chelation reaction of aluminum isopropoxide with the chelating agent ethylacetoacetate (EAA). 47
Figure 2.2 A schematic drawing of the configuration of the wide field microscope. Optical parts include optical fibers, lenses, flipper mirrors, beamsplitters, bandpass filters, longpass filter and waveplates. 50
Figure 3.1 Chemical structures of C-SNARF-1 in its protonated and deprotonated forms around the pH at (a) Structure of the first acid-base equilibrium (pKa ~ 7.6) and (b) Structure of the second acid-base equilibrium (pKa ~ 4.2). 58
Figure 3.2 Spectral data for C-SNARF-1 in aqueous solutions of pH ranging from 1 to 10. These data were obtained using a conventional fluorimeter. 58
Figure 3.3 C-SNARF-1 emission ration, R, (obtained from the data in Figure 2) as a function of pH for solutions ranging from pH 1 to 10. The solid line was used to connect the data points. 59

Figure 3.4 A pair of representative images of C-SNARF-1 in silica thin films treated by phosphate aqueous solutions. (a) Image collected by the 580 nm channel with a bandwidth of 40 nm and (b) Image collected by the 640 nm channel. They were obtained simultaneously for a single sample region. The left and right panels in (a) and (b) are displayed on identical intensity scales. 60
Figure 3.5 Density histograms of intensity ratio R ($R = I_{580} / I_{640}$) in silicate thin films treated with phosphate solutions ranging from pH 1 to pH 8. The histograms were fitted to Gaussian functions. The peak positions represent the most common pH of the microenvironments in a sample. The peak widths represent the heterogeneity in the solid matrices. (Bar height × Bin size = Probability for the range). 61
Figure 3.6 Representative images of the a) pure silicate film sample and b) the 20% Al film sample. The shape of the spots resembles the ones in the solution-treated sample images shown in Figure 3.4..... 63
Figure 3.7 Density histograms of intensity ratio R (R = I580 / I640) in aluminosilicate thin films. The histograms were fitted to double Gaussian functions since shoulder peaks appeared in the aluminum doped samples. 65
Figure 3.8 Plot of the predominant peak position as a function of Al doping. When the Al content increases, the predominant peak is shifting from large to small values of R..... 66
Figure 4.1 A drawing of the chemical structure of Violamine R. The molecule has carboxylate and sulfonate groups, which can be responsive to the pH of its surroundings. 73
Figure 4.2 Spectra of Violamine R by fluorimeter study. The dye molecule was excited at 488 nm and two characteristic peaks could be observed at 585 nm and 650 nm. 75
Figure 4.3 Violamine R emission ration, *Rv*, (obtained from the data in Figure 4.2) as a function of pH for solutions ranging from pH 1 to 7. The solid line is used to connect the data points. 76
Figure 4.4 Histograms of Violamine R emission ration, *Rv* 77
Figure 4.5 Peak locations of silica-alumina thin films samples as a function of Al content. The blue line is used to guide the trend..... 78
Figure 5.1 Schematic illustration of the procedure for lithography. a) a typical procedure for a positive photoresist. The same pattern is transferred from the photo mask onto the substrate. b) for a negative photoresist, however, the opposite pattern is transferred 86

Figure 5.2 A schematic drawing of the proton concentration distribution at the opening and inside the pores of a zeolite single crystal. In a) it is assumed that the dye molecules can not diffuse freely inside the pores and hence only the pore openings can be probed. The pH at the ends of the zeolite equals to that of the buffer solutions they are exposed to; and b) it is assumed that the dye molecules can diffuse all the way inside the zeolite pores. The concentration inside the pores is a linear distribution along the long axis described by Fick's law and the full length of the pores can be probed. 90
Figure F.1 Fluorescent pH indicators with appropriate dimensions for single molecule fluorescence studied of interior surfaces of zeolites. 102
Figure G.1 Fabrication procedures of the microfluidic device. The blue bar represents a single zeolite crystal. 105
Figure I.1 The molar ratios of the starting gel that will be examined to produce large single crystals of high yields with good morphology (no or limited crystal intergrowth) and optical transparency. 108

List of Tables

Table 1.1 Frequently used Hammett indicators for the measurement of acid strength in solid acid networks. [83,84] 12

Table 5.1 Crystalline materials with large pores[9–16] 82

Table 5.2 Fluorescence pH indicators with dimensions matching the pore sized of AlPO4 and SAPO-5. These molecules can be excited by using UV-visible light sources. 84

Table 5.3 Experiment plan for microscope calibration 91

Table 5.4 An individual zeolite single crystal imbedded firmly onto the zipcone^{TM} UA treated glass surface. The cracking of the particle can be observed and the experimental procedures need to be optimized. 93

Acknowledgements

I want to acknowledge my major advisor, Dr. Keith L. Hohn for his continuous support and contribution to my study and research. His knowledge, patience, motivation, encouragement and enthusiasm have helped me all the time throughout my Ph.D program, which is probably the most challenging experience in my life.

I want to thank Dr. Daniel A. Higgins for being my co-advisor, who has provided me with enormous amount of information and lab resources towards the completion of the doctorial degree. I could not have accomplished the thesis without his support.

I would like to express my gratitude to my committee members: Dr. Jennifer L. Anthony, and Dr. Vikas Berry for their valuable advices and kindness during all the important phases of the Ph.D program. I also would like to express my gratitude to my outside chair, Dr. Steven J. Eckels, who is willing to participate the final evaluation of my work.

I am grateful to the members in Dr. Hohn's and Dr. Higgins's research group: Myles Ikenberry, Jingyi Xie, Quanxing Zheng, Fan Zhang, Hao xu and Seok Chan Park. I appreciate the scientific discussions with them.

I am indebt to the staff in the Department of Chemical Engineering: Florence Sperman, Karey DeBardeleben, Pat Nelson and David Threewit for their assistance and cooperation in events and activities related to my research.

I want to thank my parents, my grandparents, my uncles and my cousins for their full love, encouragement and support.

I want to thank Daming Wei for his support, tolerance and encouragement.

Dedication

To my parents

Fengyang Sun

Li Chen

To my grandparents

Baomin Chen

Hongxian Lu

To my uncles

Changle Chen

Chengxing Chen

To my life partner and best friend

Daming Wei

Chapter 1 - Introduction

1.1 Acid sites on Silica-alumina

1.1.1 Significance of Solid Acid Catalysts

Heterogeneous catalysts play a vital role in modern chemistry and petrochemical industry.[1,2] It is believed that more than 80% of all chemicals precursors and intermediates have to interact with at least one catalytic material during their manufacturing processes.[3,4] It is essential to design heterogeneous analogs of the most commonly used homogeneous catalysts in order to engineer clean pathways for industrial productions.[5,6] Solid acid catalysts have received a lot of interests from scientific researchers since the nature of the active acidic sites are familiar and the acid catalyzed reactions can be explained with existing theories and models while active sites in other solid catalysts, such as metals, oxides and sulfides are difficult to rationalize.[7] From the green-chemistry point of view, solid acid catalysts have the advantages of replacing hazardous mineral acids (such as H_2SO_4 or HF),[8] reducing the environmental impacts of the large volumes of wasted disposal from the neutralization and eliminating a separation step to recover the catalyst.[9,10] For solid acid catalysts, product separation is simplified and the reactions are often under milder conditions.[11]

The acidity of the solid acid catalysts is related to the number and the strength of the Brønsted and/or Lewis acidic sites on the framework.[11] The Brønsted acidity of a material is the ability to donate or at least partially transfer a proton to reactants in proximity and the Lewis acidity is the ability to accept an electron pair to form a coordination bond.[7] When designing a catalyst, it is very important to understand the type of acidity needed for different reactions, the strength of sites required to activate the reactants molecules and the approach to maximize the number of the active catalytic sites.[7] The efficiency of catalytic reactions could be optimized by the tuning of the chemical properties of the catalysts. Another strategy to improve the performance of the catalysts is to control the porous structures, which have an essential influence on the absorption of the reactants and the selectivity of intermediates or products.[12] A good solid acid catalyst should also possess high thermo/hydro stability and mechanical strength to ensure the reusability, which adds up to the advantages of economical and environmental concerns.[13]

Amorphous silica-alumina

Amorphous silica-alumina was the first solid acid catalyst commercialized and used in industry at a large scale.[7] The catalytic activity of the material is closely related to the acid sites in the solid network, which arise from the substitution of aluminum atom in the silicon matrix. The surface acidity of silica-alumina is less known compared to zeolite type of catalysts since the surface composition of these mixed oxides is more complex.[14] The detailed mechanism of the formation of the acid sites will be discussed in future chapters.

Amorphous silica-alumina has been used for a large number of important industrial chemical and petrochemical reactions. Their Brønsted acidity makes them very useful for reactions such as catalytic hydrocracking of heavy hydrocarbons, isomerization and oligomerization of olefins, hydrogenation of olefins to paraffins, and alkylation of aromatics with alcohols.[7,14–16] Besides the acidity, the manipulation of the pore size of amorphous silica-alumina is also related to the catalytic performance of the material since the porous structure determines the surface area, which is related to the accessibility of active sites on the catalysts. Both microporous (in the 30 ~ 60 Å range)[17] and mesoporous (in the 10 ~ 100 Å range)[18] amorphous silica-alumina have been synthesized in labs and in industry. The pore size of the catalysts can be tailored by using appropriate surfactants with appropriate chain lengths or by choosing post-synthetic treatment to change the pore configurations.[19]

There are several different procedures to synthesize the amorphous silica-alumina. For the co-precipitation method, amorphous silica-aluminas are prepared starting from homogeneous aqueous solutions containing aluminum salts (e.g. aluminum nitrate). Silica is then suspended in the solution. To deposit aluminum atoms on silica, the suspension is basified. The amount of aluminum can be controlled by varying the starting concentration of the aluminum salt.[20,21] The amorphous silica-alumina catalysts can also be synthesized by a co-gelation method, which starts from a sodium silicate and aluminum salt solution, followed by steps of precipitation, filtration and ion-exchange to have the material recovered finally.[14,22] Another route is to use organometallic precursors as the silicon (e.g. tetramethylorthosilicate) and aluminum source (e.g. aluminum isopropoxide). A homogeneous sol solution is obtained first. The sol is then converted to a solid gel. Depending on the composition of the starting materials, the gelation time, and the storage conditions, the solid gel can be either transparent or opaque.[23] Since the clear solution is directly transformed to a gel, the aluminum to silicon ratio is directly related to the starting raw

materials. This method is claimed to have a molecular level mixing of the alumina and silica,[24] and hence the aluminum doping into the silica matrix can be strictly monitored. This method is selected to synthesize the amorphous silica-alumina thin film samples for this research, which requires optically transparent samples and controllable amount of aluminum doping in the silicon framework.

Zeolite and zeolite-type catalysts

Zeolites and zeolite-type catalysts are being successfully used in oil refining, petrochemistry, chemistry and fine chemical manufacture because of their Brønsted acidity and controllable structural properties, such as particle sizes, pore dimensions and micro/meso-channel orientations. Zeolites belong to the silica-alumina family. Unlike amorphous silica-alumina, they have well-defined crystalline structures with ordered pores and cavities in the solid matrix.[25] Compared to other solid acid catalysts, zeolites have certain properties that make them a unique type of catalysts. These properties include: relatively high surface area, controllable catalytic sites, various acid strength, molecular confinement and shape selective effects.[26]

In the zeolites network, the local distortions in bonding are prevented by a global readjustment of the bond structure. therefore, the long-range effects are more significant compared to that of amorphous silica-aluminas. It is probable that zeolititic materials have stronger acidity since the symmetry energies cannot be relaxed as in the case of amorphous materials.[8] The acidity or the acid sites in a zeolite is controlled by the aluminum doping in the silicon framework.[27] When an aluminum atom is inserted into the neutral tetrahedron SiO_2 framework to replace a four coordinating 4+ charged silicon atom, the 3+ charged aluminum cation leaves a negative charge in the framework. The negative charges can be balanced by protons, forming Brønsted acid sites. These sites, acting as proton donors, are believed to be located on the oxygen bridges connecting a tetrahedral coordinated silicon and an aluminum cation.[28,29] The Brønsted acidic bridging hydroxyl protons is shown in Figure 1.1a. Silanol groups at the external surface of zeolite crystals are show in Figure 1.1b and the acidity of this type of hydroxyl groups is low. Formation of hydroxyl groups on aluminum species may also occur (shown in Figure 1.1c), depending on the post-synthesis conditions.

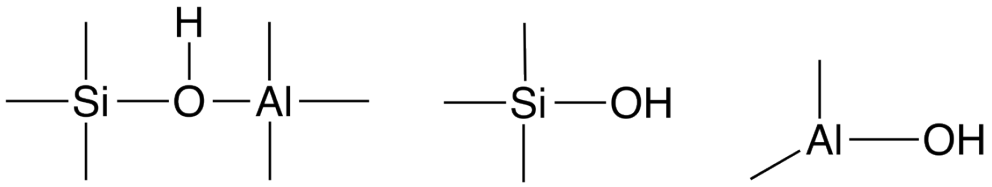

a **b** **c**

Figure 1.1 Schematic drawings of different types of hydroxyl groups representing different types of acid sites in zeolite network. a) A bridging hydroxyl group connecting a tetrahedral silicon and an aluminum cation. b) A terminal surface silanol group on the external surface. c) A hydroxyl group on a surface aluminum atom.

Aliminophosphates (AlPOs) and silicoaluminophosphates (SAPOs) are of much scientific interests in the studies of the physicochemical properties of zeolite-type materials and their applications in commercialized manufacturing processes.[30] By using structure directing agents, these zeolite-type crystals can be synthesized to possess an AFI-type molecular sieve structure, which has unidimensional linear channel systems.[31] AlPOs and SAPOs exhibit excellent thermal stability and have the potential to be used in catalysis, separation,[32] membranes, sensors and nonlinear optics.[33] The pore openings of AlPOs and SAPOs can be 0.75 nm and this size is accessible for guest molecules with kinetic diameter as large as a benzene ring (~ 5.9 Å).[34] The introduction of silicon atoms to the neutral AlPOs results in negatively charged SAPOs which are capable of inducing Brønsted acid sites in the network. Since SAPOs have a stronger interaction with the hydrocarbons, it shows the potential to be used as acid catalysts providing low to medium acidity.[30,31,35] The AlPOs and SAPOs can be synthesized to giant single crystals, with a dimension of 150 μm and up to 600 μm in low yield.[36] The synthesis method has been developed and optimized to generate large crystals in high yields. These crystals are of interests in this study for the following reasons: 1) they are optically transparent and it is possible to study them with single molecule fluorescence microscopes. 2) the giant crystal size makes it easy to manipulate individual AlPOs or SAPOs particles. 3) the ordered porous structure provides simple systems to study the behavior of the guest molecule interacting with the host. and 4) the large pore openings allows it to be loaded with large organic fluorescent molecules for the single molecule fluorescence microscopic studies. In a later chapter, a proposal of studying the interior surface inside the AlPOs or SAPOs pores will be described.

Metal oxides

Sulfate-modified metal solids were reported to have super acid sites and be capable of catalyzing a variety of reactions under relatively mild conditions.[37] Oxides such as ZrO_2, TiO_2, $Fe2O_3$ and HfO_2 can be treated either by sulfuric acid or ammonium sulfate to carry remarkable surface acidity and catalytic activity.[7,38] To prepare the material, the oxide precursors are immersed in sulfating solutions, followed by filtration, drying and calcination. It was found that the preparation and post-synthesis conditions affects the physical and chemical properties and hence the procedures need to be optimized for the best performances of the catalysts.[39] As for the acidity of the catalysts, it is believed that both Brønsted and Lewis acid sites exist on sulfated metal oxides. For example, studies for sulfated zirconia show Brønsted acidity,[40] Lewis acidity[41] and the coexistence of the two.[42] Different mechanisms have been proposed to explain the acidity of the sulfated metal oxides. Many researchers concluded that an intermediate carbenium ion is generated during the acid catalysis.[43] Other researchers proposed that the high one-electron oxidizing ability of sulfated metal oxides is the key in the hydrocarbon conversions.[44] Even if a lot of studies have shown the extraordinary catalytic performance of the sulfated metal oxide solids, there is still a long way to go before this type of catalysts to be commercialized. Coke can be formed on the surface of the catalysts and this leads to the poisoning of the active sites. Another practical problem for sulfated metal oxides is that they deactivate very quickly, due to the easy loss of sulfur during the catalytic processes in H_2 containing environment.[45,46] Sulfur can also be removed during the catalyst regeneration when exposed to relatively high temperature and the existence of carbon monoxide. More researches are needed to promote the behavior of the catalysts. Besides sulfate, tungstate has been proposed to be added as a promoter for zirconia.[47] The additional metallic components have also been reported to suppress the deactivation of the sulfated metal oxide during catalysis.[48,49]

Resins

Ion-exchange resins play an important role in the modern heterogeneous catalysis and have been commercialized for solid acid catalysts in many areas. Resins are functionalized cross-linked polymers and the two main classes of ion-exchange resins are the styrene-based sulfonic acids and the perfluorosulfonic acid-based catalyst.[50,51] It is generally accept that perfluorinated resin sulfonic acids are stronger acids. Another difference between the two is that styrene-based resins have a larger number of acid sites compared with the perfluorosulfonic acid-based resins.

Resins are used as resin beads of various sizes. Those beads may have porous structures with pore size ranging from smaller than 20 Å to larger 100Å or they can be totally non-porous.[51] The surface area and the pore size of the material are determined by the content of the cross-linking components. The level of cross-linking decides the extent of swelling of the ion-exchange resins which in turn controls the accessibility of reactants to the acid sites.[52] The acid sites can locate on the exterior surface of the resin beads, on the interior surface inside the pores or on both. Resins are often used for esterification or transesterification reactions, which are catalyzed by the protons bonded to sulfonic groups. This material has been developed to new forms like resin/silica nano-composites which have shown increased catalytic activity and fine pore structures with narrow distributions of pore dimensions.[52,53]

Heteropolyacids

Heteropolyacids have long been recognized as effective solid acid catalysts for a variety of acid catalyzed reactions. The reactions can be either homogeneous or heterogeneous depending on the composition of the catalysts and the reacting medium.[54] Among different types of heteropolyacids, 12-tungstophosphoric acid is very popular because of its high activity.[55] It is reported that these catalysts have strong Brønsted acidity, even stronger than conventional acids such as H_2SO_4, zeolites and acidic resins. $H_3PW_{12}O_{40}$ displays a Keggin structure which has an oxygen tetrahedral-coordinated heteroatom (PO_4) surrounded by 12 edge-shared oxygen octahedral-coordinated addenda atoms (WO_6). When combined with monovalent cations such as NH_4^+, K^+ or Cs^+, the Keggin heteropolyacids are transformed to solid acid catalysts. The acidity of the material arise from the large size of the polyanion, which has low and delocalized surface charge density, so that the interaction between the polyanion and the proton is weak, generating strong acid sites.[56] They have been widely used for transesterification, hydration and polymerization reactions.[57] It has also been reported that heteropolyacids have been used for biodiesel synthesis.[58] From the practical point of view, heteropolyacids suffer from deactivation over time, and they can not be regenerated by combustion since the catalysts will not be stable under elevated temperatures. Strategies for solving this problem include providing H_2-containing working conditions or using bifunctional catalysts.[59,60]

Other solid acid catalysts

Some other solid acid catalyst systems have received increasing attentions in recent years. For example, nanotubes and nanoparticles coated with functional groups have been used for a variety of industrial organic transformations by using their acid sites.[61] Sulfonated muti-walled carbon nanotubes were used to synthesis biodiesel.[62] Catalysts supported on magnetic nanoparticles (usually iron particles) have been grafted with carboxylic acid or sulfonic acids. The advantage of these magnetic nanoparticles is that all the active sites are on the external surfaces, which eliminates the internal diffusion limitations.[63]

1.1.2 Chemistry of Amorphous Silica-alumina

Catalytic processes play essential roles in the chemical, petrochemical and oil refining industries. Heterogeneous catalyst is receiving more and more attention for economic and environmental concerns, as discussed above. Catalytic solids are very complex systems. The study of the chemistry of the active sites provides important information of the mechanisms of reaction, which in turn helps to design catalysts with efficient conversion of the starting materials and high selectivity of the desired products.[3,6465,66] The use of amorphous silica-aluminas as solid acid catalysts has a long history and natural materials, such as clays were the first solid acid catalyst commercialized for industrial manufacture.[65,66] Compared with zeolites, which are a type of aluminosilicate with a crystalline structure, amorphous silica-aluminas have only low to moderate acidities shown by different characterization studies, such as NMR, IR and ad/desorption methods. However, amorphous silica-aluminas are still indispensable solid acid catalysts especially in some petrochemical processes, in which bifunctional catalytic systems are frequently required and low to moderate acidity of the active sites are preferred.[67] For example, metal sulfides are often combined with amorphous silica-alumina as hydrocracking catalysts, where the dehydrogenation function is performed by the sulfides and the Brønsted acid sites are provided by the amorphous silica-alumina. In this process, only moderate acidity or much lower acidity than that of zeolite is required in order to obtain high selectivity to gas oil or kerosene. On the other hand, too low acidity will lead to low activity of the catalysts and a detailed study of adjusting the strength of the acid sites turns out to be very important.[68]

Despite the industrial importance of amorphous silica-aluminas, an accurate explanation of the acidic properties has not yet been developed. The amorphous nature of the material makes

their structures and chemical properties more complex compared to the crystalline analogue of zeolites.[67] The Brønsted acidity of the solids can depend on the starting materials, synthesis procedures, chemical compositions (like Si/Al ratio and water content), post-synthesis treatment and other parameters. [67]

Different models have been proposed to describe the nature of the acid sites. Thomas[69] and Tamele[70] proposed the more widely accepted explanation in 1940s. They postulated that the cracking catalytic activity of the amorphous silica-alumina is related to the Brønsted acidity on the solids, which is originated from the tetrahedral Al^{3+} substituting Si^{4+} in the silica network. In the pure silica network (shown in Figure 1.2a), each silicon atom is surrounded by four oxygen atoms so that the valence of both silicon and oxygen atoms are satisfied. When one silicon atom is replaced by an aluminum atom, which has a valence of three, the valence of the oxygen atoms around the aluminum atom can not be satisfied and they all have negative valence as is shown in Figure 1.2b. A positive hydrogen ion is needed to neutralize the negative charge of the four oxygen atoms and this H^+ should possess Brønsted acidity. It was argued that the maximum acidity could be obtained when the silica to alumina ratio is one, which results in the maximum number of the Si-O-Al bonds. The calculating of the valence also explained the reason why neither pure silica nor pure alumina is active for hydrocracking process.

Gates et al.[71] argued that the different acid strength in the amorphous silica-alumina and zeolite catalysts is due to the fact that the bridging hydroxyl groups proposed in Thomas and Tamele's work are not the active Brønsted acid sites in the material. Instead, the terminal silanol groups are responsible for the catalytic activity of the amorphous silica-alumina materials. They claimed that the unsaturated Al^{3+} ions have Lewis acidity and the surface silanol groups next to them are the active Brønsted acid sites. Busca et al.[72] performed the FT-IR experiments to prove that the addition of the aluminum ions did shift the peak of the silanol group, which is the evidence of the neighboring aluminum surface atoms invoke the Brønsted acidity of the silanol groups. Ugliengo et al.[73] agreed on absence of the bridging hydroxyl groups in amorphous silica-alumina and they hypothesized that water molecules break down the original bridging hydroxyl Brønsted centers and interact with the surface aluminum cation and H-bonded with the silanol group next to it. The new specie of the AlOH groups are the Brønsted acid sites responsible for the catalytic activity.

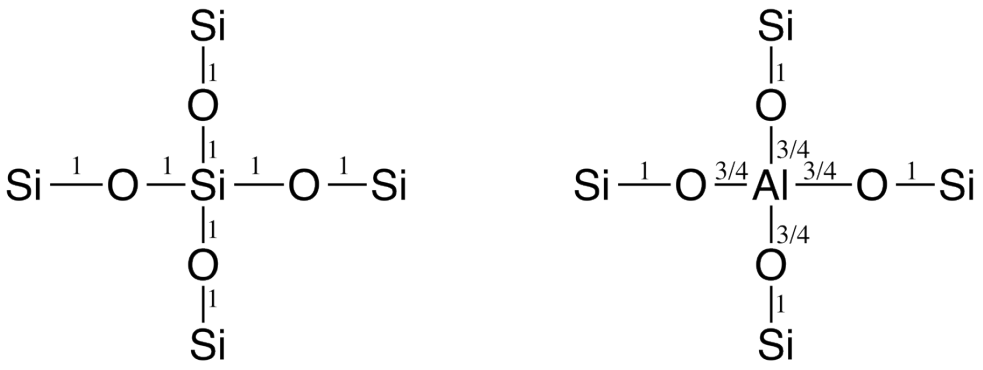

Figure 1.2 Illustration for the valence distribution on silicon and aluminum atoms. a) The valence is satisfied for both silicon and oxygen atoms in absence of aluminum atoms. b) When a tetrahedral aluminum atom replaces one silicon atom in the framework, the valence of the oxygen atoms does not satisfy and a hydrogen ion is needed to associate with the oxygen atoms. And this hydrogen ion possesses Brønsted acidity.

The absence/existence of the hydroxyl groups as strong Brønsted acid sites is always in argument, and numerous spectroscopic studies have been conducted to address this issue. Leydier et al.[74] suggested that instead of accurately assigning the FT-IR spectra, it is more important to study different behaviors of the acid sites in the amorphous silica-alumina. They proposed new sites of pseudo-bridging silanol groups in the network, which interact with the aluminum atoms through electrostatic interaction rather than covalent bonds, as is the case in zeolite solids. By FT-IR experiments and theoretical calculations, it was indicated that the role of aluminum atoms in the silica network is to stabilize the deprotonated species and hence to promote the Brønsted acidity of the silanol groups compared that is in the pure silica network. This study also proposed another type of acid sites in the amorphous silica-alumina that take part in the proton transfer processes. These sites are water molecules absorbed on aluminum atoms, which are not involved in hydrogen bonding with the adjacent hydroxyl groups. Protons of these water molecules can be transferred to basic molecules that are deprotonated by probing molecules (like lutidine used in the study). The process is named as a “cascade proton transfer” and the aluminum molecules function like “acidic water reservoirs” in the network. Ugliengo et al also raised the idea of water molecules behaving like Brønsted acid sites as mentioned above. The uniqueness of their thought is that the Brønsted acidity comes from the stabilization of the

conjugated base species originated from the proton transfer processes instead of the hydroxyl groups themselves.

Despite of the argument on the nature of the Brønsted sites in the amorphous silica-alumina, it is generally agreed that the tetrahedral aluminum atoms inserted into the silica network actually enhance the Brønsted acidity of different types of hydroxyl groups. Zeolitic materials are the crystalline analogues of amorphous silica-aluminas. The ordered structure of zeolites makes it easier to study the effect of the Si/Al ratio on the acidic properties of the material. The "next nearest neighbor" concept is used to describe how acidity change with aluminum doping in the zeolites network. In this theory, each aluminum atom is connected through four oxygen atoms to four silicon atoms and these nine atoms are named as the "next nearest neighbors". The lower number of the aluminum atoms results in higher acidity, which means that a completely isolated aluminum atom has the highest acid strength.[75] In the case of amorphous silica-alumina, however, the less rigid structure causes the agglomeration of aluminum rich domains and this is believed to be one of the reason why amorphous materials have a lower acid strength with the same Si/Al ratios compared to their zeolite counterparts.[76] The four-coordinated aluminum atoms are widely agreed to be the cause of the acid sites, so it is possible to maximize the number of the four-coordinated aluminum atoms to enhance the Brønsted acidity in the amorphous silica-alumina.[77] Uytterhoeven et al.[78] discovered that in alumina rich samples (> 80% Al_2O_3), the six-coordinated aluminum atoms are the dominant specie while in the alumina lean samples (< 30% Al_2O_3), the dominant aluminum specie is the four-coordinated aluminum atoms. These types of aluminum atoms can reversibly transform between Brønsted and Lewis acid sites upon water addition/ removal[79] shown in Figure 1.3. In this research, the aluminum doping into the silica network is within the alumina lean range. It was also mentioned in some literature that the more homogeneous distribution of SiO_2 and Al_2O_3 could lead to more Brønsted and/or Lewis sites.[80] For this reason, a sol-gel method is used for the sample synthesis in this study. Calcination was used to diffuse more aluminum atoms into the silica network to enhance mixing, as is recommended by other studies.[67]

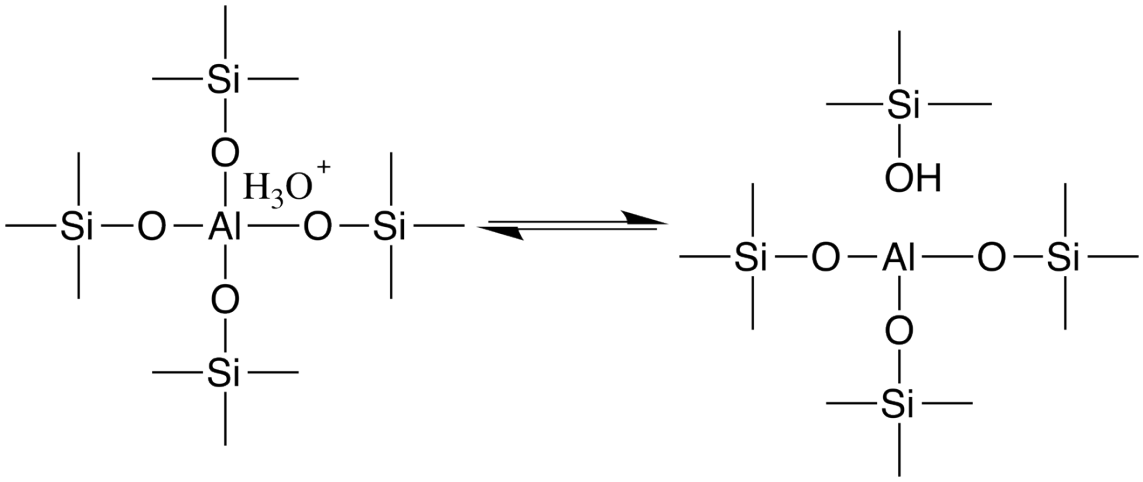

Figure 1.3 Scheme of the reversible conversion of Brønsted and Lewis aid site upon water addition and removal in the amorphous silica-alumina.

1.1.3 Characterization Methods for Studying Acidity in Solid Frameworks

Hammett Titration

Titration methods have been used for the characterization of the acid sites on the surface of the amorphous silica-alumina since the 1940s, when Thomas and Tamele firstly tried to explain the acidity on the material.[70,81] Hammett indicators are a series of non-ionized or neutral molecules that can interact with the acid sites on the solid surfaces, the color change of which can be used to estimate a range of acid strength.[82] The term of acidity function (H_0) is used to quantitatively describe the ability of the acid sites to add a proton per molecule on the indicators to form its conjugate acid.

$$H_0 = pKa + log\,[B]/[BH^+] \qquad 1$$

In Equation 1, the activity of the species is approximated to concentration. [B] is the concentration of the neutral indicator while [BH^+] is the concentration of the conjugate acid of the basic indicator. pKa is pK_{BH^+} (pK_{BH^+} = -log[B][H^+]/[BH^+]). The acidity function can be used to describe the acidity ranging from dilute solutions to 100% sulfuric acid and it is considered as an extension of the pH scale to the negative values. Table 1.1 lists some indicators that are being frequently used to characterize the surface acidity on different solid materials. These molecules are uncharged bases capable of being converted to their conjugated acid forms by media with sufficient acid strength to transfer a proton to the indicators. By observing the color change of the indicators, the surface acidity of the solids can be estimated. For example, if the color is the

acid form of the indicator, then the value of the H_0 function of the solid is equal to or lower than the pKa of the indicator.

Table 1.1 Frequently used Hammett indicators for the measurement of acid strength in solid acid networks. [83,84]

Indicator	Color Base Form	Color Acid Form	pKa
Neutral red	yellow	red	+6.8
Methyl red	yellow	red	+4.8
Phenylazonaphtylamine	yellow	red	+4.0
p-Dimethylaminoazobenzene	yellow	red	+3.3
2-Amino-5-azotoluene	yellow	red	+2.0
Benzeneazodiphylamine	yellow	purple	+1.5
Crystal violet	blue	yellow	+0.8
p-Nitrobenzeneazo-(p'-nitro-dipehylamine)	orange	purple	+0.43
Dicinnamalacetone	yellow	red	-3.0
Benzalacetophenone	colorless	yellow	-5.6
Anthraquinone	colorless	yellow	-8.2
2,4,6-Trinitroaniline	colorless	yellow	-10.10
p-Nitrotoluene	colorless	yellow	-11.35
m-Nitrotoluene	colorless	yellow	-11.99
p-Nitrofluorobenzene	colorless	yellow	-12.44
p-Nitrochlorobenzene	colorless	yellow	-12.70
m-Nitrochlorobenzene	colorless	yellow	-13.16
2,4-Dinitrotoluene	colorless	yellow	-13.75
2,4-Dinitrofluorobenzene	colorless	yellow	-14.52
1,3,5-Trinitrotoluene	colorless	yellow	-16.04

The original assumption for this method is that the performance of the indicators is independent of the acid medium in which they present. However, there are far more complicated processes happening between the indicator molecules and the solid surfaces other than the simple proton transfer.[85] Those processes might be responsible for the color change of the indicators but not included in the expression of the acidity function (H_0). For example, Lewis himself argued that the strength of the Lewis acid sites depend on both the medium of the solvent and the base that is used as the reference. Since amorphous silica-aluminas have complicated structures as well as the chemical properties, the titration method needs to be combined with other characterization method in order to describe the acid strength in the networks.

Nuclear magnetic resonance

Nuclear magnetic resonance (NMR) spectroscopy has been evolving to probe the local environment of silicon, aluminum and proton atoms，providing important information about acidity of amorphous silica-alumina in relation to framework atoms, synthesis procedures and post synthesis treatments.[68] NMR provides information on the quantum properties of the atoms, which cannot be obtained by other characterization methods.[86] In 1959, Andrew et al. figured out a way to improve the NMR experiments for solids by spinning the sample about an axis and the method is often referred as the magic angle spinning (MAS) NMR.[87] Several nuclei are frequently used to characterize amorphous silica-alumina, such as ^{1}H, ^{29}Si, and ^{27}Al. By designing NMR experiments, the information of nature, structure and acidic properties of the materials can be obtained, providing valuable information to design catalysts with desired functionality.

^{29}Si MAS NMR studies have shown that different types of silicates existing in the amorphous silica-alumina. These studies help to understand the acidic properties changing upon varying amount aluminum atoms existing in the framework.[80,88] The ^{29}Si chemical shift is mostly affected by the atomic composition of the first and second coordination atoms (the first coordination atoms refer to the atoms directly attached to a silicon atom and the second coordination atoms refer to the atoms attached to the first coordination atoms). Q^n is used to describe different silicon species. For example, Q^4 represents a situation in with a silicon atom has four tetrahedral oxygen in the first coordination and another four silicon atoms in the second coordination. [80] For the co-gelled amorphous silica-aluminas, the removal of aluminum atoms

(the original alumina content is 14 wt%) in the silicon matrix narrows the silicates characteristic bands into separate peaks at around – 108.7 ppm. A peak for Q^3 coordination (with three silicon atoms and one other atoms at the second coordination) is resolved at low aluminum samples.[89] For the samples synthesized by deposition method, however, the amount of aluminum (from 5 wt% to 15 wt% Al_2O_3) does not change the Q^3 peak, indicating that a separate aluminum phase grows on the SiO_2 solids instead of a mixing between SiO_2 and Al_2O_3 phases.[88] By the ^{29}Si MAS NMR study, it is possible to recognize the Q^3 type of the silicate species which are attached to either an aluminum tetrahedron or a hydroxyl group and these two groups are responsible for the acid sites in the material. These two studies demonstrated that different synthesis methods influenced the chemical properties of the amorphous silica-alumina materials.

The ^{27}Al MAS NMR is an important tool to characterize the acidic properties in the amorphous silica-alumina solid frameworks by understanding the nature and the local environments of aluminum atoms. It has been reported that at low aluminum doping content, the tetrahedral aluminum is the dominating specie, which is widely believed to be related to the Brønsted acidity of the material.[89–91]When the low aluminum sample was further dealuminated, the catalytic activity decreased, corresponding to the loss of the four-coordinated aluminum in the network. At high aluminum samples, six and five-coordinated aluminum atoms also exist in the matrix.

^1H MAS NMR could be used to recognize different types of H atoms, which are assigned to be acid sites with different Brønsted acidity. One of the earliest experiments was designed by Hunger et al. [90,91] In their work, they recognized two types of signals for H atoms in the network. The signal at 7ppm was assigned to be the non-acidic silanol groups while the one at 2 ppm was considered to be the strong acidic groups, which are responsible for the Brønsted acidity in amorphous silica-alumina and zeolitic materials. The position of the signal was claimed to be the H atoms of silanols or the bridging hydroxyl groups under the electrostatic interaction with the oxygen atom and the interaction is affected by the framework tetrahedral aluminum atoms.[86,92] At the position of 3ppm, a broad signal has been reported on the dehydrated, but not dehydroxylated, silica-aluminas. This position was attributed to the surface hydroxyl groups on aluminum atoms, which can be converted to bridging hydroxyl groups when water is absorbed.[93] By assigining signals to different hydrogen atoms, it has been proved that there might be a small

domain in the amorphous silica-alumina that has the acidic strength comparable to that in H-faujasite and H-mordenite samples. [93]

Infrared spectroscopy

The infrared (IR) spectroscopic method is considered to be the most direct tool to study the type, concentration and the strength of the acid sites by observing the stretching of the hydroxyl groups at different location and around different chemical environments in the amorphous silica-aluminas. Simple IR studies recognize the silanols at a wavenumber of 3470-3740 cm^{-1} and the bridging hydroxyl groups at 3550-3680 cm^{-1}. The amount of aluminum in the silica network has a strong effect on the polarity that is shown in the shifting of the wavenumber in the spectra.[94] There are several modes of IR experiment designed to work on different types of sample systems. The transmission-absorption mode works on thin films and samples are processed to wafers in order to be examined. The diffuse reflectance infrared Fourier transform spectroscopy (DRIFTS) is used to study powder samples which can be strongly scattering or absorbing.

In order to characterize acidic properties, ab/desorption of probing molecules are used since the strength of solid acids is defined with respect to a base. Several molecules are used frequently in IR studies, such as ammonia, pyridine, benzene, and carbon monoxide (CO). The perfect probing molecule should present different behaviors upon different types and strength of acid sites and different spectra can be obtained. For example, pyridine molecules can bind with strong Brønsted acid sites to form pyridinium ions or coordinatively bind with strong Lewis acid sites. The ring vibration of the molecules gives peaks at 1544 cm^{-1} and 1455 cm^{-1}, respectively. Weak Lewis acid sites result in a band between 1448 cm^{-1} and1442 cm^{-1}. Several studies using IR methods have provided spectroscopic evidence that the Brønsted sites change with composition of the material and the calcination temperature in the amorphous silica-aluminas. [13,79,95]

Temperature programmed desorption

Temperature programmed desorption (TPD) is a very convenient method to quickly determine the acidic properties of the solid network. TPD of a base molecule is based on the adsorption equilibrium.[96,97] In a typical experiment, an adsorbate is first absorbed on the solid surface and a detector at downstream (such as a thermal conductivity detector, mass or UV-

visible spectrometer) is used to monitor the change of the properties of the inert carrier gas. Two types of molecules can be used at the on the same material in order to increase the resolution of the method. For example, ammonia, which is mostly widely used for the solid acid characterization, can be coupled with 2,6-dimethylpyriddine. Ammonia itself can be adsorbed on Brønsted and Lewis sites in a solid network, 2,6-dimethylpyriddine, however, can only interact with Brønsted sites because of the steric effect of methyl groups.[98] These experiments provide information on the Brønsted and Lewis acid sites distribution on amorphous silica-aluminas.

1.2 Single Molecule Fluorescence Microscopy

The characterization methods mentioned above provide the ensemble-averaged information about solid matrices. In the ensemble methods, it is assumed that heterogeneous catalysts have a homogeneous distribution of the properties everywhere on the surface of the solids. However, variations of different length scales do exist across catalyst beds, single particles and thin films. New characterization techniques are needed to look at the local environment that lead to macroscopic properties. The size of the domains can be down to micrometer or nanometer length scales. Single molecule (SM) fluorescence microscopic methods provide a way to look at the heterogeneous catalysts with high spatial and time resolution. The property distribution, molecular transport phenomenon and *in situ* catalytic activities can be observed.

1.2.1 Principles of Fluorescence Microscopy

A simple three-level energy Jablonski diagram is used to describe the photophysical processes of dye molecules during the single molecule fluorescence microscopic studies (the Jablonski diagram is shown in Figure 1.4). A dye molecule can be pumped by a laser with radiation energy of hv (h is the Planck constant and v is the optical frequency of the excitation laser) from the singlet ground state, S_0, to a singlet excited state, S_1. After the absorption of a photo, the molecule can return to the ground state through a radiative process by emitting a photon or through a nonradiative process. After the emission, the molecule goes back to the vibrational ground state S_0. The timescale for this transition is of the order of 1 ~ 10 nanoseconds. In some cases, the molecule can also relax through intersystem crossing into the triplet state, T_1. From T_1, the molecule can return to S_0 by emission of a phosphoresce photon. This is a slower process with a timescale of microseconds to even up to seconds after excitation and therefore the

molecule seems to be invisible for a certain amount of time. This phenomenon is often referred to triplet blinking.

The organic molecules suitable for SM studies need to have a high quantum yield, ϕ_F, which is defined as the ratio of the number of the emitted photons to the number of the absorbed photons. ϕ_F can also be defined by the rate constants of different processes shown in Equation 2.

$$\phi_F = \frac{number\ of\ emitted\ photons}{number\ of\ absorbed\ photons} = \frac{k_{rad}}{k_{rad}+k_{nonrad}} \qquad 2$$

where k_{rad} represents the rate constant of the radiative process and k_{nonrad} represents the rate constant of the nonradiative process. A high absorption cross-section area of dye molecules, σ, is also preferred for SM experments. This area is interpreted as the effective area for a molecule to be able to absorb excitation photons from a laser source. σ is directly related to the electronics structure of the fluorophores.

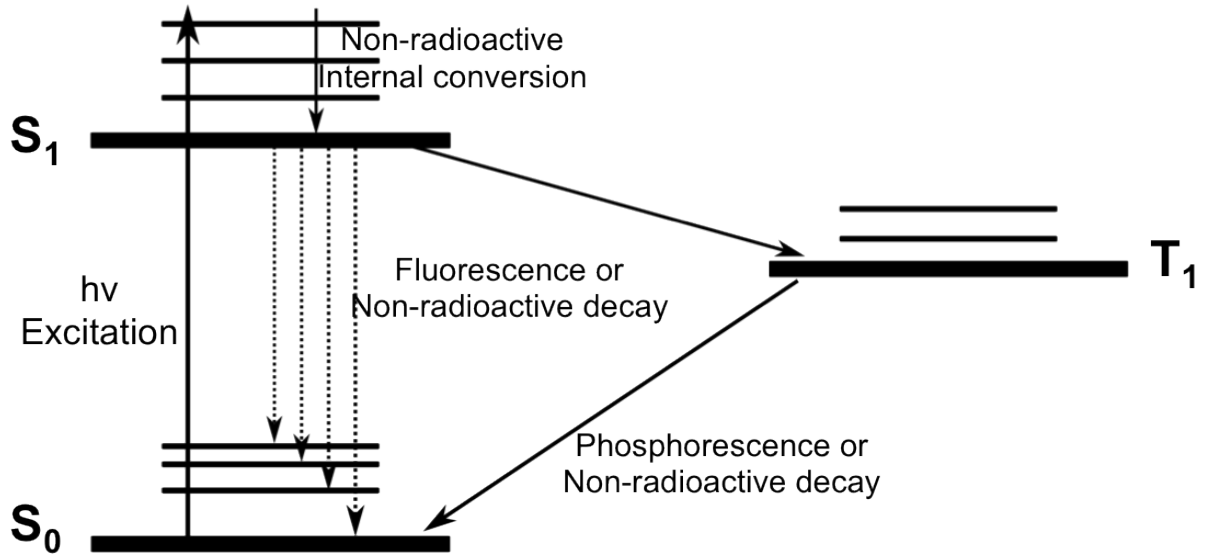

Figure 1.4 Jablonski Diagram. A simplified and typical energy level scheme to describe the single molecule fluorescence process and other competing processes. S_0 represents the ground state, S_1 represents the first excited state, and T1 represents the lowest triplet state. There are several levels of vibrational states in each electronic state. Photons with a energy of hv can excite the transition from the ground state to excited states. Fluoresce, nonfluorescence or intersystem crossing processes are of different rates and all of them can bring back the excited molecule to the ground state.

Photoblinking and photobleaching are two processes that limit the quality of signal collected from individual molecules since they make the fluorescent molecules become non-fluorescent. Unfortunately, these two processes are unavoidable for experiments at room temperature. Photobleaching happens when the dyes go through several cycles of excitation-emission transitions and the molecules get oxidized and hence the chemical structure responsible for the fluorescent behavior is destroyed. The impact from photobleaching can be reduced by simply decreasing the amount of the oxygen in the experiment environment, such as nitrogen gas purging.

The spatial resolution of the SM method is conveniently defined as the size of the spot that a light beam of certain wavelength can be focused into. Airy pattern (or Airy disc) is the mathematical description of the spot. The pattern has a series of concentric rings and has an intensity maximum in the center. Abbe et al.[99] solved the equation by using Bessel functions and derived the expression (shown in Equation 3) for the radius of the diffraction-limited spot, which is used as the transverse resolution for SM fluorescence microscopic measurements.

$$\delta_{min} = \frac{0.61\lambda}{NA} \qquad 3$$

In the equation, λ is the wavelength of light in vacuum. *NA* is the numerical aperture for the objective ($NA = nsin\theta$), and it is defined by the refractive index, *n*, of the medium in which light travels and the convergence angle, θ. For modern objectives, *NA* can be very high (between 1.3 and 1.5) by using water or oil as the medium instead of air.

1.2.2 Fluorescence Techniques for the Observation of Single Molecules

Fluorescence microscopic methods have been proven to be extremely sensitive and can be used for the detection of fluorescence signals from a single molecule. The earliest works were done by Moerner et al.[100] in 1980's via observation of absorption spectrum and by Orrit et al.[101] by studying excitation spectrum of dye molecules. The first experiments were completed at liquid-helium temperatures in order to immobilize the fluorophores so they could be observed as extremely narrow spectra in environments of different properties. Nowadays a large variety of microscopic techniques have been developed and allow collecting information from one molecule, which carries physicochemical information of a small domain that is in interaction

with the fluorophore. Modern experiments are based on the detection of the fluorescence light that is filtered out from the excitation light source and environmental radiations. Hence SM fluorescence microscopy is essentially a dark field method, which is of high signal-to-background as well as high signal-to-noise ratios compared with absorption or excitation measurements. The dye molecules can be immobilized and spatially separated in films, on surfaces, or in solutions. Modern SM experiments can be done at room temperature without requiring a cryogenic condition, which was considered as the major limitation of SM fluorescence methods.

There are also other widely used and very robust methods that can achieve the same or much better spatial resolutions compared with the SM fluorescence methods, such as the advanced electron microscopy (EM), scanning probing microscopy or atomic force microscopy (AFM), and scanning tunneling microscopy (STM). However, these methods either work under harsh conditions (such as high vacuum) or require special preparation (such conductive surface) that will destroy the structures or properties of scientific interests. Besides the noninvasive manner, SM fluorescence methods provide more chemical information than EM and AFM. Another advantage of the optical methods is the easy labeling strategy, which can be a powerful and convenient tool for studying of biological systems. The fact that SM fluorescence methods can be used under an ambient environment makes it very applicable and flexible for different sample systems and research purposes.

Near-field Fluorescence Microscopy

The diffraction limit in conventional microscopy has led to the development of near-field scanning optical microscopy (NSOM), the design of which allows a sub-wavelength spatial resolution.[102] In the early 20th century, Synge[103–105] proposed a type of new optical microscopic method that overcomes the diffraction limit. He proposed a microscopic aperture with a dimension much smaller than the wavelength of the optical light beam and the aperture was supposed to positioned in extreme proximity to the sample under examination. The light beam passing through the aperture would not diffract before it hit the sample surface and only the portion right beneath the aperture could be illuminated and imaged by an optical detector. In this configuration, the resolution is limited by the dimension of the aperture instead of the wavelength of the excitation light. Figure 1.5 is a schematic drawing of the set-up. At that time, Synge realized the difficulties of an actual experiment such as the aperture construction and

sample handling. Synge's theory was first demonstrated experimentally in 1972 by Ash and Nicholls[106] who used microwave with wavelength up to 3 cm as the radiation source. It was not until in the mid 1980s that Pohl[107,108] and Lewis,[108] working independently, reported the subdiffraction-limited imaging based on a theory proposed half a century ago.

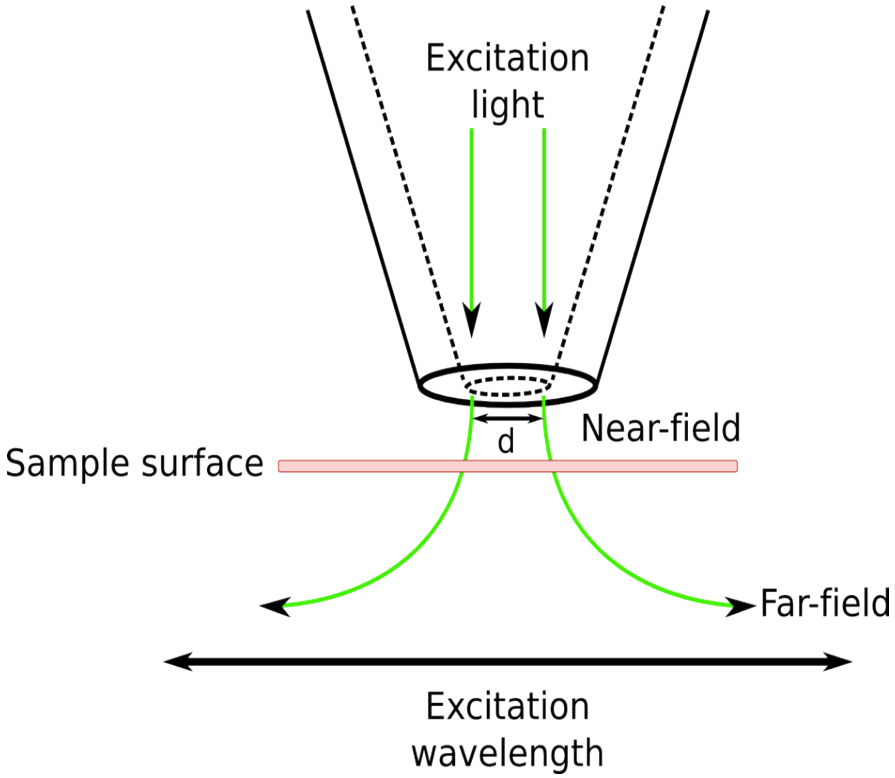

Figure 1.5 A schematic drawing of a near-field scanning optical microscope. The spatial resolution of the technique is defined by the dimension of the aperture, d, which is smaller than the wavelength of the excitation light. The sample is very close to the aperture in order to get excited before the light can diffract.

In 1993, Betzig and Chichester[109] reported the individual fluorescence molecules were detected by using NSOM with subwavelength resolution. Other experiments designed by other research groups soon followed to report the application of NSOM for SM spectra and fluorescence lifetime measurements. It is worth mentioning that Betzig and Chichester's experiment was the first demonstration of using optical microscopy at room temperature for SM detection. Betzig and Chichester's work was considered as a landmark for both NSOM and SM experiments.

Fluorescence correlation spectroscopy

Fluorescence correlation spectroscopy (FCS) is a very powerful tool for SM studies of diffusing molecules. This technique is based on the autocorrelation statistical analysis of fluorescence fluctuations of mobile dye molecules at very low concentration in a small excitation volume. A schematic drawing of the experiment is shown in Figure 1.6. Unlike other fluorescence technique, the emission intensity itself is not of direct interest but the intensity variations caused by small deviations of the volume oscillating around the thermal equilibrium of the bulk system. The parameters that could stimulate fluorescence fluctuation to be detected include the photophysical characteristics of the dye molecules (like triplet blinking and fluorescence lifetime), local concentration, diffusion constants, inter- or intramolecular reactions or conformational changes.[110,111]

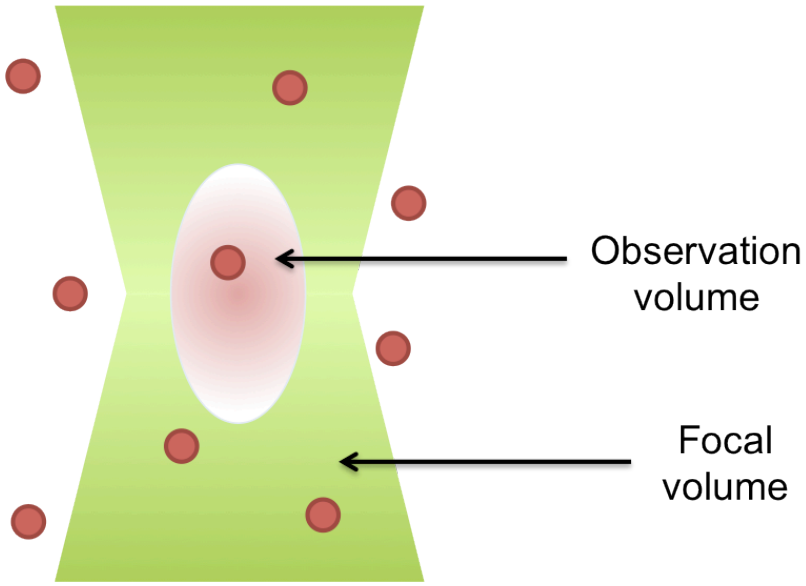

Figure 1.6 A schematic drawing of a focal volume of an objective for FCS experiments. The red dots represent the dye molecules. They are doped in a solution at the single molecule level and move into and out of the focal volume.

The autocorrelation is to compare the fluorescence signal at time t with the signal itself at time $t + \tau$ and hence the data is collected by recording the fluorescence intensity over a given time. An autocorrelation process is performed on the time transient after the data is obtained. The autocorrelation function is show in Equation 4.

$$C(\tau) = \frac{\delta F(t) \cdot \delta F(t+\tau)}{F(t)^2} \qquad 4$$

$C(\tau)$ is the autocorrelation function and it is normalized by the square of the average fluorescence.[112,113] $\delta F(t)$ and $\delta F(t+\tau)$ are the intensity fluctuation at time t and $t + \tau$ respectively. The autocorrelation function is influenced by the number of the dye molecules in the excitation volume. For one particular molecule, its effect on the measured fluorescence intensity declines when the bulk concentration increases. As a result, it is desired to have very dilute concentrations of dye molecules for FCS studies.

Wide-field Methods

Wide-field fluorescence microscopy is a very convenient and simple method for SM detection. As is indicated by the name, a light source is used to illuminate a relatively large area on the sample with several microns in diameter, which is a dimension larger that the size of the focused spot. A lot of fluorophores can be excited at the same time and the fluorescence signals are all collected by an array detector, which in most of cases is a charged coupled device (CCD) chip. Besides the size of the imaged area, another characteristic of using a wide-field microscope set-up is that images can be taken at near video rates, providing an avenue to monitor the molecule behaviors almost in real time.[113] The frame rate allows a temporal resolution of 30 ms. The spatial resolution of the wide-field method is the size of the diffraction-limited spots, which are of dimensions of around 250 nm, as is estimated by Equation 3. Each single molecule appears to be a spot composed of pixels in wide-field images. The intensity distribution in pixels is obtained by fitting the real intensity profile to a 2-dimension Gaussian profile.

It is possible to locate an individual molecule with a much better precision statistically than the diffraction limitation. The precision of measuring the position of a molecule can be defined as the confidential level, $ts/\sqrt{N}$, and N is the number of measurements. In SM detections, N equals to the number of the photons collected from one molecule. The measured mean position of the molecule then can be expressed in Equation 5.

$$\mu = \bar{x} \pm \frac{ts}{\sqrt{N}} \qquad 5$$

In the expression, t is the student value and s is the stand deviation determined by the diffraction limitation. The precision to which a single molecule is located can be down to around 20 nm.[105] This value is determined by the pixel size of the CCD camera and the magnification of the microscope.[104] Even with a small pixel size, large pixel array and magnification, this accuracy is still difficult to achieve since many factors can diminish the signal to noise ratio, such as photobleaching and photo blinking processes, which can decrease the number of photons to be detected and the CCD camera itself has unavoidable read-out noises.

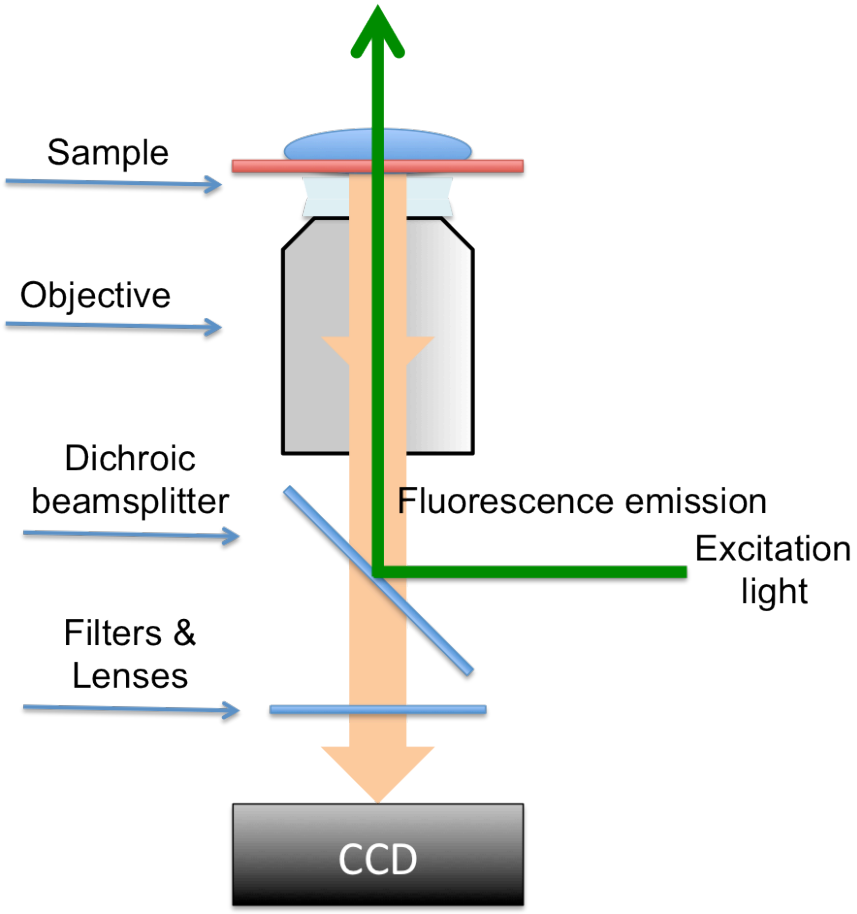

Figure 1.7 A schematic drawing of an epifluorescence microscope. The excitation depth is infinite and the molecules from the out-of focal plan in the sample are excited, becoming a source of background noise.

There are two modes of wide-field fluorescence method for SM detection. The first one is the epifluorescence microscopy. A simplified schematic drawing of the microscope is shown in Figure 1.7. A round area with diameter of several micrometers is illuminated by a light source. In

order to create an illuminating spot, the light is focused on the back aperture of the microscope objective. A high numerical aperture is preferred in order to maximize the detected fluorescence signals and to improve the resolution. It can be derived from Equation 3 that, $NA = nsin\theta$,, so immersion oil with high refractive index, n, is used as the medium. The fluorescence signals from the examined sample pass through the same objective, which is used to focus the illuminating light source. Additional optical parts, such as lenses and filters along the emission pathway, are used to get rid of the residual excitation light and other background signals. This set-up minimizes the noise coming from the excitation light. However, the excitation depth is through the entire sample thickness and the dye molecules from out of the focal plane can also be excited, which in turn becomes a source of noise, decreasing the image quality.

Total internal reflection fluorescence (TIRF) microscopy is the other mode for the wide-field method and a schematic drawing is shown in Figure 1.8a. In this mode, an evanescent field is used to excite the dye molecules. TIRF mode is constructed according to the Snell's law, which describes how light is refracted or reflected at the interface of two media with different refractive indexes. When propagating in a medium, light will be totally reflected when it hits the interface, which has a medium with smaller refractive index on the other side. In a common TIRF experimental set-up, the first medium is glass (glass coverslip) and the second medium is water or a sample system supposed to have very similar refractive index to that of water. Even if light cannot pass into the second medium (such as water or the medium of a sample under examination), an evanescent field still can pass through the interface and propagate for a small distance. The intensity profile along the propagating direction is shown in Equation 6.

$$I(z) = I(0)\exp(-z/d) \qquad 6$$

where $I(0)$ is the excitation light intensity at the interface, and d is the exponential decay distance that is defined in Equation 7

$$d = \frac{\lambda_0}{2\pi}(n_2^2 sin^2\theta - n_1^2)^{-1/2} \qquad 7$$

where λ_0 is the wave length of the excitation light in vacuum and n_1 and n_2 are the refractive indexes of the two media, respectively. A typical value of d for a green light is ~ 150 nm and this value indicates that only a very thin layer in the sample that is very close to the glass/water

(sample) interface can be illuminated and hence a limited number of dye molecules can be excited by the evanescent field. TIRF mode obviously avoids the background noise from inside the sample compared with the epifluorescence mode.

There is also a prism-based TIRF microscopy and the schematic set-up is shown in Figure 1.8b. The excitation light does not pass through the objective but is guided into a prism in this mode. The prism is positioned right on top of the sample and the evanescent pass through the interface to excite the dye molecules in a thin layer.

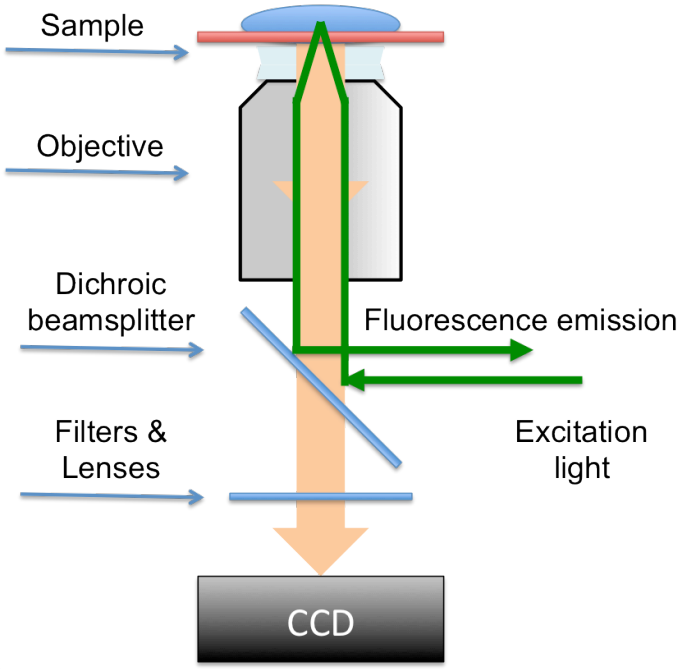

a

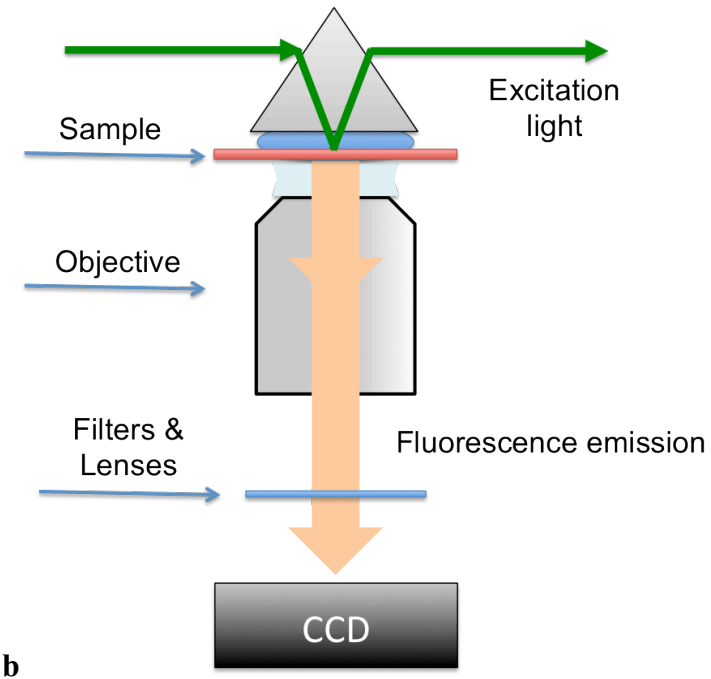

b

Figure 1.8 Schematic drawings for two experimental configurations for TIRF experiments based on different excitation pathways. a) The configuration for the through-the-objective mode. The excitation light passes through the objective, overlapping with the fluorescence signal pathway for a short distance. b) The configuration for the prism-based mode. In both configurations, only a small volume of the sample can be excited by the light source, lowing the background from the out-of-focus fluorescence.

Confocal Methods

Confocal microscopy is a very important and powerful method for SM detection experiments. A representative scheme is shown in Figure 1.9. The excitation light only illuminates an area of the smallest diffraction-limited spot size determined by Equation 3. The collimated light is used and focused into a certain depth of the sample. The fluorescence emission from the dye molecules as well as the back-scattered excitation light is collimated by the same objective. The residue excitation light can be screened out by a dichroic mirror, an interference filter or a beam splitter such as the configuration in a wide-field microscope. A tube lens is used to focused the fluoresce signal to a pinhole in the detection pathway, which serves to block the out-of-focal plane light in order to increase the resolution, The dimension of the pinhole defines the depth of field for a confocal image. Only the dye molecules existing in the excitation volume, which is as small as femtoliters, can be excited and recorded by a point

detector such as a photo-multiplier tubes or avalanche photo diodes (APDs). A scanning motion is required to raster on the sample and to obtain images with larger size than the diffraction limited spot. A computer-controlled piezo-electric state is normally coupled with a confocal microscope in order to scan point by point precisely. Optical parts or other detectors can be added to a confocal microscope configuration to extend its applicability to collect more interesting information of a sample. A polarizer can be used to study the orientation of the fluorophores. The spectrum of the fluorescence signal can be obtained by grafting with a prism and a CCD camera. A confocal microscope can also be used for FCS studies, in which signals from dye molecules diffusing into the excitation volume can be detected and recorded.

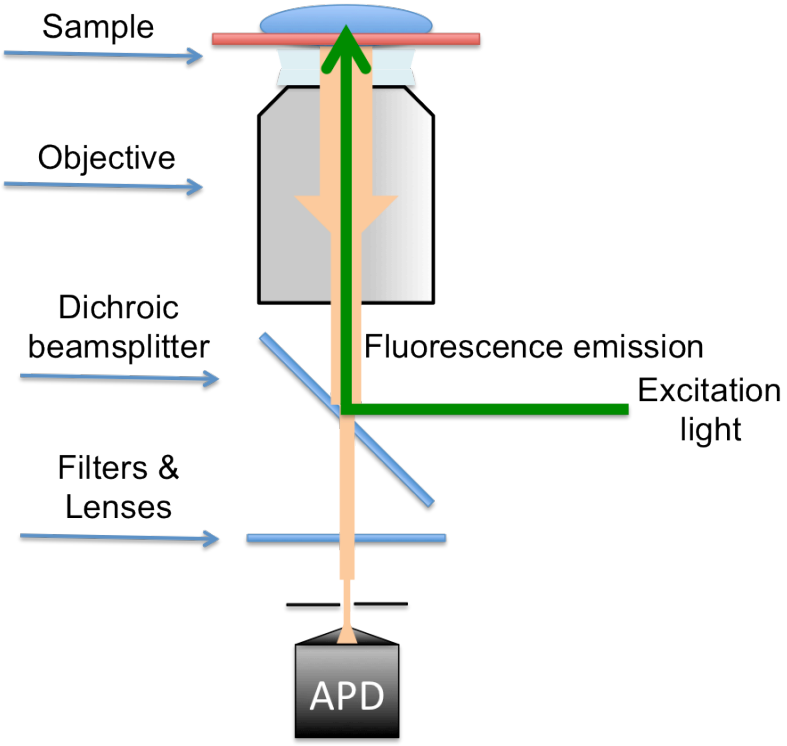

Figure 1.9 A schematic drawing of confocal microscopy. Only the molecules in the focal volume can be excited and emitted fluorescence signals to. This configuration decreases the background to a great extent for the small excitation volume. The signal is focused by a tube lens through an aperture and reject the out-of-focal plan fluorescence automatically. A point detector, such as an avalanche photo diodes (APD) is used to count the number of photons from individual fluorophores.

Fluorescence resonance energy transfer

Fluorescence resonance energy transfer (FRET) is another frequently used technique for single molecule detection. It has been developed into a very useful tool for physical chemistry and biophysical studies for more than 30 years.[114,115] FRET occurs when a donor fluorophore is excite by a light source, and the energy is transferred to an acceptor molecule in proximity through a non-radiative process. The excited acceptor molecule then releases energy by emitting photons with a longer wavelength. The energy transfer process between this pair of molecules is named as Förster dipole-dipole interaction and it can only when the emission spectrum of the donor overlaps with the absorption of the acceptor as is depicted in Figure 1.10.[116] The energy transfer is a strong function with the donor-acceptor distance and the extent of the overlap of the spectra. Equation 8 gives the rate of a FRET process.

$$k_T(r) = \frac{1}{\tau_D}\left(\frac{R_0}{r}\right)^6 \qquad 8$$

where r is the distance between the donor and acceptor molecules, and τ_D is the fluorescence lifetime of the donor without any energy transfer. R_0 is the Förster radius. The Förster radius is a characteristic distance, between which 50% of the energy is transferred from the donor to the acceptor. R_0 is affected by several factors, such as the extent of spectral overlap between a pair of donor and acceptor, the donor fluorescence lifietime, τ_D, the quantum yields, and orientaions of the transition dipoles of the two molecules. Typical values for R_0 is between 20 ~ 60 angstroms.[98,117,118] This range is comparable to the sizes of a lot of biological macromolecules. For this reason, FRET is known as a spectroscopic/molecular ruler for measurements between labeled sites on macromolecules such as proteins.

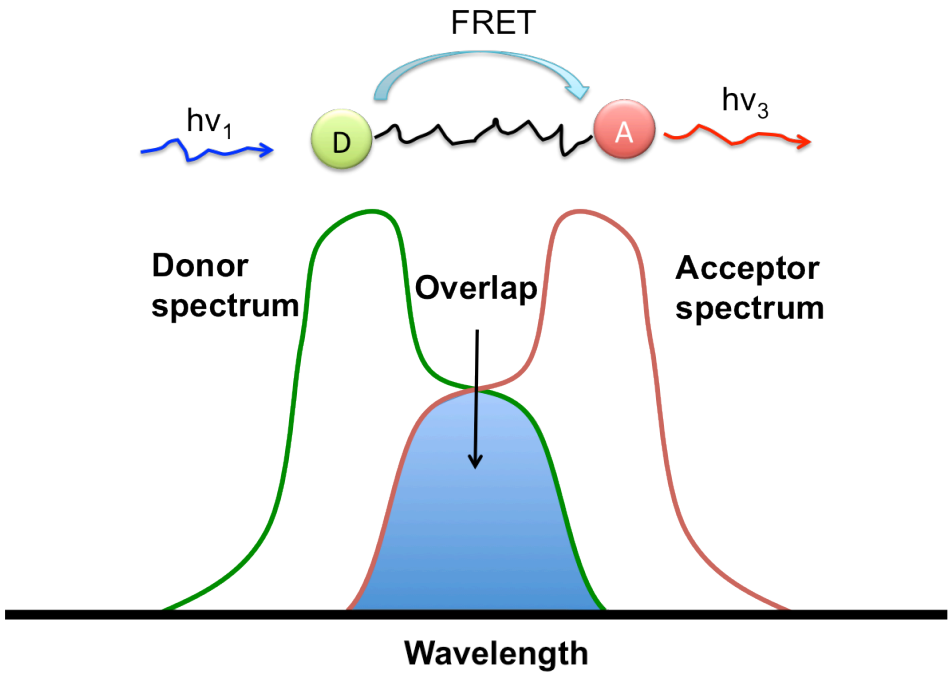

Figure 1.10 An illustration of a fluorescence resonance energy transfer process. A light source is used to excite the donor and the energy is transferred to the acceptor through a nonradiative process. The excited donor then can release the energy through radiative or nonradiative processes. The FRET process can only happen when there is an overlap of the spectra of the two fluorophores and when there is an appropriate distance between the two.

The instrumentation for FRET measurement can be similar to that of a wide-field or a confocal single molecule fluorescence detection configuration. In the case of a wide-field configuration, a beam splitter is used to separate the fluorescence signal spectrally and two images can be formed on a CCD camera simultaneously for the donor and acceptor molecules, respectively. In the confocal configuration, a similar dichroic beamsplitter is used and two point detectors (two APDs, for example) are used together to record two images.

1.2.3 Solid Catalysts Characterization with Single Molecule Methods

Catalytic domains with nanometer or Ångströms dimensions are distributed on and within the network of heterogeneous catalysts. The active sites can exhibit varying performances because of different local elemental compositions, structures and their accessibility to reactant molecules.[119] Many characterization methods have been used to understand material properties at different scales. Particularly noteworthy are those techniques that probe the catalysts at the

atomic scale, the scale at which chemical reactions occur.[120] Recently, SM fluorescence techniques have shown their potential to be applied to solid catalyst characterization by many research groups, obtaining information about molecular diffusion, ad/desorption phenomenon, reaction kinetics and chemical conversions. Single molecule fluorescence microscopic method makes it possible to investigate the molecular dynamics in pores and on surfaces of catalytic systems at small length scales with high resolution.[9] Signals such as fluorescence intensity, spectrum, polarization light can be interpreted as the properties of the solid matrix.

Activity mapping

The local compositional and structural differences can have strong effects on the catalytic activity of catalyst surfaces. Roeffaers et al.[121] designed SM fluorescence experiment with a wide-field microscope to map active sites for different reactions over individual layered double hydroxide (LDH) crystals with sizes about 10 ~ 20 μm. Two fluorogenic reactions catalyzed by LDH particles were studied and the distribution of the fluorescent products provided evidence of catalytic sites with different activity on the basal surfaces and edges on the same crystal. The dye molecule，which is also the reactant itself is 5-carboxyfluorescein diacetate (C-FDA). This molecule can be catalyzed by LDH for transesterification reaction with alcohols or hydrolysis in a water-containing medium. In the image of the transesterification reaction, bright spots representing reaction products were all over the crystal while in the image of the hydrolysis reaction, most of the bright spots appeared on the edges of the crystal, indicating that active sites capable of catalyzing the hydrolysis of C-FDA mainly existed on the edges rather than the basal faces of the crystal.

Reaction kinetics

Reaction kinetics can be studied by SM fluorescence microscopy. Xu et al.[122] studied the conversion of nonfluorescent Resazurin to fluorescent resorufin in NH_2OH aqueous solutions. The reaction was catalyzed by Au nanoparticles with sizes of 1.7-6.7 nm. The particles were well separated and dispersed on quartz slides. Diffraction-limited fluorescence spots were detected, indicating that a molecule of fluorescent resorufin was produced. Since a real-time movie was recorded, each bright spot burst was recognized as one reaction catalyzed by one Au nanoparticle. The time before a fluorescence burst happened was considered as the waiting time for a nonfluorescent Resazurin molecule diffuse to a nanoparticle, get absorbed on an active site

and thermal-activated for the reaction. The time duration for a fluorescence burst was reported as the waiting time for a product molecule diffusing away from an Au nanoparticle. Several control experiments were designed to prove that only when products combined on the Au nanoparticle surface， the fluorescence bursts could be observed. Two waiting times were used to obtain the kinetic and thermodynamic parameters for the reaction, such as the ab/desoption and reaction rate constants and equilibrium constants. It should be noted that the single particle investigation in this study allowed reaction to be followed on individual active sites, which cannot be achieved with ensemble characterization methods.

Molecular diffusion in the pores and on the surfaces

The single molecular tracking technique allows monitoring the diffusion patter of guest molecules in a solid matrix. Zurner et al.[123] and Jung et al.[124] combined the SM fluorescence and the high-resolution electron microscopy methods to study mesoporous hexagonal silica films. The interaction between the guest molecule and the host environment was investigated in detail. The dye molecule used for the SM study was terrylene diimide (TDI), which is a highly fluorescence molecule. Individual dye molecules appeared as 2-dimensional Gaussian profiles, which gave the location and the orientation of the transition dipole moments of the molecules. The same transition dipole moments for all TDI dye molecules everywhere in the image indicated that the imaged domains had highly ordered mesoporous structures. This work proved that the SM fluorescence method could be used to study the structure of the solid framework. In order to study the influence of the host environment on the diffusion pathway of the TDI molecules, the samples were exposed to air of varying humidities and to different organic solvents. It was found that TDI fluorophores were immobilized in low humidity conditions and diffused only slowly in higher humidity. In the chloroform atmosphere, however, high mobility of the molecules was observed and the mobility could be stopped by simply replacing the chloroform atmosphere with air. The researchers concluded that the chloroform acted as a lubricant-like phase inside the pores and influenced the interaction of the TDI molecules with silanol groups and template molecules. With the same experimental strategy, it was observed that TDI dye molecules could be bounced back when they hit a dead end in an ordered material or they can escape from a channel to another channel via a bypass route. Some other studies with TDI dye molecule have demonstrated that it is possible to distinguish the TDI molecules

diffusing on the external surface and inside the pores by observing the mobility.[125] These studies directly related the behavior of the dye molecules to the structural information of the solid matrix.

1.2.4 Single molecule fluorescence studies of acidity in solid catalysts

Acidity characterization by pH-sensitive dye molecules

Fluorescent, pH-sensitive dye molecules have been widely used for intracellular pH studies. The pH dependent behaviors of the fluorophores can be used for qualitative measurements of pH values. Some dye molecules can be turned on and off by sharply defined pH values and the emission intensities can be functions of pH values. One problem with these dye molecules is that their fluorescence signals are influenced by many factors, such as optical path length, temperature, excitation light intensity and emission detection efficiencies. For ratiometric methods, the dye molecules are responsive to the pH value of the environments by varying at least two emission (or excitation) wavelengths.[126,127] Dual emission pH-sensitive dye molecules have been synthesized by a number of researchers.[128] These molecules have two distinct emission bands for their protonated and deprotonated forms. The intensity ratios of the signal at two characteristic wavelengths can be calibrated to quantitatively indicate pH values. Equation 9 depicts the relation between the pH value and the measurable fluorescent intensity ratio, R.[129,130]

$$pH = pK_a + c\times\log\left(R - R_{min}/R_{max} - R\right) + \log\left[I^a/I^b\right] \qquad 9$$

where c is the slope obtained by linear regression analysis. R is the measured emission intensity at two wavelengths, with maximum and minimum limiting values of R_{max} and R_{min}. I^a and I^b are the emission intensity at the fully acid or fully basic form of the dye molecule, respectively.

A study by Fu et al. has shown the potential of using the ratiometric method to obtain the microenvironmental acidity in silica thin films. A pH-sensitive dye molecule, C-SNARF-1, is used to study the acidic properties of silanol sites. It was reported that the as-synthesized silica thin films had an average pH of ~ 4.8, which was influenced by the acid-catalyzed sample preparation procedure. They tried to control the local film acidity by exposing the samples to external solutions of different pH values for 1 h and 8 h, respectively. Histograms of intensity ratio, R, were made from fluorescence of individual molecules to present the acidity distribution in silica films. The trend of R changing with pH was in agreement with that was acquired from

bulk solutions. It was shown that films treated for only 1 h had wider *R* distributions, indicating more heterogeneous acidic environments in the samples. This work proved the evidence of the kinetic factors limiting the accessibility of the external solutions to certain film environments. They also observed the influence of silanols on the local pH in the thin films. Narrow *R* distribution was found at pH 8 and 9, indicating more homogeneous acidities buffered by silanol groups in the sample. Wide *R* distribution at pH 7 was attributed to the most sensitive response of C-SNARF-1, where the average pH was close to the pKa of the dye molecule. Fu's work provided insightful information about silica networks that could not be observed by averaged-ensemble characterization methods.

Characterization by fluorogenic reactions

A fluorogenic reaction involves a substrate whose fluorescent properties can be induced or enhanced by adding another molecule entity. Some reactions can specifically happen at a Brønsted acid site, allowing researchers to map the acidity distribution as well as the catalytically active domains on solid frameworks. For example, Roeffaers et al.[131,132] utilized the acid-catalyzed self-condensation reaction of furfuryl alcohol to monitor the spatial and temporal dependence of the product formation on ZSM-5 crystals. The reaction route is shown in Figure 1.11. Two furfuryl alcohol molecules **1** initially were catalyzed to form a colorless bis(furfuryl)methyl group **2**. This molecule was capable of transferring a hydride ion to a primary carbenium ion produced from another molecule of furfuryl alcohol. Visible absorption occurred from the resonance-stablized bis(furfuryl)methyl carbenium ion **3** or its conjugated structure of **4**. When excited by visible light, only compounds **3** and **4** and their related structures fluoresce. The absorption and emission spectra red-shifts as the degree of oligomerization and conjugated increased, providing an avenue to observe the product formation as a function of time and location. By using a confocal microscope, the fluorescent species were observed on the (100) phase of the crystal after 10 minutes of reaction. By adjusting the focal depth, fluorescence could be observed within the crystal. After 16 hours of reaction, fluorescence products were observed on the edges of the crystal. It was concluded that all parts of the catalyst could be reached by furfuryl alcohol molecules. After 50 days of reaction, however, the tips of the crystals had the most fluorescence. It was argued that after long reaction time, the catalysts were deactivated by pore plugging. Meanwhile, the desorption of the product molecule became slow and gave rise to

extensive oligomerization reaction. This work was able to probe individual zeolite crystals and observe the temporal and spatial relation to the Brønsted acidity in the solid network.

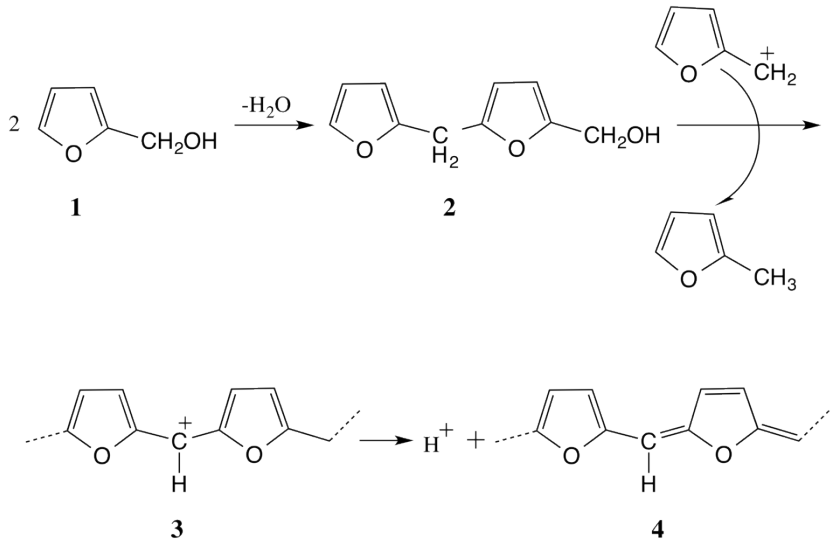

Figure 1.11 Acid-catalyzed self-condensation reaction of furfuryl alcohol.

In a second example, Weckhuysen et. al[64] reported SM fluorescence experiment for mapping the catalytic activity of individual fluid catalytic cracking (FCC) zeolite particles. In this study, two dye molecules were used at the same time to obtain both the activity and the matrix information. The fluorogenic reaction of thiophene oligomerization was employed to monitor the acidic domains on the catalyst since the reaction could only happen on Brønsted acid sites. The green fluorescence from the products served as the indicator of the acidity, which was also the catalytic activity for the FCC process. Stronger intensity indicated stronger acidity of the catalytically active domains. The second dye molecule is Nile Blue A, which had red fluorescence. The size of Nile Blue A prevented it from accessing the pore structure and this dye molecule was used to reveal the porous matrix of the zeolite particle. This study mapped the porous structure of the FCC catalysts as well as the acidity distribution across the network. Changes in Brønsted acidity over time was observed by studying the catalysts after different deactivation procedures, using thiophene as the indicator. As the researchers predicted, the fluorescence intensity dropped for deactivated catalysts, indicating the loss of Brønsted acid sites, which were responsible for the formation of fluorescence carbocations.

Other molecules with fluorogenic properties, such as hydroxyalkylation of anisole and dehydration of 1,3-diphenyl- 1,3-propanediol were also used for the characterization of the Brønsted acidity of the solid catalysts. These studies have successfully proved the potential of

applying SM fluorescence microscopy for characterization of solid acid catalysts. The high sensitivity, high time and spatial resolution allows to map the acidity on single particles or single crystals. *In situ* characterization procedures can be conveniently designed to observe the evolvement of the reaction and the deactivation of the active sites. SM fluorescent methods is very promising to acquire structural as well as catalytic insights in solid acid systems.

Reference

(1) Hagen, J. *Industrial catalysis: a practical approach*. 2006.

(2) Second, C.. Ertl, G.. Knözinger, H.. Schüth, F. Handbook of Heterogeneous Catalysis. 2008.

(3) Rase, H. *Handbook of commercial catalysts: heterogeneous catalysts*. 2000.

(4) Anderson, J.. Garcia, M. *Supported metals in catalysis*. 2005.

(5) Clark, J. H. Catalysis for green chemistry. *Pure and Applied Chemistry.* 2001, *73*, 103–111.

(6) Poduval, D. G.. van Veen, J. a R.. Rigutto, M. S.. Hensen, E. J. M. Brønsted acid sites of zeolitic strength in amorphous silica-alumina. *Chemical communications (Cambridge, England)*. 2010, *46*, 3466–8.

(7) Corma, A. Inorganic solid acids and their use in acid-catalyzed hydrocarbon reactions. *Chemical reviews.* 1995.

(8) Corma, A. Solid acid catalysts. *Current Opinion in Solid State and Materials Scienc.e* 1997.

(9) Niemantsverdriet, J. *Spectroscopy in catalysis*. 2007.

(10) Thomas, J. M.. Thomas, W. J. *Principles and practice of heterogeneous catalysis*. 1997. Vol. 171, p. 669.

(11) Clark, J. Solid acids for green chemistry. *Accounts of chemical research.* 2002.

(12) Price, P.. Clark, J. Enhanced Selectivity in the Preparation of Linear Alkylbenzenes Using Hexagonal Mesoporous Silica Supported Aluminium Chloride1. *Process Research & Development.* 1998.

(13) Sharma, Y.. Singh, B.. Korstad, J. Advancements in solid acid catalysts for ecofriendly and economically viable synthesis of biodiesel. *Biofuels, Bioproducts and Biorefining.* 2011.

(14) Scherzer, J.. Gruia, A. *Hydrocracking science and technology*. 1996.

(15) Matar, S.. Ph.D.. Hatch, L. F. *Chemistry of Petrochemical Processes.* Gulf Professional Publishing. 2001. p. 356.

(16) Weitkamp, J. Catalytic Hydrocracking—Mechanisms and Versatility of the Process. *ChemCatChem.* 2012.

(17) Bellussi, G.. Perego, C.. Carati, A. Amorphous mesoporous silica-alumina with controlled pore size as acid catalysts. *catalys.* 1994.

(18) Beck, J. S.. Vartuli, J. C.. Roth, W. J.. Leonowicz, M. E.. Kresge, C. T.. Schmitt, K. D.. Chu, C. T. W.. Olson, D. H.. Sheppard, E. W. A new family of mesoporous molecular sieves prepared with liquid crystal templates. *Journal of the American Chemical Society.* 1992, *114*, 10834–10843.

(19) Beck, J.. Calabro, D.. McCullen, S. Method for functionalizing synthetic mesoporous crystalline material. *Patent 5,145,81.6.* 1992.

(20) Brace, X.. Matijević, E. Coprecipitation of silica with aluminum hydroxide. *Colloid and Polymer Science Kolloid Zeitschrift & Zeitschrift für Polymere.* 1977, *255*, 153–160.

(21) Kriesel, J.. Sander, M.. Tilley, T. Block copolymer-assisted synthesis of mesoporous, multicomponent oxides by nonhydrolytic, thermolytic decomposition of molecular precursors in nonpolar media. *Chemistry of materials.* 2001.

(22) Hosier, P. Method for Controlling Hydrocarbon Fermentations and Apparatus. *US Patent 3,586,605.* 1971.

(23) Yoldas, B. Alumina gels that form porous transparent Al2O3. *Journal of Materials Science.* 1975.

(24) Yoldas, B. A transparent porous alumina. *Am. Ceram. Soc. Bull.* 1975.

(25) Flanigen, E.. Bekkum, H. van. Jansen, J. *Introduction to Zeolite Science and Practice*. 1991.

(26) Weitkamp, J.. Puppe, L. *Catalysis and zeolites: fundamentals and applications*. 1999.

(27) Elanany, M.. Koyama, M.. Kubo, M.. Broclawik, E.. Miyamoto, A. Periodic density functional investigation of Lewis acid sites in zeolites: relative strength order as revealed from NH3 adsorption. *Applied Surface Science.* 2005, *246*, 96–101.

(28) Lercher, J.. Jentys, A. Application of microporous solids as catalysts. *Handbook of Porous Solids.* 2002.

(29) Schuth, F.. SING, K.. Weitkamp, J. Handbook of porous solids (5 vols). 2002.

(30) Gale, J.. Payne, M. Comparing the acidities of zeolites and SAPOs from first principles. *Chemical Communications.* 1997.

(31) Utchariyajit, K.. Wongkasemjit, S. Effect of synthesis parameters on mesoporous SAPO-5 with AFI-type formation via microwave radiation using alumatrane and silatrane precursors. *Microporous and Mesoporous Materials.* 2010.

(32) Wilson, S.. Lok, B. Aluminophosphate molecular sieves: a new class of microporous crystalline inorganic solids. *Journal of the American Chemical Society.* 1982.

(33) Caro, J.. Finger, G.. Kornatowski, J.. Richter-Mendau, J.. Werner, L.. Zibrowius, B. Aligned molecular sieve crystals. *Advanced Materials* 1992, *4*, 273–276.

(34) Schunk, S.. Demuth, D. Element distribution and growth mechanism of large SAPO-5 crystals. *Microporous Materials.* 1996.

(35) Jacobsen, C.. Madsen, C. Mesoporous zeolite single crystals. *Journal of the Ameriacn Chemical Society.* 2000.

(36) Mueller, U.. Unger, K. Preliminary studies on the synthesis of alkaline-free large crystals of ZSM-5. *Zeolites.* 1988.

(37) Arata, K. Solid superacids. *Adv. Catal.* 1990.

(38) Song, Y.. Liu, H.. Liu, S.. He, D. Partial Oxidation of Methane to Syngas over Ni / Al 2 O 3 Catalysts Prepared by a Modified Sol-Gel Method. 2009, 1925–1930.

(39) Brown, A.. Hargreaves, J. Sulfated metal oxide catalysts. Superactivity through superacidity? *Green Chemistry.* 1999.

(40) Lunsford, J.. Sang, H.. Campbell, S. An NMR study of acid sites on sulfated-zirconia catalysts using trimethylphosphine as a probe. *Catalysis letters* 1994.

(41) Pinna, F.. Signoretto, M.. Strukul, G.. Cerrato, G.. Morterra, C. Isomerization ofn-butane on sulfated zirconia: Evidence for the dominant role of Lewis acidity on the catalytic activity. *Catalysis letters.* 1994.

(42) Adeeva, V.. Dehaan, J.. Janchen, J. Acid sites in sulfated and metal-promoted zirconium dioxide catalysts. *of Catalysis* 1995.

(43) SONG, X.. SAYARI, A. Sulfated Zirconia-Based Strong Solid-Acid Catalysts: Recent Progress. *Catalysis Reviews.* 1996, *38*, 329–412.

(44) Ghenciu, A.. Fărcaşiu, D. The mechanism of conversion of hydrocarbons on sulfated metal oxides. Part II. Reaction of benzene on sulfated zirconia. *Journal of Molecular Catalysis A: Chemical.* 1996.

(45) Ng, F.. Horvát, N. Sulfur removal from ZrO_2/SO_4^{2-} during n-butane isomerization. *Applied Catalysis A: General.* 1995.

(46) Mao, R. L. Van. Xiao, S.. Le, T. Thermal stability of the Pt bearing sulfate-promoted zirconia in the presence of hydrogen. *Catalysis letters.* 1995.

(47) Larsen, G.. Raghavan, S.. Márquez, M.. Lotero, E. Tungsta supported on zirconia and alumina catalysts: temperature-programmed desorption/reaction of methanol and pyridine DRIFTS studies. *Catalysis letters.* 1996.

(48) Brown, A. S. .. Hargreaves, J. S. .. Rijniersce, B. A study of the effect of sulphation on iron oxide catalysts for methane oxidation. *Catalysis Today.* 1998, *45*, 47–54.

(49) Brown, A. S. C.. Hargreaves, J. S. J.. Rijniersce, B. A study of the structural and catalytic effects of sulfation on iron oxide catalysts prepared from goethite and ferrihydrite precursors for methane oxidation. *Catalysis Letters.* 1998, *53*, 7–13.

(50) Sainio, T.. Laatikainen, M.. Paatero, E. Phase equilibria in solvent mixture–ion exchange resin catalyst systems. *Fluid phase equilibria.* 2004.

(51) Rao, L. Solid Acid Catalysts in Green Chemistry. 2007, 65–75.

(52) Harmer, M.. Michalczyk, M. Unique silane modified perfluorosulfonic acids as versatile reagents for new solid acid catalysts. *Chemical Communications.* 1997.

(53) Harmer, M.. Sun, Q. Solid acid catalysis using ion-exchange resins. *Applied Catalysis A: General.* 2001.

(54) Baba, T.. Ono, Y. Heteropolyacids and their salts supported on acidic ion-exchange resin as highly active solid-acid catalysts. *Applied catalysis.* 1986.

(55) Dias, J.. Osegovic, J.. Drago, R. The solid acidity of 12-tungstophosphoric acid. *Journal of Catalysis.* 1999.

(56) Kozhevnikov, I.. Sinnema, A.. Bekkum, H. Van Proton sites in Keggin heteropoly acids from17O NMR. *Catalysis letters.* 1995.

(57) Kozhevnikov, I. Catalysis by heteropoly acids and multicomponent polyoxometalates in liquid-phase reactions. *Chemical Reviews.* 1998.

(58) Narasimharao, K.. Brown, D.. Lee, A. Structure–activity relations in Cs-doped heteropolyacid catalysts for biodiesel production. *Journal of catalysis.* 2007.

(59) Oliveira, C.. Dezaneti, L. Esterification of oleic acid with ethanol by 12-tungstophosphoric acid supported on zirconia. *Applied Catalysis A.* 2010.

(60) Savelieva, G.. Abdukhalykov, D.. Dossumov, K. Research of the Activity of Catalysts on the Base of H3PW12O40 in Partial Oxidative Conversion of C3–C4 alkanes. *Catalysis letters.* 2009.

(61) Corma, A.. Garcia, H. Silica-Bound Homogenous Catalysts as Recoverable and Reusable Catalysts in Organic Synthesis. *Advanced Synthesis & Catalysis.* 2006, *348*, 1391–1412.

(62) Shu, Q.. Zhang, Q.. Xu, G.. Nawaz, Z. Synthesis of biodiesel from cottonseed oil and methanol using a carbon-based solid acid catalyst. *Fuel Processing Technology.* 2009.

(63) Gill, C.. Price, B.. Jones, C. Sulfonic acid-functionalized silica-coated magnetic nanoparticle catalysts. *Journal of Catalysis.* 2007.

(64) Weckhuysen, B. Chemical imaging of spatial heterogeneities in catalytic solids at different length and time scales. *Angewandte Chemie International Edition.* 2009.

(65) Rao, L. Solid acid catalysts in green chemistry. *Resonance.* 2007.

(66) Corma Inorganic Solid Acids and Their Use in Acid-Catalyzed Hydrocarbon Reactions. 1995.

(67) Scherzer, J.. Gruia, A. *Hydrocracking science and technology*. 1996.

(68) Crépeau, G.. Montouillout, V. Nature, structure and strength of the acidic sites of amorphous silica alumina: an IR and NMR study. *The Journal of Physical Chemistry B.* 2006.

(69) Thomas, C. L. Chemistry of Cracking Catalysts. *Industrial & Engineering Chemistry.* 1949, *41*, 2564–2573.

(70) Tamele, M. Chemistry of the surface and the activity of alumina-silica cracking catalyst. *Discussions of the Faraday Society.* 1950.

(71) Nilsen, B.. Onuferko, J.. Gates, B. Silicated aluminas prepared from tetraethoxysilane: catalysts for skeletal isomerization of butenes. *Industrial & engineering Chemistry Fundamentals.* 1986.

(72) Busca, G. Acid catalysts in industrial hydrocarbon chemistry. *Chemical reviews.* 2007, *107*, 5366–410.

(73) Garrone, E.. Onida, B.. Bonelli, B. Molecular water on exposed Al3+ cations is a source of acidity in silicoaluminas. *The Journal of Pysical Chemistry B.* 2006.

(74) Leydier, F.. Chizallet, C.. Chaumonnot, A.. Digne, M.. Soyer, E.. Quoineaud, A.-A.. Costa, D.. Raybaud, P. Brønsted acidity of amorphous silica–alumina: The molecular rules of proton transfer. *Journal of Catalysis.* 2011, *284*, 215–229.

(75) Baerlocher, C.. McCusker, L.. Olson, D. *Atlas of zeolite framework types*. 2007.

(76) Kato, Y.. Shimizu, K.. Matsushita, N.. Yoshida, T.. Yoshida, H.. Satsuma, A.. Hattori, T. Quantification of aluminium coordinations in alumina and silica–alumina by Al K-edge XANES. *Physical Chemistry Chemical Physics.* 2001, *3*, 1925–1929.

(77) Robinson, W. R. A. .. van Veen, J. A. .. de Beer, V. H. .. van Santen, R. . Development of deep hydrodesulfurization catalysts. *Fuel Processing Technology.* 1999, *61*, 103–116.

(78) Fripiat, J. Structure and Properties of Amorphous Silicoaluminas. II. Lewis and Brønsted Acid Sites. *The Journal of Physical Chemistry.* 1965.

(79) Basila, M.. Kantner, T.. Rhee, K. The Nature of the Acidic Sites on a Silica-Alumina. Characterization by Infrared Spectroscopic Studies of Trimethylamine and Pyridine Chemisorption1. *The Journal of Physical Chemistry.* 1964.

(80) Góra-Marek, K.. Derewiński, M.. Sarv, P.. Datka, J. IR and NMR studies of mesoporous alumina and related aluminosilicates. *Catalysis today.* 2005.

(81) Thomas, C. Chemistry of cracking catalysts. *Industrial & Engineering Chemistry.* 1949.

(82) Hammett, L.. Deyrup, A. A series of simple basic indicators. I. The acidity functions of mixtures of sulfuric and perchloric acids with water1. *Journal of the American Chemical Society.* 1932.

(83) Akc, M. Acidity of Silica-Alumina Catalysts By Amine Titration Using Hammett Indicators and FT-IR Study of Pyridine Adsorption. 1999, *23*, 319–327.

(84) Tanabe, K.. Misono, M.. Ono, Y.. Hattori, H. New Solid Acids andBases. *Stud. Surf. Sci. Catal.* 1989.

(85) Benesi, H. Acidity of catalyst surfaces. I. Acid strength from colors of adsorbed indicators. *Journal of the American Chemical Society.* 1956.

(86) Freude, D.. Ernst, H.. Wolf, I. Solid-state nuclear magnetic resonance studies of acid sites in zeolites. *Solid State Nuclear Magnetic Resonance.* 1994, *3*, 271–286.

(87) Andrew, E.. Bradbury, A.. Eades, R. Removal of dipolar broadening of nuclear magnetic resonance spectra of solids by specimen rotation. 1959.

(88) Hensen, E. J. M.. Poduval, D. G.. Magusin, P. C. M. M.. Coumans, a. E.. Veen, J. a. R. Van Formation of acid sites in amorphous silica-alumina. *Journal of Catalysis.* 2010, *269*, 201–218.

(89) Man, P. P.. Peltre, M. J.. Barthomeuf, D. Nuclear magnetic resonance study of the dealumination of an amorphous silica?alumina catalyst. *Journal of the Chemical Society, Faraday Transactions.* 1990, *86*, 1599.

(90) Hunger, M.. Freude, D.. Pfeifer, H. Magic-angle spinning nuclear magnetic resonance studies of water molecules adsorbed on Brønsted- and Lewis-acid sites in zeolites and amorphous silica?aluminas. *Journal of the Chemical Society, Faraday Transactions.* 1991, *87*, 657.

(91) Hunger, M.. Freude, D.. Pfeifer, H.. Bremer, H.. Jank, M.. Wendlandt, K. P. High-resolution proton magnetic resonance and catalytic studies concerning brønsted centers of amorphous Al2O3-SiO2 solids. *Chemical Physics Letters.* 1983, *100*, 29–33.

(92) Wolf, I.. Freude, D. Low-temperature and echo 1H magic-angle spinning nuclear magnetic resonance studies of dealuminated and weakly rehydrated zeolites H-Y. *Microporous Materials.* 1995, *5*, 69–75.

(93) Heeribout, L.. Vincent, R. Brønsted acidity of amorphous silica–aluminas studied by 1H NMR. *Catalysis letters.* 1998.

(94) Sanderson, R. *Chemical Bonds and Bonds Energy*. 1976.

(95) Pieta, I.. Ishaq, M.. Wells, R.. Anderson, J. Quantitative determination of acid sites on silica–alumina. *Applied Catalysis A: General* 2010.

(96) Sawa, M.. Niwa, M.. Murakami, Y. Relationship between acid amount and framework aluminum content in mordenite. *Zeolites.* 1990, *10*, 532–538.

(97) Karge, H. G.. Dondur, V. Investigation of the distribution of acidity in zeolites by temperature-programmed desorption of probe molecules. I. Dealuminated mordenites. *The Journal of Physical Chemistry.* 1990, *94*, 765–772.

(98) Moerner, W.. Fromm, D. Methods of single-molecule fluorescence spectroscopy and microscopy. *Review of Scientific Instruments.* 2003.

(99) Abbe, E. Resolution of microscopes, Arch. *Mikrosk. Anat* .1873.

(100) Moerner, W.. Kador, L. Optical detection and spectroscopy of single molecules in a solid. *Physical Review Letters.* 1989.

(101) Orrit, M.. Bernard, J. Single pentacene molecules detected by fluorescence excitation in a p-terphenyl crystal. *Physical review letters.* 1990.

(102) Enderle, T.. Ha, T.. Chemla, D.. Weiss, S. Near-field fluorescence microscopy of cells. *Ultramicroscopy.* 1998.

(103) Synge, E. H. XXIII. An application of piezo-electricity to microscopy. *Philosophical Magazine Series 7.* 1932, *13*, 297–300.

(104) Synge, E. H. XXXVIII. A suggested method for extending microscopic resolution into the ultra-microscopic region. *Philosophical Magazine Series 7.* 1928, *6*, 356–362.

(105) Synge, E. H. III. A microscopic method. *Philosophical Magazine Series 7.* 1931, *11*, 65–80.

(106) Ash, E.. Nicholls, G. Super-resolution aperture scanning microscope. 1972.

(107) Pohl, D. W.. Denk, W.. Lanz, M. Optical stethoscopy: Image recording with resolution λ/20. *Applied Physics Letters.* 1984, *44*, 651.

(108) Lewis, A.. Isaacson, M.. Harootunian, A.. Muray, A. Development of a 500 Å spatial resolution light microscope. *Ultramicroscopy.* 1984, *13*, 227–231.

(109) Betzig, E.. Chichester, R. J. Single molecules observed by near-field scanning optical microscopy. *Science (New York, N.Y.).* 1993, *262*, 1422–5.

(110) Aragon, S.. Pecora, R. Fluorescence correlation spectroscopy and Brownian rotational diffusion. *Biopolymers.* 1975.

(111) Felekyan, S. Full correlation from picoseconds to seconds by time-resolved and time-correlated single photon detection. *Review of scientific Instruments.* 2005.

(112) Maiti, S.. Haupts, U.. Webb, W. Fluorescence correlation spectroscopy: diagnostics for sparse molecules. *Proceedings of the National Academy of Sciences of the United States of America.* 1997.

(113) Hess, S. T.. Huang, S.. Heikal, A. A.. Webb, W. W. Biological and Chemical Applications of Fluorescence Correlation Spectroscopy: A Review †. *Biochemistry.* 2002, *41*, 697–705.

(114) Steinberg, I. Long-range nonradiative transfer of electronic excitation energy in proteins and polypeptides. *Annual review of biochemistry.* 1971.

(115) Fairclough, R.. Cantor, C. The use of singlet-singlet energy transfer to study macromolecular assemblies. *Methods in enzymology.* 1978.

(116) Gabor, G. Radiationless energy transfer through a polypeptide chain. *Biopolymers.* 1968.

(117) Meer, B.. Coker, G.. Chen, S. Resonance energy transfer: theory and data. *Cambridge: VCH.* 1994.

(118) Joseph, R.. Lakowicz, R. Principles of Fluorescence Spectroscopy. *Kluwer Academic/Plenum Publishers, New York.* 1999.

(119) Weckhuysen, B. M. Chemical imaging of spatial heterogeneities in catalytic solids at different length and time scales. *Angewandte Chemie (International ed. in English).* 2009, *48*, 4910–43.

(120) De Cremer, G.. Sels, B. F.. De Vos, D. E.. Hofkens, J.. Roeffaers, M. B. J. Fluorescence micro(spectro)scopy as a tool to study catalytic materials in action. *Chemical Society reviews.* 2010, *39*, 4703–17.

(121) Roeffaers, M. B. J.. Sels, B. F.. Uji-I, H.. De Schryver, F. C.. Jacobs, P. a. De Vos, D. E.. Hofkens, J. Spatially resolved observation of crystal-face-dependent catalysis by single turnover counting. *Nature* 2006, *439*, 572–5.

(122) Xu, W.. Kong, J. S.. Yeh, Y.-T. E.. Chen, P. Single-molecule nanocatalysis reveals heterogeneous reaction pathways and catalytic dynamics. *Nature materials.* 2008, *7*, 992–6.

(123) Zürner, A.. Kirstein, J.. Döblinger, M.. Bräuchle, C.. Bein, T. Visualizing single-molecule diffusion in mesoporous materials. *Nature.* 2007, *450*, 705–8.

(124) Jung, C.. Kirstein, J.. Platschek, B.. Bein, T.. Budde, M.. Frank, I.. Müllen, K.. Michaelis, J.. Bräuchle, C. Diffusion of oriented single molecules with switchable mobility in networks of long unidimensional nanochannels. *Journal of the American Chemical Society.* 2008, *130*, 1638–48.

(125) Kirstein, J.. Platschek, B.. Jung, C.. Brown, R.. Bein, T.. Bräuchle, C. Exploration of nanostructured channel systems with single-molecule probes. *Nature materials.* 2007, *6*, 303–10.

(126) O'Connor, N.. Silver, R. Ratio Imaging: Practical Considerations for Measuring Intracellular Ca^{2+} and pH in Living Cells. *Methods in cell biology.* 2007.

(127) Bright, G.. Fisher, G. Fluorescence ratio imaging microscopy. *Methods Cell Biol.* 1989.

(128) Whitaker, J. E.. Haugland, R. P.. Prendergast, F. G. Spectral and photophysical studies of benzo[c]xanthene dyes: dual emission pH sensors. *Analytical biochemistry.* 1991, *194*, 330–44.

(129) Babcock, G.. Callahan, P. Redox-linked hydrogen bond strength changes in cytochrome a: implications for a cytochrome oxidase proton pump. *Biochemistry.* 1983.

(130) Grynkiewicz, G.. Poenie, M.. Tsien, R. A new generation of Ca2+ indicators with greatly improved fluorescence properties. *Journal of Biological Chemistry.* 1985.

(131) Beale, A.. Jacques, S. Tomographic energy dispersive diffraction imaging as a tool to profile in three dimensions the distribution and composition of metal oxide species in catalyst bodies. *Angewandte Chemie International Edition.* 2007.

(132) Roeffaers, M.. Sels, B.. Uji‐i, H. Space‐and Time‐Resolved Visualization of Acid Catalysis in ZSM‐5 Crystals by Fluorescence Microscopy. *Angewandte.* 2007.

Chapter 2 - Sample Preparation and Experimental Setup

2.1 Preparation of C-SNARF-1 doped phosphate bulk solutions for conventional spectra study by a fluorimeter

The dye molecule in this study is a pH sensitive dye ((5' and 6')-carboxy-10-(dimethylamino)-3-hydroxy-spiro[7H-benzo-[c]xanthene-7,1'(3H)-isobenzofuran]-3'-one (C-SNARF-1). It was purchased from Invitrogen and used to prepare a 22 μM stock solution in absolute ethanol and HPLC grade water. The C-SNARF-1 stock solution was diluted to 200 nM, 10nM, and 1nM in water. C-SNARF-1 possesses several functional groups that can be protonated and deprotonated through dynamic equilibriums. In order to understand the pH response of C-SNARF-1, its fluorescence behavior was firstly studied in aqueous phosphate solutions by bulk spectroscopic experiments. These solutions were also used for controlling the acidic properties in the silica thin films. These samples provided the pH response of C-SNARF-1 in a solid network at the single molecule level.

Phosphate salt was purchased in Sigma-Aldrich. For the bulk solution studies, 0.1 mM solutions doped with 100 nM dye molecules were prepared in deionized water. The solutions were titrated with 0.1 mM hydrochloride (HCl) solution and 0.1 mM sodium hydroxide (NaOH) solution to different pH values, ranging from pH 1 to pH 8. For the acidity controlling in silica thin films, no dye molecule is doped.

2.2 Preparation of silica and amorphous silica-alumina thin films

The amorphous silica-alumina thin films were prepared by a sol-gel approach. The synthesis was developed from a procedure reported by B. E. Yoldas[1] for preparation of gels, glass and ceramic materials. The precursors are metal alkoxides., Tetramethyl orthosilicate (TMOS) was used as the silicon source and aluminum alkoxides for the aluminum source. The sol-gel process is superior to other synthesis methods in its ability to ensure molecular level mixing of different components. This is a very important characteristic since the excess charge caused by the of Al-O-Si bonds is the key for the formation of acid sites in amorphous silica-alumina.[2] Mizukami et al.[3] found that the Al-O-Si bonds could be formed more efficiently in the sol-gel silica-alumina compared with those synthesized by other methods. A sol-gel process is very convenient since a simple reactor is needed for the synthesis. To prepare samples, a

homogeneous solution is formed first by the hydrolysis of metal alkoxides, followed by condensation, drying and calcination. The Al/Si ratio can be strictly controlled by mixing different amount of the precursors with high purity. Bulk samples, including thin films and fibers, can be obtained by the sol-gel process.[4] A chelating agent ethylacetoacetate (EAA) was used to better solvate aluminum alkoxide. The chelation process is shown in Figure 2.1. The chelated product was like new molecular precursors, which could be co-condensed with hydrolyzed silicic acid ($Si(OH)_4$)[5]. Before spin casting the sols on to the cover slip, a surfactant (cetyltrimethylammonium bromide (CTAB)) was added in order to generate mesoporous structures and increase the surface area.

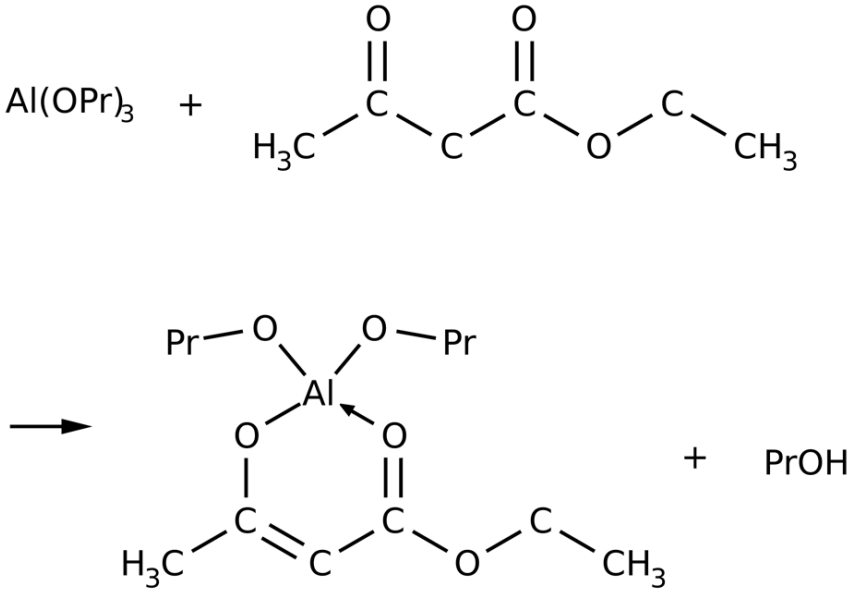

Figure 2.1 The chelation reaction of aluminum isopropoxide with the chelating agent ethylacetoacetate (EAA).

2.2.1 As-synthesized Films

Pure silica samples

Acid-catalyzed hydrolysis and condensation starts immediately after the pure silica sols were prepared by mixing tetramethyl orthosilicate (TMOS), absolute ethanol (EtOH), water, hydrochloric acid (HCl) and a stoichiometric amount of EAA. The mixture was stirred at room

temperature vigorously for 1 hour on a magnetic stir plate. It was then allowed to stand overnight at room temperature. 0.024g Cetyltrimethylammonium bromide (CTAB, Aldrich) was added to 2 ml of sol. The new mixture was vigorously stirred for 1 hour at room temperature. The sol was then deposited on the cover slip (FisherFinest Premium) by spin casting. The spin rate was typically at around 5000 rpm for 30 s. The wet films were let sit over night in a desiccator.

Silica-alumina samples

Silica-alumina samples were prepared by co-condensation of separately pre-hydrolyzed precursor sols. The silica sol was prepared as described above. For the alumina sol, hydrolysis of aluminium isopropoxide in HPLC grade isopropanol was performed in the presence of ethyl acetoacetate (EAA) as a chelating agent, and stoichiometric quantities of water in relation to the number of alkoxide groups. In cases where a precipitate formed, a small amount of concentrated nitric acid was added to obtain a clear sol. This solution was stirred for 2 hours at the room temperature. A series of silica-alumina sols were then obtained by mixing appropriate amounts of the pre-hydrolyzed solutions.

2.2.2 Calcined Films

Surfactant, solvent and acid catalyst (HCl) were removed by calcination in a temperature programmed muffle furnace, ruling out their influence on the acidity in the films. In this process, the temperature was first ramped at 1 °C/min from room temperature to 110 °C where it was held for 90 minutes. The temperature was then increased to 500 °C at a ramp rate of 1 °C /min, where it was held for 5 hours. The temperature finally decreased to room temperature at a rate of 1 °C /min. During the calcination, an air pump is used to flow air into the muffle furnace to avoid char or tar formation from the decomposition of organic molecules. After cooling, the films were cleaned in an air plasma cleaner (Harrick Plasma) for 5 minutes to remove luminescent residues. The final thickness of the films was measured to be 30 ± 3nm by spectroscopic ellipsometry.

Since the calcination process would decompose the organic molecules. Dye was loaded to the pure silica as well as the silica-alumina samples after synthesis. The calcined films were loaded with C-SNARF-1 molecules by spin casting a 0.5 nM solution.

2.2.4 Buffered Thin Films

Pure silica films were used to explore the pH-dependent response of C-SNARF-1 in thin films. These samples were prepared by the acid catalyzed sol-gel method described above. The films were subsequently exposed to 0.1 mM phosphate solutions with pH values ranging from 1 to 8 for overnight. This time scale is sufficiently long for the microenvironments in the films to equilibrate with the treatment solutions.[6] The films were rinsed with a small amount of water and dried under a stream of nitrogen, and subsequently loaded with dye at nanomolar concentration by spin casting, as described above.

2.3 Instrumentation

2.2.1 Single molecule setup

All SM studies were conducted on an existing wide-field fluorescence microscope. This system is built on an inverted epi-illumination microscope (Nikon TiE). A schematic drawing of the microscope is illustrated in Figure 2.1. Light from a Nd:YVO4 laser (Coherent, Verdi, 532nm) was used to excite the dye molecules. The incident laser power was maintained between 0.75 and 1.5 mW. It was first focused into a spinning optical diffuser and then collected and passed through a polarization scrambler before being directed into the epi-illumination port of the microscope. The light was reflected from a dichroic beam splitter (Chroma Q555LP) and focused into the back aperture of an oil immersion objective (Nikon Apo TIRF 100X, 1.49 N.A.). Fluorescence from the sample was collected and separated from the incident laser light by passing back through the beam splitter and a 550 nm long pass filter. The fluorescent signal was subsequently directed into an image splitter (Cairn Research, OptoSplit II), where it was further split by a second dichroic beam splitter (Chroma, 610dcxr). The two signal beams were individually directed through two band-pass filters: one centered at 580 nm, the other at 640 nm, both having 40 nm passbands, and then simultaneously detected by a back-illuminated EM-CCD camera (Andor iXon DU-897).

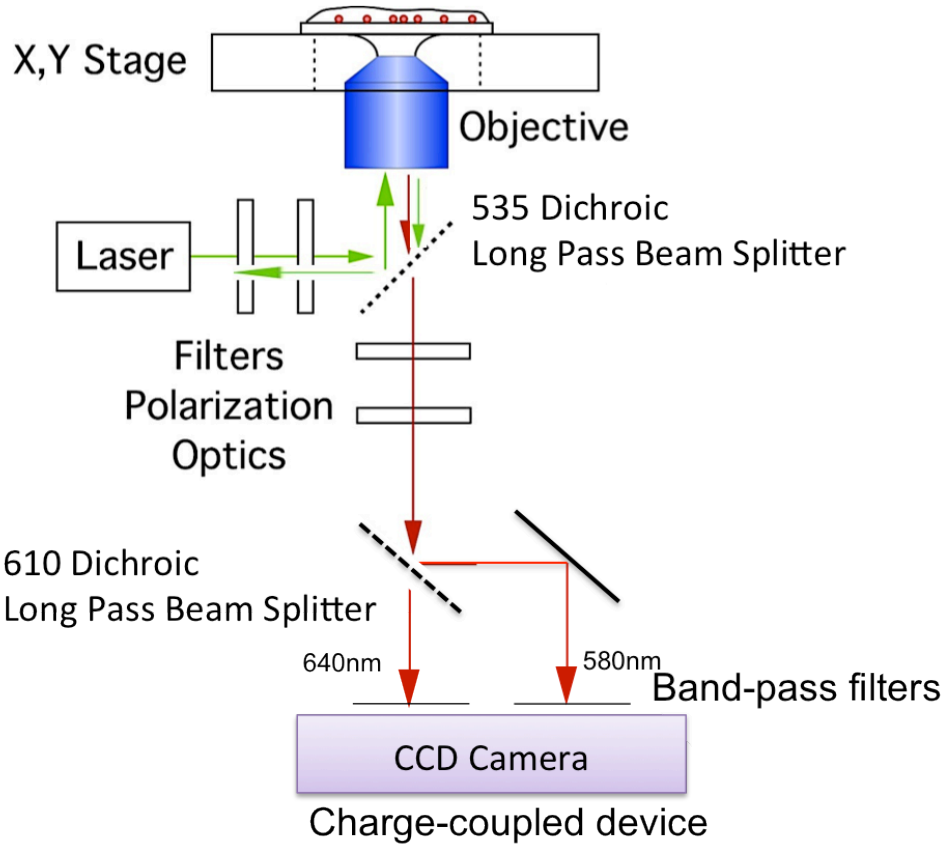

Figure 2.2 A schematic drawing of the configuration of the wide field microscope. Optical parts include optical fibers, lenses, flipper mirrors, beamsplitters, bandpass filters, longpass filter and waveplates.

2.2.2 Fluorometer

A commercial fluorometer (Fluoromax, Spex) was used to study the pH sensitive behaviors of C-SNARF-1 in the aqueous solutions. An excitation light, centered at 532 nm was used to stimulate the fluorophores. Both the excitation and the emission slit widths were set to 3 nm. The scan range was from 550 nm to 700 nm with 1 nm increment and 0.1 s in integration per data point. The 100 nM C-SNARF-1 phosphate solutions with pH ranging from 1 to 8 were examined. Spectra of the samples were collected. Distilled water was used as the background. The experiment was performed at room temperatures.

2.3 Data analysis

The individual, well-separated dye molecules appeared as well-defined pairs of spots in two images recorded simultaneously by the back-illuminated EM-CCD camera. A software package written in house (based on the National Instruments Labview platform) was used to recognize and locate the individual spot pairs. The profiles of spots were fitted to two-dimensional Gaussian functions. The amplitudes of the Gaussian fits were used to determine the intensity ratio of the spot pairs and the intensity ratio, R, could be obtained for each fluorescent dye molecule.

Reference

(1) Yoldas, B. Preparation of glasses and ceramics from metal-organic compounds. *Journal of Materials Science.* 1977.

(2) Yabuki, M.. Takahashi, R.. Sato, S. Silica–alumina catalysts prepared in sol–gel process of TEOS with organic additives. *Physical Chemistry Chemical Physics.* 2002.

(3) Mizukami, F.. Kiyozumi, Y.. Sano, T.. Niwa, S.. Toba, M. Effect of Solvent Diols and Ligands on the Properties of Sol-Gel. 1998, *1031*, 1027–1031.

(4) Dunn, B.. Zink, J. Optical properties of sol–gel glasses doped with organic molecules. *J. Mater. Chem.*. 1991.

(5) R Nass, H. S. Synthesis of an alumina coating from chelated aluminium alkoxides.

(6) Fu, Y.. Collinson, M. M.. Higgins, D. a Single-molecule spectroscopy studies of microenvironmental acidity in silicate thin films. *Journal of the American Chemical Society*. 2004, *126*, 13838–44.

Chapter 3 - Single Molecule Studies of Acidity Distributions in Mesoporous Silica-Alumina Thin Films

3.1 Introduction

It is widely acknowledged that catalysts play a vital role in modern industry.[1,2] It is estimated that more than 80% of all chemicals have to interact with at least one catalytic material during their manufacturing processes.[3,4] Compared to homogeneous systems, solid catalysts could help to reduce the environmental impact of chemical synthesis because these systems can replace hazardous mineral acids and eliminate a separation step to recover the catalyst.[5,6] To develop more clean pathways, heterogeneous analogs of the most commonly used homogeneous catalysts must be implemented.[7] The Brønsted acidity of aluminosilicate (Al-Si) materials, such as zeolites and amorphous silica-aluminas, makes them suitable for use as solid acid catalysts in several petrochemical processes, including hydrocracking, isomerization and oligomerization of alkenes and alkylate aromatics and other important reactions.[8–11] The insertion of tetrahedral Al atoms into the silica matrix gives rise to catalytically active sites because of the compensation of the resulting extra negative charge by a proton.[12,13] This Al-for-Si substitution model was proposed by Thomas[14]and Tamele[15] to explain the acidity Al containing materials.

Many approaches have been used to study the acidity properties of Al-Si materials. Temperature-programmed desorption (TPD) and FTIR are frequently used to measure their acidity by probing interactions between their intrinsic acid sites and weak bases (e.g., ammonia and pyridine) to which they are exposed.[16–19] NMR spectroscopy (i.e., 1H MAS, magic angle spinning) has also been employed to study the number and strength of Brønsted acid sites in solid acid catalysts.[16,17] Classical titration measurements have also been reported.[20] These techniques all provide valuable data on average materials acidity at the ensemble level. However, few microenvironments in these materials are likely to possess average properties. Rather, their acidity properties are more likely to vary widely between different sites. The exact local properties of these individual microenvironments govern the physical and chemical interactions between guest molecules and the solid matrix necessary for efficient catalysis.[17] Therefore, new methodologies are needed to probe the distribution of microenvironment acidity in heterogeneous catalysts.

Recently, single molecule (SM) fluorescence microscopy has been implemented in a number of catalyst studies because of its high temporal and spatial resolution.[7,21] Valuable information can be extracted by analyzing the fluorescence intensity, spectrum and polarization[22,23] of guest molecules interacting with a catalyst medium. SM methods can also provide information on structural heterogeneities,[24,25] reaction pathways,[26] catalyst kinetics[24] and catalytic dynamics[27] in solid materials. While pH sensitive dyes have been used to study acidity in a variety of media, including biological systems,[28,29] and agarose gels.[30] In previous work from the Higgins group,[31,32] the pH sensitive dye ((5' and 6')-carboxy-10-(dimethylamino)-3-hydroxy-spiro[7H-benzo-[c]xanthene-7,1'(3H)-isobenzofuran]-3'-one, C.SNARF-1) was used to explore the local acidity properties of pure SiO2 films that had been exposed to solutions of different pH.[33] The results showed that the C-SNARF-1 single molecules were sensitive to the local pH, as determined by the solutions and by surface SiOH groups incorporated in the materials. To our knowledge, SM methods have not yet been used to probe microenvironment acidity in common solid catalyst materials.

Ideally, the proper dye molecule for SM studies of materials acidity should exhibit clear and well-defined changes in its emission spectrum with pH. C-SNARF-1 is a dual emission probe, yielding fluorescence in two bands centered at 580 nm and 640 nm. The ratio of fluorescence emission in these two bands changes with pH in bulk solution and thus provides a means to study the local pH in close proximity to a dye molecule in solid materials.[34,35] C-SNARF-1 is most commonly employed to probe pH near (i.e., within 1-2 pH units) the pKa of the first protonation process (pKa ~ 7.6)[36] shown in Figure 3.1a. In this range, the emission ratio $R=I_{580}/I_{640}$ shows a dramatic increase with decreasing pH. However, C-SNARF-1 also shows a more subtle response at lower pH, due to a second protonation process indicated in Figure 3.1b, that can be used to probe the properties of much more acidic environments.

In this work, we study the acidity properties of individual microenvironments found within mesoporous silica-alumina thin films by SM methods. These materials serve as effective models for amorphous silica-alumina solid acid catalysts. C-SNARF-1 is employed as the probe molecule in these studies. Its pH-dependent emission properties are first explored at low pH (i.e pH < 4) in solution and in mesoporous films, prior to implementation in SM studies of mesoporous silica-alumina thin films. In all SM studies, the dye is immobilized in the matrix at nanomolar concentrations so that the spatially well-separated single molecules can be located

and their spectral emission characteristics determined. A wide-field fluorescence microscope is employed to collect dual color fluorescence images (for emission near 580 nm and 640 nm) of 15 to 20 20 x 20 μm^2 regions in each sample. The pairs of fluorescent spots produced by each molecule are fit to Gaussian functions to determine their emission ratios ($R=I_{580}/I_{640}$). Histograms of the emission ratios are then employed to obtain acidity distribution information. The shape, width and peak position of each histogram is assessed. These data show clear changes as a function of the level of Al doping in each silica-alumina thin film. The results are interpreted to reflect a clear trend towards incorporation of more acidic microenvironments with increasing Al content.

3.2 Experimental section

3.2.1 Sample preparation

C-SNARF-1 was purchased from Invitrogen and diluted to prepare a stock solution in absolute ethanol and HPLC grade water. Silica-alumina thin film samples were prepared by co-condensation of separately pre-hydrolyzed precursor sols.[37–39] For the alumina sol, hydrolysis of aluminium isopropoxide in isopropanol was performed in the presence of ethyl acetoacetate (EAA) as a chelating agent, and stoichiometric quantities of water in relation to the number of alkoxide groups. In cases where a precipitate formed, a small amount of concentrated nitric acid was added to obtain a clear sol. This solution was stirred for 2 hours. Silica sols were prepared by mixing tetramethyl orthosilicate, absolute ethanol, water, hydrochloric acid and a stoichiometric amount of EAA. The mixture was stirred at room temperature for 1 hour. A series of silica-alumina sols were then obtained by mixing appropriate amounts of the pre-hydrolyzed solutions. These sols were stirred for 1 hour and allowed to stand overnight. 0.024 grams of Cetyltrimethylammonium bromide (CTAB, Aldrich) was then dissolved in the 2ml solutions by stirring for 1 hour. The co-condensed sols were spin cast onto glass microscope coverslips (FisherFinest Premium) to obtain mesoporous thin films. These samples were stored in a desiccator overnight. Surfactant, solvent and acid catalyst were removed by calcination, ruling out their influence on the acidity in the films. In this process, the films were first heated at 110 °C for 90 minutes. The temperature was then increased to 500 °C at a ramp rate of 1 °C /min, where it was held for 5 hours. After cooling, the films were cleaned in an air plasma cleaner (Harrick Plasma) for 5 minutes to remove luminescent residues. The calcined films were then

loaded with probe molecules by spin casting a 0.5 nM C-SNARF solution. The final thickness of the films was measured to be 30 ± 3nm by spectroscopic ellipsometry.

Pure silica films were used to explore the pH-dependent response of C-SNARF-1 in thin films. These samples were prepared by the acid catalyzed sol gel method described above. The films were subsequently exposed to 0.1 mM phosphate solutions with pH values ranging from 1 to 8 for overnight. This time scale is sufficiently long for the microenvironments in the films to equilibrate with the treatment solutions.[40] The films were rinsed with a small amount of water and dried under a stream of nitrogen, and subsequently loaded with dye by spin casting, as described above.

3.2.2 Instrumentation and method

All SM studies were conducted on an existing wide-field fluorescence microscope.[41,42] This system is built on an inverted epi-illumination microscope (Nikon TiE). Light from a Nd:YVO4 laser (Coherent, Verdi, 532nm) was used to excite the dye molecules. The incident laser power was maintained between 0.75 and 1.5 mW. It was first focused into a spinning optical diffuser and then collected and passed through a polarization scrambler before being directed into the epi-illumination port of the microscope. The light was reflected from a dichroic beam splitter (Chroma Q555LP) and focused into the back aperture of an oil immersion objective (Nikon Apo TIRF 100X, 1.49 N.A.). Fluorescence from the sample was collected and separated from the incident laser light by passing back through the beam splitter and a 550 nm long pass filter. The fluorescent signal was subsequently directed into an image splitter (Cairn Research, OptoSplit II), where it was further split by a second dichroic beam splitter (Chroma, 610dcxr). The two signal beams were individually directed through two band-pass filters: one centered at 580 nm, the other at 640 nm, both having 40 nm passbands, and then simultaneously detected by a back-illuminated EM-CCD camera (Andor iXon DU-897). The individual, well-separated dye molecules appeared as well-defined pairs of spots in two images positioned side-by-side on the camera. A software package written in house (based on the National Instruments Labview platform) was used to locate the individual spot pairs and to fit their profiles to Gaussian functions. The amplitudes of the Gaussian fits were used to determine the desired intensity ratio, R, for each fluorescent molecule.

3.3 Result and discussion

3.3.1 Bulk pH studies of C-SNARF-1 in aqueous solutions.

The probe molecule selected for assessing the local pH within the alumina-doped silica films was C-SNARF-1 (see chemical structure in Figure 3.1). C-SNARF-1 is commonly used to probe the pH of solutions around the pH of its first protonation equilibrium (pKa ~ 7.6). In this work, we sought to employ its response in lower-pH environments to monitor the acidity in silica films. This required careful, quantitative investigations of its response in a pH range (pH < 5) where it is typically not employed. The pH response of C-SNARF-1 was first studied in aqueous solutions with varying pH values, using a conventional fluorimeter. The C-SNARF-1 fluorescence spectrum is comprised of two dominant emission bands centered at 580 nm and 640 nm. The intensity ratio, R ($R = I_{580}/I_{640}$), changes with pH and provides a way to assess the acidity of the surrounding medium. To characterize the pH response of C-SNARF-1, we recorded its fluorescence sprectra in a series of solutions with pH ranging from 1 to 10. These spectra are shown in Figure 3.2. A plot of R as a function of pH is plotted and the two pH ranges in which C-SNARF-1 is most sensitive to changes in the local pH are identified in Figure 3.3. From pH 5 to 10, R decreased with increasing pH, in agreement with the results of previous studies in Higgins's group.[32,43] However, in the low pH range, from pH 4 to 1, R decreased with a decrease in pH. The spectral response of C-SNARF-1 in the low pH range arises from a second acid-base equilibrium shown in Figure 3.1b. It is likely that the benzoic acid groups, having pKa of ~ 4.2, are protonated over this pH range. The clear response of C-SNARF-1 in the low pH range is important, because it allows for the acidity properties of acidic catalyst networks to be explored. These results demonstrate the potential for using C-SNARF-1 to study solid acid matrices.

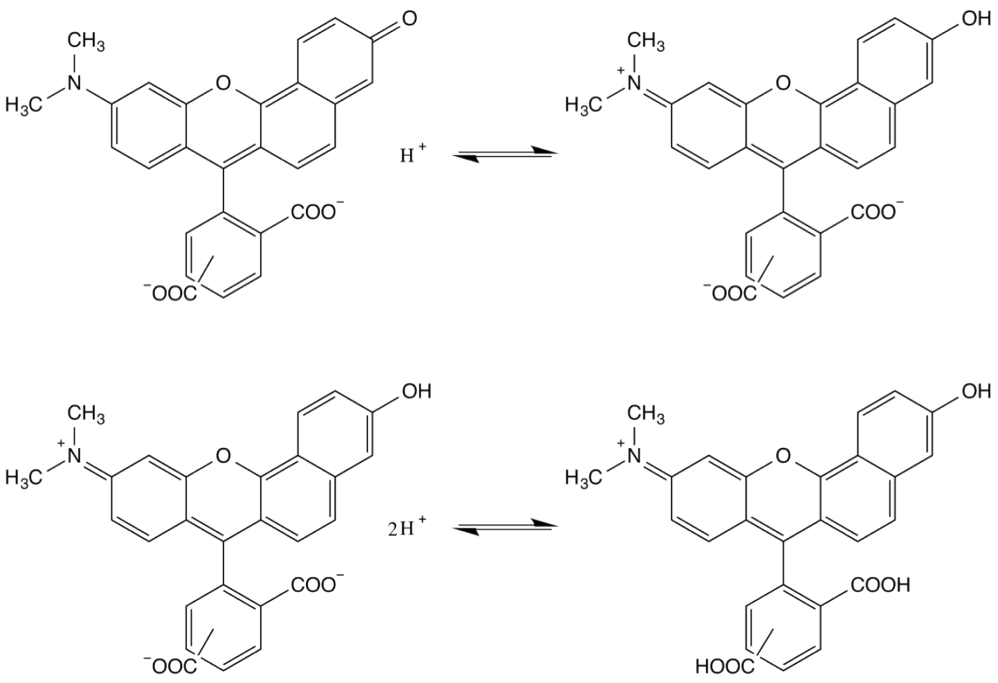

Figure 3.1 Chemical structures of C-SNARF-1 in its protonated and deprotonated forms around the pH at (a) Structure of the first acid-base equilibrium (pKa ~ 7.6) and (b) Structure of the second acid-base equilibrium (pKa ~ 4.2).

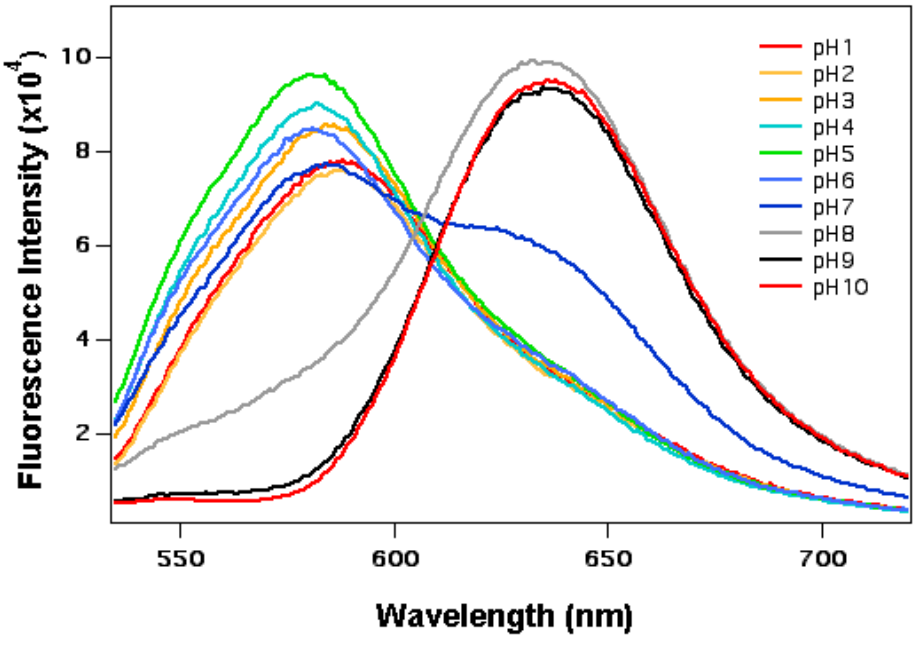

Figure 3.2 Spectral data for C-SNARF-1 in aqueous solutions of pH ranging from 1 to 10. These data were obtained using a conventional fluorimeter.

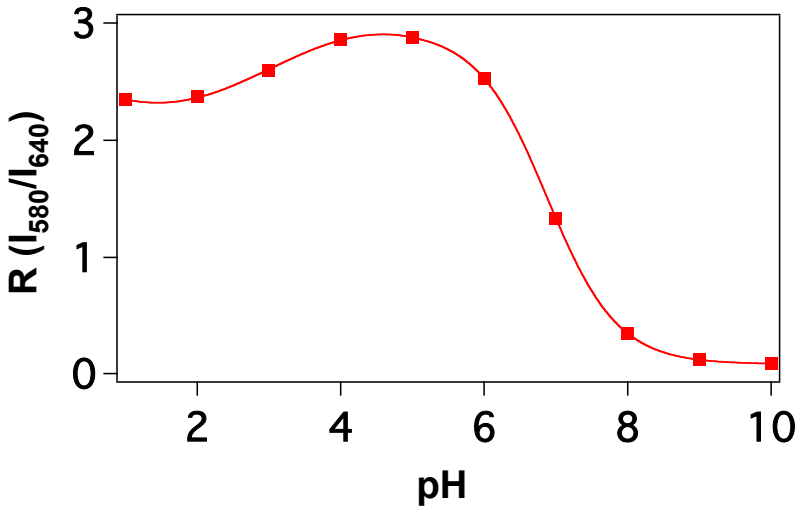

Figure 3.3 C-SNARF-1 emission ration, R, (obtained from the data in Figure 2) as a function of pH for solutions ranging from pH 1 to 10. The solid line was used to connect the data points.

3.3.2 C-SNARF-1 pH response in thin films at the single molecule level.

Pure silica films were prepared and treated overnight with phosphate solutions of varying pH values (from pH 1 to pH 8). Dye molecules (0.5 nanomolar concentration) were loaded into the films by spin coating. The films were then imaged on the wide field fluorescence microscope. The intensity ratios of the fluorescent spots produced in the two detection channels (580 nm and 640 nm) were obtained. Figure 3.4a and Figure 3.4b depict a pair of representative images obtained. The two images were recorded simultaneously by the CCD camera and were of the exact same coordinates. Each individual dye molecule in the film appears in both images as bright spots because of the dual emission of C-SNARF-1. As is shown in the figure, the dye molecules were well dispersed onto the thin films, interacting with the local environment. The resolution of the fluorescence microscope is limited by the wavelength (532 nm) of the laser used to excite the dye molecules. Equation 1 is used to quantitatively estimate the resolution which gives a value of ~ 217 nm. This value indicates the distance required to resolve the fluorescent molecules and the precision of locating an individual molecule. The dye molecules were doped at 0.5 nM level and they appeared to be well-separated spots in the images. The distance between the molecules was at ~ 600 nm length scale (1 pixel in the image represents

125 nm) and different intensity ratios indicated the spatial variation of the acidity in the silicate thin films.

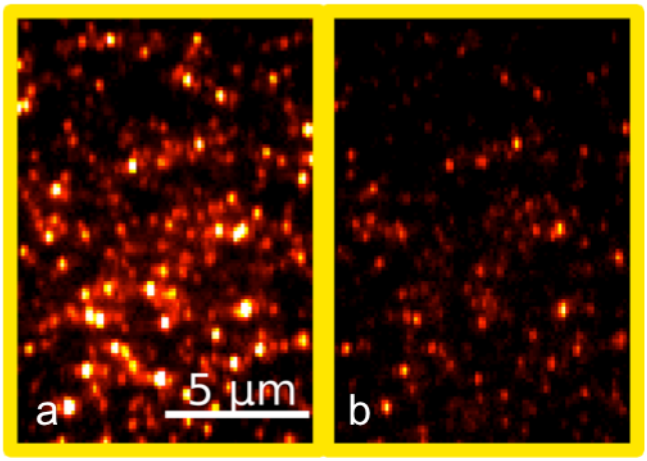

Figure 3.4 A pair of representative images of C-SNARF-1 in silica thin films treated by phosphate aqueous solutions. (a) Image collected by the 580 nm channel with a bandwidth of 40 nm and (b) Image collected by the 640 nm channel. They were obtained simultaneously for a single sample region. The left and right panels in (a) and (b) are displayed on identical intensity scales.

Histograms of the R values obtained from individual molecules in each sample are plotted in Figure 3.5. These histograms depict the acidity distributions for the nanoscale environments within each film. It can be seen that the treated films are heterogeneous with distinct distributions in each of them. Since all the histograms were positively skewed, the most common pH value of individual microenvironments was found to be different from the mean pH in the solid acid network. Each histogram was fitted to a Gaussian function to obtain information that could be interpreted to the film acidity and the dye behaviors. The peak position was used to represent the most common pH value, which was mainly influenced by the buffer solutions. From pH 1 to 5, the peak position shift to bigger values of R with an increase of pH while from pH 5 to 9, the trend was the opposite. This observation agreed with that observed in the bulk solution studies, indicating that it is possible to use C-SNARF-1 to probe the acidity of a solid matrix, at the single molecule level.

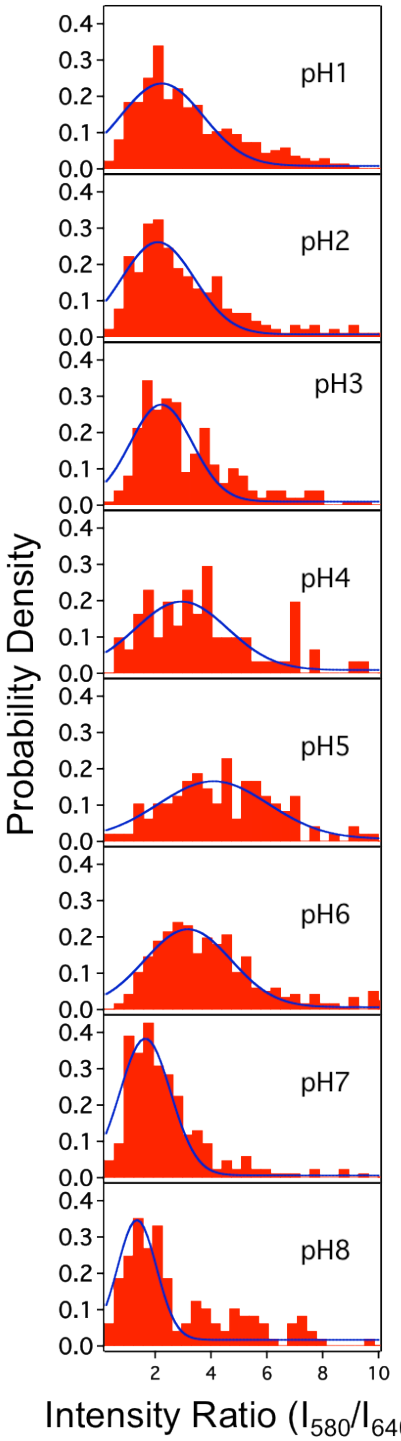

Figure 3.5 Density histograms of intensity ratio *R* (*R* = I_{580} / I_{640}) in silicate thin films treated with phosphate solutions ranging from pH 1 to pH 8. The histograms were fitted to Gaussian functions. The peak positions represent the most common pH of the microenvironments in a sample. The peak widths represent the heterogeneity in the solid matrices. (Bar height × Bin size = Probability for the range).

The width obtained from the histogram also provided interesting information about the silica framework and the behavior of C-SNARF-1. The fluorimeter study revealed that when the pH was around 4 and 7, the molecule was the most sensitive to pH variations. The R value would change a lot when the pH changed slightly in these two regions. The increased sensitivity of the dye in this region is expected to lead to wider histograms from the single molecule results. However, at pH 7, we observed a narrow peak rather than a wide one. Similar results were reported in previous studies from our group.[42] This unexpected narrowing of the distribution was attributed to buffering of the nanoscale pH by surface –SiOH groups, which have a pKa near 7.5.[44] In this region, the pH distribution in the thin film was the most homogeneous. At pH 4, the peak was relatively wide but the widest peak appeared at pH 5. The narrowing of the peak near pH 4 is again attributed to the buffering effect of surface –SiOH groups. A small population of –SiOH sites are expected to have a pKa of around 4 as described by Eisenthal and coworkers.[45] The single molecule fluorescence studies of the silica films exposed to environments with different pH suggest that two competing factors influence the correlation between intensity ratio and pH: the sensitivity of C-SNARF-1 tends to broaden the peak while the buffering effect of two types of –SiOH groups tends to narrow the peak.

3.3.3 Acidity properties of mesoporous Si-Al composite films probed by single molecule fluorescent spectroscopic methods

The Al-Si composite films were prepared with 0% to 20% (molar ratio) alumina dopants. The C-SNARF-1 dye molecules were incorporated into these films as described above. The imaging method and data analysis procedure were the same as the pH film study. Figure 3.6a is a pair of representative images of the pure silicate film sample and Figure 3.6b represents the 20% Al film sample. The shape of the spots resembles the ones in the solution-treated sample images shown in Figure 3.4. The dye molecules were doped at the same level but few spots appeared in the alumina doped samples. This is because the negatively charged surface of the films repelled the dye molecules when alumina was doped into to pure silica framework. The net negative charge arose when the oxygen anions were shared between Si^{4+} and Al^{3+} since Al^{3+} was present in tetrahedral coordination with oxygen.[46] When exposed to aqueous environments(the moisture was provided by the solution during the loading of dye molecules), protons came to compensate the net charge and give rise to Brønsted acidity in the alumina doped film samples.

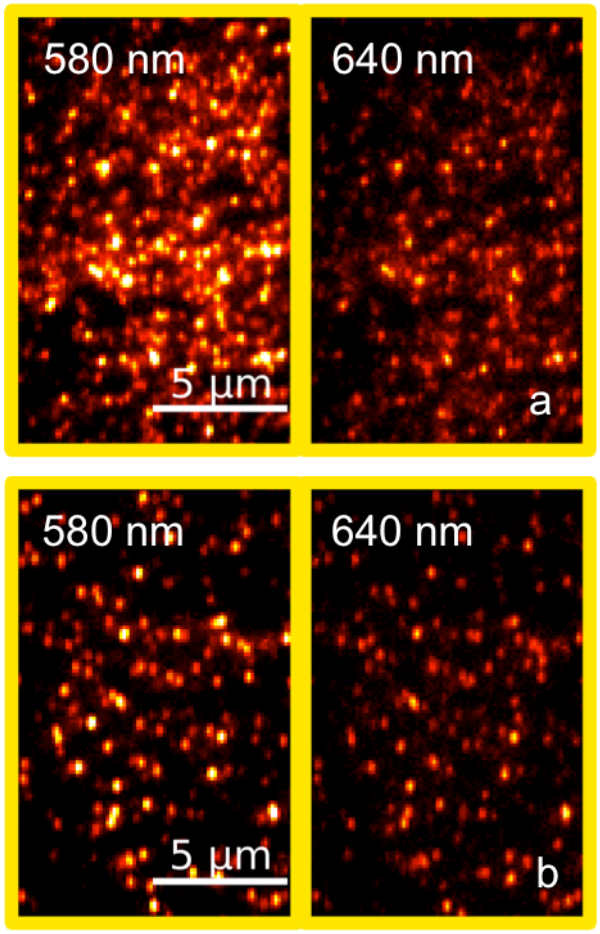

Figure 3.6 Representative images of the a) pure silicate film sample and b) the 20% Al film sample. The shape of the spots resembles the ones in the solution-treated sample images shown in Figure 3.4.

The histograms of intensity ratios were obtained for each film and were fitted to double Gaussian functions (in Figure 3.7). A more complicated fitting procedure was employed here because the histogram data appeared to depict the presence of at least two distinct environments in the samples doped with Al. Specifically, a new shoulder peak at higher intensity ratios (in the tail part of the histogram) was observed in the presence of Al dopant.

Undoped silica (i.e., 0% Al) was found to yield the least acidic microenvironments in this study, and the acidity was influenced by the two types of Si–OH groups with pKas around 7.5 and 4 in the pH film study. Introducing tetrahedral Al atoms into the films should decrease the pKa because of the inducing effect of the negatively charged Al atoms into the silica framework.[8,47] The observation of a new peak (constitute with fluorescence spots with larger R

values) in the single molecule histogram data obtained from the Al-doped films is indicative of an increase in their acidity. By comparison of these results with the pH film data, the shape and the intensity ratio (3.0 to 4.4) of the second peak indicates this population had a pH value of around 4 and 5. In the histogram obtained from the 0% Al sample, the tail in this range was small, indicating that the population of microenvironments with pH 4 was small. When Al was added, however, the second peak started to appear, suggesting that the doping of Al created more microenvironments with pH around 4.5.

Figure 3.8 is the plot of the position of the predominant peaks shifting with different amount of the Al doping. The predominant peak in the 0% Al samples was mainly attributed to pKa 7.5 –SiOH groups. Upon incorporation of Al dopant sites, the center of this peak shifted to smaller values of R representing either pH values greater than 7 or smaller than 4 according to the trend predicted by both fluorimeter and film pH studies. It was reported in the literature that in Si rich systems (Si/Al > 3), the presence of Al sites increases the Brønsted acidity of the matrix. So the trend can best be explained by attributing the shift in R to surface sites with pH values smaller than 3. The shift of the average of the major peak to smaller values of R indicated that the number of microenvironments with pH values smaller than 3 increased with more Al doping and these sites might originate from pka 4.5 –SiOH groups.

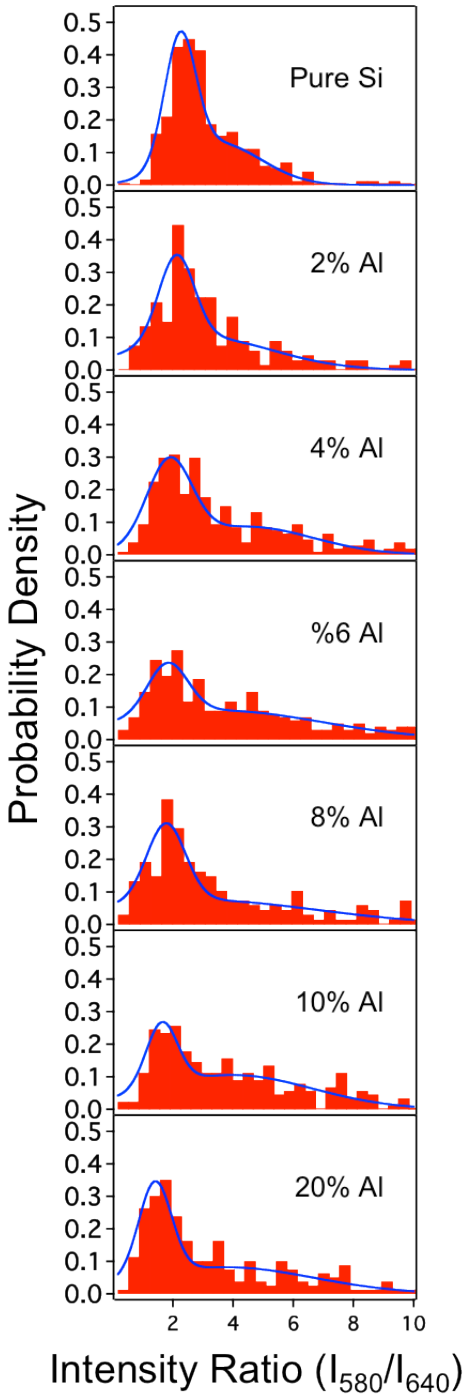

Figure 3.7 Density histograms of intensity ratio *R* (*R* = I_{580} / I_{640}) in aluminosilicate thin films. The histograms were fitted to double Gaussian functions since shoulder peaks appeared in the aluminum doped samples.

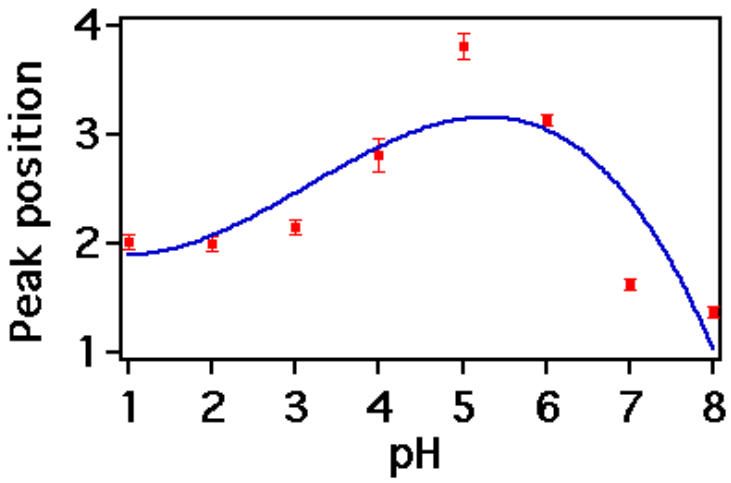

Figure 3.8 Plot of the predominant peak position as a function of Al doping. When the Al content increases, the predominant peak is shifting from large to small values of R.

3.3 Conclusion

Single-molecule fluorescence spectroscopic methods have been employed to investigate the microenvironmental acidity distributions in mesoporous aluminosilicate thin films that serve as models for solid acid catalysts. C-SNARF-1 was shown to be an effective probe of the local pH in media of low pH (i.e., $1 < pH < 4$). Histograms of the emission intensity ratios of C-SNARF-1 single molecules were used to access the acidity distributions in mesoporous silica films treated under solutions of different pH and for Al-Si films of varying Al content. Studies of the solution-treated silica films revealed the pH dependent response of C-SNARF-1 in solid materials and also provided data on the heterogeneity of the microenvironments found in these materials. The acidity properties of the microenvironments were found to be most homogeneous when treated with solutions of pH near the known pKas of incorporated silanol sites. In aluminosilicate thin films, the SM data revealed an increase in film acidity with increasing Al content. The results were interpreted to depict an initial increase in microenvironments having pH values around 4-5, with a subsequent shift to environments having $pH < 3$, as the Al content was increased to 20%. The distributions obtained were extremely broad, depicting a high degree of heterogeneity in the acidity properties of these films.

This work provides important new information on the distribution of Brønsted acidity in solid acids that cannot be obtained by conventional techniques. It demonstrates that SM methods can be used to characterize the heterogeneity of solid acid catalysts.

Reference

(1) Second, C.. Ertl, G.. Knözinger, H.. Schüth, F. Handbook of Heterogeneous Catalysis. **2008**.

(2) Hagen, J. *Industrial Catalysis: A Practical Approach (Google eBook)*. John Wiley & Sons, 2006. p. 525.

(3) Rase, H. *Handbook of commercial catalysts: heterogeneous catalysts*. 2000.

(4) Anderson, J.. Garcia, M. *Supported metals in catalysis*. 2005.

(5) Niemantsverdriet, J. *Spectroscopy in catalysis*. 2007.

(6) Principles and Practice of Heterogeneous Catalysis http://tocs.ulb.tu-darmstadt.de/18209491X.pdf (accessed Jul 3, 2013).

(7) Weckhuysen, B. M. Chemical imaging of spatial heterogeneities in catalytic solids at different length and time scales. *Angewandte Chemie (International ed. in English)* **2009**, *48*, 4910–43.

(8) Poduval, D. G.. van Veen, J. a R.. Rigutto, M. S.. Hensen, E. J. M. Brønsted acid sites of zeolitic strength in amorphous silica-alumina. *Chemical communications (Cambridge, England)* **2010**, *46*, 3466–8.

(9) Corma Inorganic Solid Acids and Their Use in Acid-Catalyzed Hydrocarbon Reactions. **1995**.

(10) Scherzer, J.. Gruia, A. J. *Hydrocracking Science and Technology*. Marcel Dekker, Incorporated, 1996. p. 305.

(11) Busca, G. Acid catalysts in industrial hydrocarbon chemistry. *Chemical reviews* **2007**, *107*, 5366–410.

(12) Rabo, J. A.. Gajda, G. J. Acid Function in Zeolites: Recent Progress. *Catalysis Reviews* **1989**, *31*, 385–430.

(13) PINE, L. Prediction of cracking catalyst behavior by a zeolite unit cell size model. *Journal of Catalysis* **1984**, *85*, 466–476.

(14) Thomas, C. L. Chemistry of Cracking Catalysts. *Industrial & Engineering Chemistry* **1949**, *41*, 2564–2573.

(15) Tamele, M. Chemistry of the surface and the activity of alumina-silica cracking catalyst. *Discussions of the Faraday Society* **1950**.

(16) Meziani, M. J.. Zajac, J.. Jones, D. J.. Partyka, S.. Rozière, J.. Auroux, A. Number and Strength of Surface Acidic Sites on Porous Aluminosilicates of the MCM-41 Type Inferred from a Combined Microcalorimetric and Adsorption Study. *Langmuir* **2000**, *16*, 2262–2268.

(17) Beck, J. S.. Vartuli, J. C.. Roth, W. J.. Leonowicz, M. E.. Kresge, C. T.. Schmitt, K. D.. Chu, C. T. W.. Olson, D. H.. Sheppard, E. W. A new family of mesoporous molecular sieves prepared with liquid crystal templates. *Journal of the American Chemical Society* **1992**, *114*, 10834–10843.

(18) Rivera, D.. Harris, J. M. In Situ ATR-FT-IR Kinetic Studies of Molecular Transport and Surface Binding in Thin Sol−Gel Films: Reactions of Chlorosilane Reagents in Porous Silica Materials. *Analytical Chemistry* **2001**, *73*, 411–423.

(19) Inaki, Y.. Yoshida, H.. Yoshida, T.. Hattori, T. Active Sites on Mesoporous and Amorphous Silica Materials and Their Photocatalytic Activity: An Investigation by FTIR, ESR, VUV−UV and Photoluminescence Spectroscopies. *The Journal of Physical Chemistry B* **2002**, *106*, 9098–9106.

(20) Mbaraka, I.. Shanks, B. Design of multifunctionalized mesoporous silicas for esterification of fatty acid. *Journal of Catalysis* **2005**, *229*, 365–373.

(21) Roeffaers, M. B. J.. De Cremer, G.. Uji-i, H.. Muls, B.. Sels, B. F.. Jacobs, P. a. De Schryver, F. C.. De Vos, D. E.. Hofkens, J. Single-molecule fluorescence spectroscopy in (bio)catalysis. *Proceedings of the National Academy of Sciences of the United States of America* **2007**, *104*, 12603–9.

(22) Ogawa, M. Incorporation of Pyrene into an Oriented Transparent Film of Layered Silica-Hexadecyltrimethylammonium Bromide Nanocomposite. *Langmuir* **1995**, *11*, 4639–4641.

(23) Huang, M. H.. Dunn, B. S.. Zink, J. I. In Situ Luminescence Probing of the Chemical and Structural Changes during Formation of Dip-Coated Lamellar Phase Sodium Dodecyl Sulfate Sol−Gel Thin Films. *Journal of the American Chemical Society* **2000**, *122*, 3739–3745.

(24) Tachikawa, T.. Majima, T. Single-molecule, single-particle approaches for exploring the structure and kinetics of nanocatalysts. *Langmuir : the ACS journal of surfaces and colloids* **2012**, *28*, 8933–43.

(25) Roeffaers, M. B. J.. Sels, B. F.. Uji-I, H.. De Schryver, F. C.. Jacobs, P. a. De Vos, D. E.. Hofkens, J. Spatially resolved observation of crystal-face-dependent catalysis by single turnover counting. *Nature* **2006**, *439*, 572–5.

(26) Xu, W.. Kong, J. S.. Yeh, Y.-T. E.. Chen, P. Single-molecule nanocatalysis reveals heterogeneous reaction pathways and catalytic dynamics. *Nature materials* **2008**, *7*, 992–6.

(27) Buurmans, I. L. C.. Ruiz-Martínez, J.. Knowles, W. V. van der Beek, D.. Bergwerff, J. a. Vogt, E. T. C.. Weckhuysen, B. M. Catalytic activity in individual cracking catalyst particles imaged throughout different life stages by selective staining. *Nature chemistry* **2011**, *3*, 862–7.

(28) Betzig, E.. Patterson, G. H.. Sougrat, R.. Lindwasser, O. W.. Olenych, S.. Bonifacino, J. S.. Davidson, M. W.. Lippincott-Schwartz, J.. Hess, H. F. Imaging intracellular fluorescent proteins at nanometer resolution. *Science (New York, N.Y.)* **2006**, *313*, 1642–5.

(29) Huang, B.. Wang, W.. Bates, M.. Zhuang, X. Three-dimensional super-resolution imaging by stochastic optical reconstruction microscopy. *Science (New York, N.Y.)* **2008**, *319*, 810–3.

(30) Castro, A.. Shera, E. B. Single-molecule detection: applications to ultrasensitive biochemical analysis. *Applied optics* **1995**, *34*, 3218–22.

(31) Fu, Y.. Collinson, M. M.. Higgins, D. a Single-molecule spectroscopy studies of microenvironmental acidity in silicate thin films. *Journal of the American Chemical Society* **2004**, *126*, 13838–44.

(32) Ye, F.. Collinson, M. M.. Higgins, D. a What can be learned from single molecule spectroscopy? Applications to sol-gel-derived silica materials. *Physical chemistry chemical physics : PCCP* **2009**, *11*, 66–82.

(33) Beck, J. S.. Schmitt, K. D.. Higgins, J. B.. Schlenkert, J. L. New Family of Mesoporous Molecular Sieves Prepared with Liquid Crystal Templates. **1992**, 10834–10843.

(34) Owen, C. S. Comparison of spectrum-shifting intracellular pH probes 5′(and 6′)-carboxy-10-dimethylamino-3-hydroxyspiro[7H-benzo[c]xanthene-7, 1′(3′H)-isobenzofuran]-3′-one and 2′,7′-biscarboxyethyl-5(and 6)-carboxyfluorescein. *Analytical Biochemistry* **1992**, *204*, 65–71.

(35) Owen, C. S.. Carango, P.. Grammer, S.. Bobyock, S.. Leeper, D. B. pH-dependent intracellular quenching of the indicator carboxy-SNARF-1. *Journal of Fluorescence* **1992**, *2*, 75–80.

(36) Whitaker, J. E.. Haugland, R. P.. Prendergast, F. G. Spectral and photophysical studies of benzo[c]xanthene dyes: dual emission pH sensors. *Analytical biochemistry* **1991**, *194*, 330–44.

(37) Yoldas, B. Hydrolysis of aluminium alkoxides and bayerite conversion.

(38) R Nass, H. S. Synthesis of an alumina coating from chelated aluminium alkoxides.

(39) Nampi, P. P.. Moothetty, P.. Wunderlich, W.. Berry, F. J.. Mortimer, M.. Creamer, N. J.. Warrier, K. G. High-Surface-Area Alumina-Silica Nanocatalysts Prepared by a Hybrid Sol-Gel Route Using a Boehmite Precursor. *Journal of the American Ceramic Society* **2010**, *93*, 4047–4052.

(40) Fu, Y.. Collinson, M. M.. Higgins, D. a Single-molecule spectroscopy studies of microenvironmental acidity in silicate thin films. *Journal of the American Chemical Society* **2004**, *126*, 13838–44.

(41) Kirkeminde, A.. Torres, T. Multiple diffusion pathways in pluronic f127 mesophases revealed by single molecule tracking and fluorescence correlation spectroscopy. *The Journal of Physical …* **2011**.

(42) Roy, S.. Aguirre, A.. Higgins, D. A.. Chikan, V. Investigation of Charge Transfer Interactions in CdSe Nanorod P3HT/PMMA Blends by Optical Microscopy. *The Journal of Physical Chemistry C* **2012**, *116*, 3153–3160.

(43) Ye, F.. Higgins, D. a.. Collinson, M. M. Probing Chemical Interactions at the Single-Molecule Level in Mesoporous Silica Thin Films. *Journal of Physical Chemistry C* **2007**, *111*, 6772–6780.

(44) Hair, M. L. Hydroxyl groups on silica surface. *Journal of Non-Crystalline Solids* **1975**, *19*, 299–309.

(45) Ong, S.. Zhao, X.. Eisenthal, K. B. Polarization of water molecules at a charged interface: second harmonic studies of the silica/water interface. *Chemical Physics Letters* **1992**, *191*, 327–335.

(46) La Parola, V.. Deganello, G.. Scirè, S.. Venezia, A. . Effect of the Al/Si atomic ratio on surface and structural properties of sol–gel prepared aluminosilicates. *Journal of Solid State Chemistry* **2003**, *174*, 482–488.

(47) Tsyganenko, A. A.. Storozheva, E. N.. Manoilova, O. V. Lesage, T.. Daturi, M.. Lavalley, J. Brønsted acidity of silica silanol groups induced by adsorption of acids. **2000**, *70*, 159–163.

Chapter 4 - Single molecule fluorescence studies of amorphous silica-alumina thin films by probing with Violamine R

4.1 Introduction

Single molecule fluorescence microscopy has the potential to probe the acidity in silica-alumina thin films. The method can provide information on the distribution of a certain property, indicating the micro-scale heterogeneity of the material, instead of the average bulk information obtained by characterization techniques such as FT-IR, NMR and gas de/adsorptions.[1–4] Single molecule detection requires appropriate selection of dye molecules, which should be of high quantum yield and clear pH-dependent behavior in its emission and/or excitation spectra. Ideal fluorophores should have a pKa that is close to that of the species to be probed.[5] Violamine R (VR) is a good candidate to study the acidic properties of silica-alumina thin films. A schematic drawing of chemical structure of VR molecule is presented in Figure 4.1. VR has a pKa around 3.2 for the carboxylate, but it also has the sulfonate on it that should give it some sensitivity at very low pH as well. Violamine-R is also a duel emission dye， having two characteristic peaks at 585 nm and 650. The intensity ratio of the two bands is pH sensitive and could be used to probe the acidity of an interacting medium.

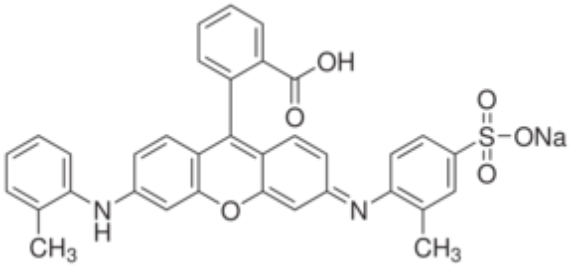

Figure 4.1 A drawing of the chemical structure of Violamine R. The molecule has carboxylate and sulfonate groups, which can be responsive to the pH of its surroundings.

VR was used to confirm the C-SNARF study, in which microenvironments with varying effective pH values were observed. The morphology, structure and acidity distribution of a material can be different depending on different synthesis procedures.[6,7] It is very difficult to simulate the thin film preparation to produce a large amount of samples for bulk characterization

study and hence it is reasonable to try to observe similar phenomenon by using another dye molecule.

VR was studied first by a commercial fluorimeter to determine its excitation/emission spectra. For the single molecule probing of silica-alumina thin films, VR was doped at nanomolar level into silica-alumina films with various silica and alumina ratios, and a wide-field microscope was then used for imaging.

4.2 Experimental section

4.2.1 Dye purification

Violamine R was purchased from Sigma Aldrich (60% pure). It needs to be purified before the pH-dependence fluorescence response can be observed. VR was purified by recrystallization. An over-saturated solution of VR was firstly prepared by adding the solid to methanol at the boiling point. Undissolved impurities as well as the excess amount Violamine R were removed by filtration. VR solids were then collected by crystallization of the filtrate at ice water temperature.

4.2.2 Sample preparation

The synthesis of amorphous silica-alumina thin films was the same as described in Chapter 3. They were calcined to remove surfactants and acid catalysts. Plasma cleaning was used to remove fluorescent residues. The thin films had aluminum contents ranging from 0% to 20% Al. Nanomolar level Violamine R were doped onto the thin films by spin coating at a rate of 5000 rpm for 30 seconds right before imaging with a wide field fluorescence microscope.

4.2.3 Instrumentation and method

The commercial fluorimeter (Fluoromax, Spex) was used to obtain the excitation/emission spectra of the purified VR in phosphate solutions titrated to different pH values.

The single molecule fluorescence studies were conducted on the similar wide-field microscope configuration as was described in Chapter 3. Based on the excitation spectra study, a 488 nm laser was used as the light source to excite the VR dye molecules. The incident power was maintained between 3 and 6 mW. The propagating pathway was the same as is depicted in

Figure 2.2. The 488 nm excitation light was first separated from the dye emission by a beam splitter and a 510 nm long pass filter. Fluorescence signals from fluorophores were subsequently split by a second beam splitter and directed to two band pass filters as was used for C-SANRF-1 studies. Images were recorded by the back-illuminated EM-CCD camera and the intensity ratio for each fluorescent molecule was obtained.

4.3 Result and discussion

4.3.1 Violamine R pH response in aqueous solutions

The pH-response of Violamine R was used to probe the acidity in silica-alumina thin films. It was first studied in aqueous phosphate solutions with carefully controlled pH values. A conventional fluorimeter was used to obtain the fluorescence spectra of VR excited by several wavelengths. 488 nm appeared to be an effective wavelength to excite the molecule to show characteristic peaks. VR was found to have two dominant emission bands centered at 585 nm and 650 nm, respectively. A ratiometric method was used and the intensity ratio *Rv (Rv = I_{580}/I_{640})* was used to access the effective pH of the solid network in silica-alumina thin films. Figure 4.2 is the emission spectra of VR excited at 488 nm.

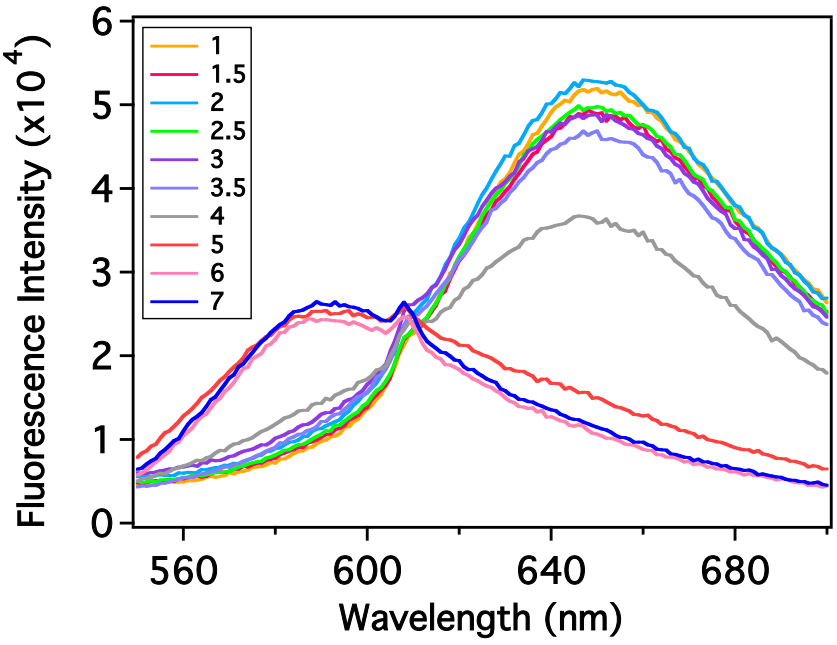

Figure 4.2 Spectra of Violamine R by fluorimeter study. The dye molecule was excited at 488 nm and two characteristic peaks could be observed at 585 nm and 650 nm.

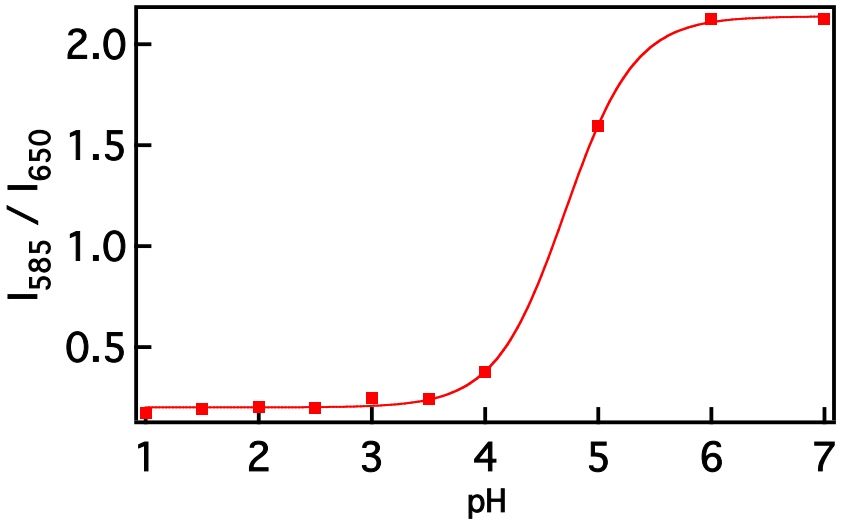

Figure 4.3 Violamine R emission ration, *Rv*, (obtained from the data in Figure 4.2) as a function of pH for solutions ranging from pH 1 to 7. The solid line is used to connect the data points.

Figure 4.3 depicts the correlation between the intensity ratio *Rv* ($Rv = I_{585} / I_{650}$) and the pH values of the titrated phosphate solutions. As was predicted from the molecular structure of Violamine R, it was sensitive at around pH 4.5 ~ 5. From these data, we can conclude that VR is an appropriate dye molecule to probe acidic environments in solid acid matrices. The intensity ratio, *Rv*, increased with the increasing of pH values in the whole pH range that was examined.

The imaging technique and data analyisis for Violamine R probing the silica-alumina thin films were very similar to that for C-SNARF-1 studies. Histograms of the intensity ratio, *Rv*, were obtained and fitted to Gaussian functions as shown in Figure 4.4. The plot of the peak location as a function of aluminum content is shown in Figure 4.5. It could be observed that the increasing doping amount of aluminum atoms in the silicon network generated more local environments with lower effective pH, which was indicated by the smaller *Rv* values. The VR single molecule fluorescence microscopic results supported the observation in the C-SNARF-1 studies, in which it was demonstrated that more acidic environments existed in the higher aluminum samples. Those environments were able to protonate the functional groups, which were responsible for the pH-dependent response on the dye molecules and fluorescence spectrum transition could be observed.

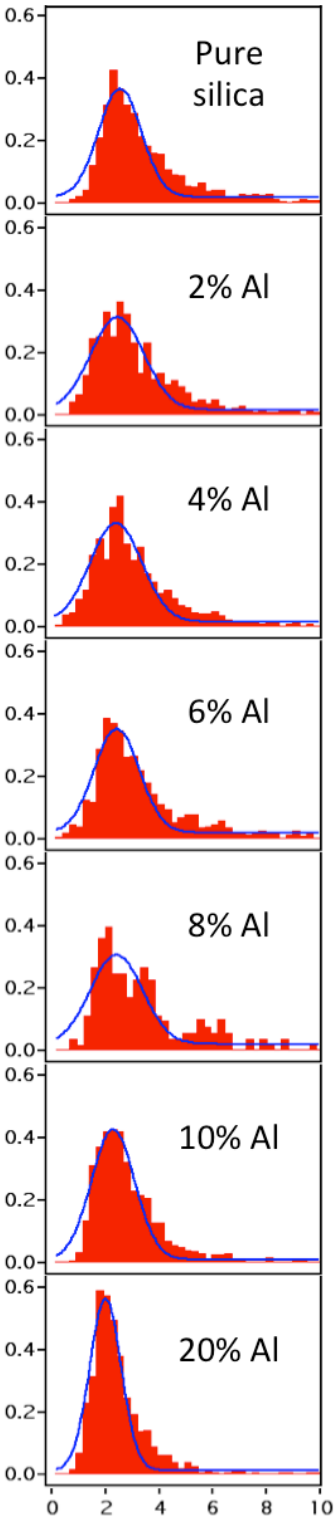

Figure 4.4 Histograms of Violamine R emission ration, *Rv*

It can be seen that the peak positions of the histograms shift from large values of *Rv* to small values when more aluminum was doped to silica network. As indicated by Figure 4.3, small *Rv* represents lower pH and hence high aluminum samples contained more microenvironments with low pH. It was learned from C-SNARF-1 data that, when aluminum was doped, microenvironments with pH around 4 ~ 5 appeared. VR was proved to be sensitive around this region and *Rv* of the dye molecules should be responsive, showing changes of the dual emission spectra. It was reasonable to interpret the histogram peaks shift as the changing of pH in the silica-alumina thin films. As shown in C-SNARF-1 study, there might also a population of local environments with pH smaller than 3 in high aluminum samples; however, VR only had one sensitive region (pH around 4 ~ 5) in the pH range of 1 ~ 7 and hence *Rv* that represented low pH values (pH < 3) might have been compiled with those represented pH of 4 ~ 5. All those *Rv's* made up to the histogram peaks and responsible for the shifting.

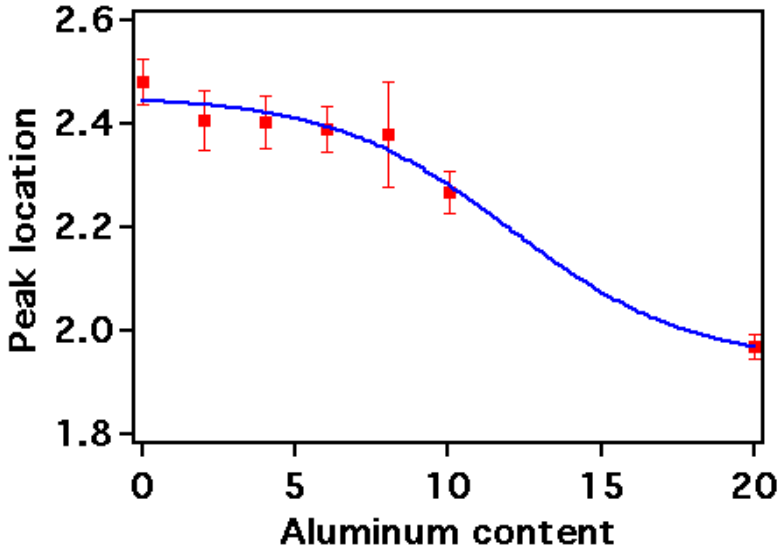

Figure 4.5 Peak locations of silica-alumina thin films samples as a function of Al content. The blue line is used to guide the trend.

The histogram peaks for C-SNARF-1 and VR were different since the molecules have different fluorescence emission behaviors. The two dye molecules for the single molecule fluorescence studies of the silica-alumina materials have their advantages and disadvantages. C-SNARF-1 has two sensitive regions and could reveal better the heterogeneity of acidity distribution of the silica-alumina thin films. VR, however, only has one sensitive region within the pH range it has been examined. It is easier to understand the acidity of the material with VR

as the probing dye molecule, yet the variations of the properties were concealed for the single trend of *Rv* as a function of pH and the single pH sensitive regions. In future studies, VR could be a good candidate to probe acidic media with low pH values (pH at around 4 ~ 5).

Reference

(1) Meziani, M. J.; Zajac, J.; Jones, D. J.; Partyka, S.; Rozière, J.; Auroux, A. Number and Strength of Surface Acidic Sites on Porous Aluminosilicates of the MCM-41 Type Inferred from a Combined Microcalorimetric and Adsorption Study. *Langmuir.* **2000**, *16*, 2262–2268.

(2) Beck, J. S.; Vartuli, J. C.; Roth, W. J.; Leonowicz, M. E.; Kresge, C. T.; Schmitt, K. D.; Chu, C. T. W.; Olson, D. H.; Sheppard, E. W. A new family of mesoporous molecular sieves prepared with liquid crystal templates. *Journal of the American Chemical Society.* **1992**, *114*, 10834–10843.

(3) Rivera, D.; Harris, J. M. In Situ ATR-FT-IR Kinetic Studies of Molecular Transport and Surface Binding in Thin Sol−Gel Films: Reactions of Chlorosilane Reagents in Porous Silica Materials. *Analytical Chemistry.* **2001**, *73*, 411–423.

(4) Inaki, Y.; Yoshida, H.; Yoshida, T.; Hattori, T. Active Sites on Mesoporous and Amorphous Silica Materials and Their Photocatalytic Activity: An Investigation by FTIR, ESR, VUV−UV and Photoluminescence Spectroscopies. *The Journal of Physical Chemistry B.* **2002**, *106*, 9098–9106.

(5) Ye, F.; Collinson, M. M.; Higgins, D. a What can be learned from single molecule spectroscopy? Applications to sol-gel-derived silica materials. *Physical chemistry chemical physics : PCCP.* **2009**, *11*, 66–82.

(6) Hensen, E. J. M.; Poduval, D. G.; Magusin, P. C. M. M.; Coumans, a. E.; Veen, J. a. R. Van Formation of acid sites in amorphous silica-alumina. *Journal of Catalysis.* **2010**, *269*, 201–218.

(7) Leydier, F.; Chizallet, C.; Chaumonnot, A.; Digne, M.; Soyer, E.; Quoineaud, A.-A.; Costa, D.; Raybaud, P. Brønsted acidity of amorphous silica–alumina: The molecular rules of proton transfer. *Journal of Catalysis.* **2011**, *284*, 215–229.

Chapter 5 - Single molecule fluorescence microscopic study of ordered porous materials

5.1 Introduction

Porous materials can interact with atoms, ions and molecules on their external and internal surfaces. They have attracted a lot of scientific and technological interest since those materials can be used for catalysis, separations and ion-exchange.[1] According to the International Union of Pure and Applied Chemistry, porous solids can be classified based on the pore sizes: microporous materials have pore sizes below 2 nm, mesoporous materials are in the range of 2 nm to 50 nm, and finally macroporous materials have pores with dimensions above 50 nm.[2] Besides the pore sizes, the order of the pore structures is also closely related to the performances of the solids, since the pore size distribution, pore shapes and the void volume of the pores affects the accessibility of the interior surfaces to the reactants, the diffusion pathway of the guest molecules and the interaction with the host.[3] It is possible to say that zeolites and zeolitic materials are the most widely used ordered porous materials in industry. They are crystalline aluminosilicates with well-defined three-dimensional framework, forming uniform pores at nanometer scales. Their channel systems can be one, two or three-dimensional with different or the same pore openings. The dimension of the highly ordered structures typically falls in a range of 0.3 to 1.5 nm.[4] The repeating unit of the solids can be expressed as TO_4 tetrahedron, where T represents either a tetrahedral silicon or aluminum atom. Pure silicate materials are electronically neutral and hydrophobic, when aluminum is doped into the framework, however, the solids become hydrophilic and contain Brønsted acidity which is sufficiently strong to carry out some chemical reactions, such as cracking of paraffins[2].

Besides silicon and aluminum, other atoms have also been introduced into the zeolite framework. Flanigen et al[5] have firstly synthesized phosphate-based zeolites in 1982. and various framework types have been developed since 2001.[6]The structure is often denoted as $AlPO_4$-n, where the number n refers to a specific type of crystallographic structure. Most of the extra-large porous crystals (with pore openings greater than 1 nm) are phosphate-based zeolites.[7] Table 5.1 lists some of the representatives in the family. The existence of large pores allow better accessibility of large molecules to the pore openings and interior surfaces, which is a way to make the active sites more available, especially those at the opening of the pores.[2] For example,

Corma[8] studied and compared the cracking activity of zeolites dealuminated by different procedures with different pore size distributions. This work showed that zeolites with small pores had better cracking activity when reacted with small molecules such as n-heptane, which can diffuse through porous structures freely. On the other hand, when the catalysts reacted with larger molecules in a vacuum gas oil, which contains molecules too large to diffuse deeply into the pores, the zeolite sample with larger pores gave better fuel conversion. This study proved the importance of large pores when larger reacting molecules are in presence. This conclusion was supported by the studies of esterification of fatty acids with alcohols.[4]

Table 5.1 Crystalline materials with large pores[9–16]

Material	Framework Composition	Pore Size (nm)
VPI-5	$AlPO_4$	1.2
AlPO-8	$AlPO_4$	< 1.0
Cloverite	$GaPO_4$	< 1.0
JDF-20	$AlPO_4$	SC
ULM-5	$GaPO_4$	ND
UTD-1	SiO_2	~ 1.0
ULM16	$GaPO_4$	ND
CIT-5	SiO_2	0.8
ND-1	$ZnPO_4$	ND
FDU-4	Ge_xO_y	ND
NTHU-1	$GaPO_4$	ND
SC, structure collapse upon removal of organic templates. ND, not determind.		

$AlPO_4$-5 and SAPO-5 zeolites are of interests in this work. They have large crystal sizes and it is possible to manipulate singe particles under a fluorescence microscope. The crystals can be synthesized in hexagonal prisms with sizes up to 1.4 mm.[17] Another advantage of those solids is their large pore dimensions, which will allow bulky dye molecules into the porous structures. $AlPO_4$-5 and SAPO-5 zeolites have an AFI type structure.The AFI-type structure gives a one-dimensional channel system parallel to the crystallographic c-axis (the long crystal axis). The diameter of the channel is typically 0.73 nm. $AlPO_4$-5 zeolites are composed of $AlO4^-$ and $PO4^+$

tetrahedrons in alternation and hence there are no framework charges. Even though $AlPO_4$ is not expected to exhibit any acidity because of its neutrality, some researchers believed that local electronegativity difference between Al^{3+} and P^{5+} and the surface hydroxyl groups (Al-OH and P-OH) as well can produce some acidic characteristics.[18] Additional elements can be added to $AlPO_4$ to generate anionic frameworks. The substitution of phosphorous atoms by silicon atoms yields SAPO-5 silicoaluminophosphate materials and a net negative charge is coupled with this structure. This negative charge gives rise to Brønsted acidity of the material, attracting catalysis research interest.[19] The atomic fraction of the framework atoms replaced by silicon can be from 0.04 to 0.20 depending on the starting materials, synthesis conditions and the structure type.[20] Besides the pore dimension and the particle size, the fact that $AlPO_4$-5 and SAPO-5 are of good optical quality, which makes them possible candidates to be examined by single molecule fluorescence microscopy.[21]

$AlPO_4$ and SAPO-5 zeolites have been studied by many characterization techniques. Researchers have tried to understand the acidity as well as the catalytic activity of the materials. These techniques include scanning electron microscopy[18], diffuse reflectance infrared Fourier transformation spectroscopy[22], temperature programmed desorption of ammonia[23] and catalytic reactions.[24] Single molecule fluorescence microscopic characterizations have not been widely applied to the study zeolites and zeolitic materials. However, several cutting-edge studies have shown the potential to use SM fluorescence microscopic methods to study the interior surfaces of zeolites with relatively large pore sizes, such as ZSM-5 (with a MFI structure and with pore sizes ranging from 5.3 Å to 5.6 Å)[25] and $AlPO_4$-5.[26] These studies demonstrated that fluorescent dye molecules with appropriate dimensions and configurations can be assembled or diffused into the zeolite pores. For example, oxazine-1 molecules could diffuse into the pores from an external solution and 1-ethyl-4-[4-(p-Dimethylaminophenyl)-1, 3-butadienyl]-pyridinium Perchlorate (Pyridine 2) have been included into the $AlPO_4$-5 zeolite single crystals during the solid synthesis.[26,27] These studies focused on the pore structure characterization of the solids instead of the chemical properties on the interior surfaces. By selecting appropriate dye molecules, which are responsive to the pH of the environment, it is possible to probe the acidity of the solids. Table 5.2 lists some dye molecules that could be introduced into the channels of $AlPO_4$ and SAPO-5. These molecules are responsive to proton concentrations and show fluorescence transition within the sensitive pH range. The dimension of the molecules was estimated by Avogadro, a

commercialized molecule editor and visualizer software, and the structures of the molecules are depicted in Appendix A.

Table 5.2 Fluorescence pH indicators with dimensions matching the pore sized of AlPO4 and SAPO-5. These molecules can be excited by using UV-visible light sources.

Dye molecule	Sensitive pH range	Molecular Diameter (Å)	green fluorescence – violet fluorescence
Acridine	5.2 – 6.6	4.59	green fluorescence – violet fluorescence
5-Aminosalicylic acid	3.1 – 4.4	4.82	nonfluorescence–lightgreen fluorescence
Anthranilic acid	1.5 – 3.0	5.65	nonfluorescence – light blue fluorescence
	4.5 – 6.0	-	light blue fluorescence – dark blue fluorescence
	12.5 – 14.0	-	dark blue fluorescence – nonfluorescence
Harmine	7.2 – 8.9	5.35	blue fluorescence – yellow fluorescence
4-Methylescelutin	4.0 – 6.2	4.81	nonfluorescence – blue fluorescence
4-Methylumbelliferone	0.0 – 2.0	4.90	green fluorescence – weak blue fluorescence
b-Naphthol	8.5 – 9.5	4.98	nonfluorescence – blue fluorescence
Naphthol AS	8.2 – 10.3	6.12	nonfluorescence – yellow/green fluorescence
a-Naphthylamine	3.4 – 4.8	5.88	nonfluorescence – blue fluorescence
b-Naphthylamine	2.8 – 4.4	5.88	nonfluorescence – violet fluorescence
o-Phenylenediamine	3.1 – 4.4	4.93	green fluorescence – nonfluorescence
p-Phenylenediamine	3.1 – 4.4	4.93	nonfluorescence – orange/yellow fluorescence
Quininic acid	4.0 – 5.0	6.64	yellow fluorescence – blue fluorescence
Resorufin	4.4 – 6.4	4.97	yellow fluorescence – orange fluorescence
Salicylic acid	2.5 – 4.0	5.30	nonfluorescence – dark blue fluorescence
Umbelliferone	6.5 – 8.0	4.98	nonfluorescence – blue fluorescence

The goal of using SM fluorescence microscopy to study the zeolites is to only exam the interior surface of single crystals. In order to avoid the outside surface from being stained by the dye molecules, a microfluidic device was designed for interior surface isolation. The strategy was to block the exterior surfaces by covering them with a dense and inert material, so that only the interior surface inside the channels was exposed to external dye solutions. The device was prepared by the photolithography technique. The photoresists were Zipcone UA^{TM}, Zipcone UE^{TM} and Norland Optical Adhensives^{TM} (NOA 74). An appropriate mixing of the photoresists is needed to give stable structures, good adherence on the glass surfaces and hydrophobicity.

With this microfluidic device, the calibration of the dye behavior in response to different concentrations of protons could be obtained and it should be possible to quantitatively measure the Brønsted acidity in the interior surface of the zeolite crystals.

5.2 Experiments

5.2.1 Photolithography of the photoresists

Photolithography is a process to transfer a geometric pattern from a photo mask onto a substrate. There are positive and negative photoresists. For positive photoresists, the exposure to ultraviolet light sources triggers chemical reactions, which allow the photoresists to be dissolved in some solutions and removed from the substrates. The negative photoresists, however, remain on the surface after the UV exposures since the light sources provide energy for the photoresist to be polymerized and hence the exposed areas are difficult to be dissolved in solutions. The pattern transferring of both types of the photoresist is shown in Figure 5.1. It can be seen that the pattern from the photo mask is directly copied onto the substrate for the positive photoresist while the oppositve occurs for the negative photoresist.

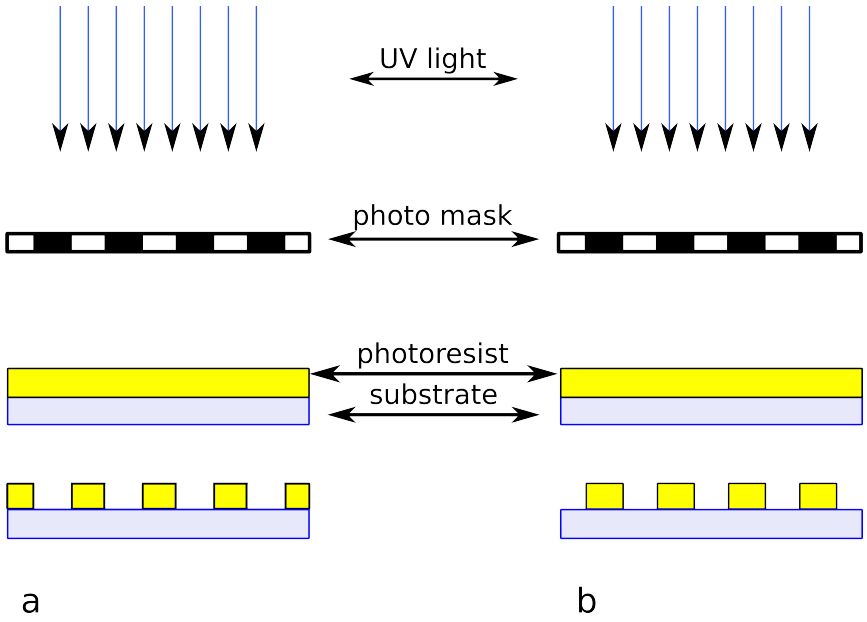

Figure 5.1 Schematic illustration of the procedure for lithography. a) a typical procedure for a positive photoresist. The same pattern is transferred from the photo mask onto the substrate. b) for a negative photoresist, however, the opposite pattern is transferred

There are several photoresist suppliers that provide different type of photoresist, such as DOW™, DuPont™, Fujifilm™ and Microchem™. The devices fabricated by these photoresists are elegant with well-defined structures.[28] However, they are not ideal candidates for single molecule studies since most of the photoresists contain fluorescent contaminants, which will increase the noise level of the SM fluorescence experiments.[29] In this work, UV cure silicone elastomers are used as the photoresists and the working mechanism is as described in Figure 5.1b. Gelest Zipcone™ U Series polymers are designed for UV cure (Zipcone™ UA is a clear acrylate modified silicone and Zipcone™ UE is an epoxycyclohexyl modified silicone) and Norland Optical Adhesive™ 74 (NOA 74) are mixed with the Gelest Zipcone™ U Series polymers at a volumetric ratio of 3:2. This ratio impacts the hardness and flexibility of the material after the UV light exposure. Zipcone™ UA and UE can also be thermo-cured at above 80 ^{0}C so that they can be used as a glue to attach the zeolite single crystals on the glass surface and no additional chemicals will be introduced into the system.

5.2.2 Fabrication of the microfluidic device

Glass surface treatment

Before the photoresist is spread on the cover slip, the glass surface needs to be thoroughly cleaned, in order to get rid of unknown fluorescent contaminants and other chemicals that might disturb the chemistry of the UV cure (for example, the radicals generated from the UV exposure might react with unknown chemicals first and hence limit the crosslinking between photoresist molecules). The cover slip was rinsed with isopropanol and water, followed by cleaning in an air plasma cleaner (Harrick Plasma) for 3 minutes to further remove the organic residues.

Fixation of a zeolite single crystal particle on the modified surface

30% of Zipcone™ UA (or UE) in isopropanol was first deposited on the glass cover slip by spin casting at a rate of 5000 rpm. A grain of zeolite crystal is immediately positioned in the center of the modified surface before it dries out so that the particle could be imbedded into the soft Zipcone™ UA (or UE) coating. The reason to dilute the photoresist is to obtain a relatively thin layer of coating on the glass surface so that the zeolite particle would not sink too deeply into the coating and the openings of the pores can be exposed. The cover slip with the zeolite fiber on top of it was then put on a hot plate for about 30 minutes at 80 ^{0}C for the Zipcone™ UA (or UE) coating to be thermo cured. The zeolite crystal was then fixed onto the modified glass cover slip during the hardening of Zipcone™ UA (or UE).

Fabrication of the microfluidic structure

80 μl of the polymer mixer (Zipcone™ U series and NOA 74 polymers) was then dropped on the zeolite-deposited cover slip by a pipette. A photo mask was used to transfer a pattern onto the photoresist. The photo mask was printed on a 3M^{TM} transparent film by a HP PSC 1350 laser printer. The exact position of the crystal needs to be localized since the cured structure is specially designed to work on individual zeolite particles. The UV light source was set to be at 250 watts and the exposure time was strictly controlled at 2.5 seconds. It is very important to control the exposure time since the insufficient exposure would yield an unstable structure and the over-exposure will destroy the fine structure of the microfluidic channels. After the UV cure, the mask was peeled off and a large amount of acetone was used to rinse away the non-polymerized photoresists to develop a well-defined microfluidic structure. A piece of dried polydimethylsiloxane (PDMS) slab (with a thickness of 0.5 cm in order to keep some rigidity of the system) is then used to cover and seal the photoresist structure, producing microfluidic

channels with dimension of 300 microns. The PDMS slab was drilled with four holes and positioned at the ends of the microfluidic channels so that external solutions could be introduced. A schematic drawing of the microfluidic device is shown in Figure 5.2

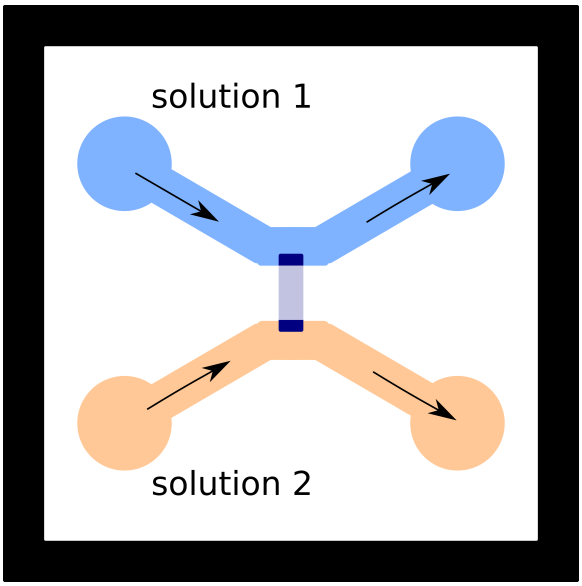

Figure 5.2 Schematic drawing of the microfluidic device. The zeolite crystal is covered with cured photoresist with only two ends exposed to the microfluidic channels. The channels will flow with dye molecule doped solutions. The design makes sure that only the pore openings are accessible to dye molecules and the molecules can only diffuse through the pore openings or the defects at two ends.

5.2.3 Calibration of the pH response of the dye molecules in the ordered zeolite porous systems

The zeolites are from Dr. Rioux, from Pennsylvania State University. They are experienced in preparing larger single crystals, such as $AlPO_4$-5 and SAPO-5. The zeolites were calcined at 550 ºC for 24 h to remove the organic templates, so that it is possible for dye molecules to diffuse onto or into the openings of the porous structures.[25,26] Otherwise, the solids will be synthesized in our lab in order to have a source of the large number of particles that will be required for this research.

A limited number of experiments were conducted to synthesize zeolite single crystals. The hydrothermal synthesis of AlPO4-5 was attempted.[30] The procedure used started from a gel solution, having a composition with mole ratios of 1 Al_2O_3: 1.3 P_2O_5: 1 tripropylamine: 40 H_2O.

Orthophosphoric acid (85%, Fisher) and aluminum isopropoxide (99%, Aldrich) were added to the water and stirred at room temperature for 60 minutes. Tripropylamine (TPA; 99%, Acros) was added and the mixture was transferred to a Teflon liner in a stainless steel autoclave. It was heated at 150 ^{o}C for 48 hours. The autoclave was then quenched in tab water and allowed to cool. The product was filtrated and centrifuged in order to collect solid particles. This procedure did not yield large single crystals of $AlPO_4$-5 by examination with a compound microscope in Dr. Daniel Higgins' lab. According to literature, the involvement of HF in the synthesis procedure would generate large single crystals and the proposed procedure is described in Appendix D for $AlPO_4$-5 and Appendix E for SAPO-5.

As is shown in Figure 5.2, the zeolite fiber should be covered with the UV cured photoresist and the two ends of the crystal should be exposed to two solutions, which are represented by two colors. The solutions could contain different dye molecules or have different pH values. Only the pore openings of the zeolite are accessible to molecules and ions in the external solutions. In order to quantify the acidity in the zeolite pores, the pH response of the dye molecules needs to be calibrated by the SM fluorescence microscopy. It is hoped to artificially create a pH gradient inside the one-dimensional linear pores of $AlPO_4$-5 and SAPO-5. Two buffer solutions, with nanomolar or micromolar concentrations of the fluorescent probes will be flowing continuously inside the channels of the microfluidic device and the dye molecules will diffuse into the zeolite pores by molecular diffusion. According to the study by Behrens et al.,[26] the dye molecules with dimensions matching the size of the pores of the zeolites can diffuse through the opening of the pores by molecular diffusion even though the process is very slow and a time window can be as long as 3 months. In the study, they successfully introduced oxazine-1 molecules into the pores of $AlPO_4$-5 by observation of the dye distribution patters in the pores of the single zeolite particles. Since they soaked the whole particles in the dye solution, they could not distinguish between the dye molecule diffusing through defects of the crystal surface or through the openings of the pores.

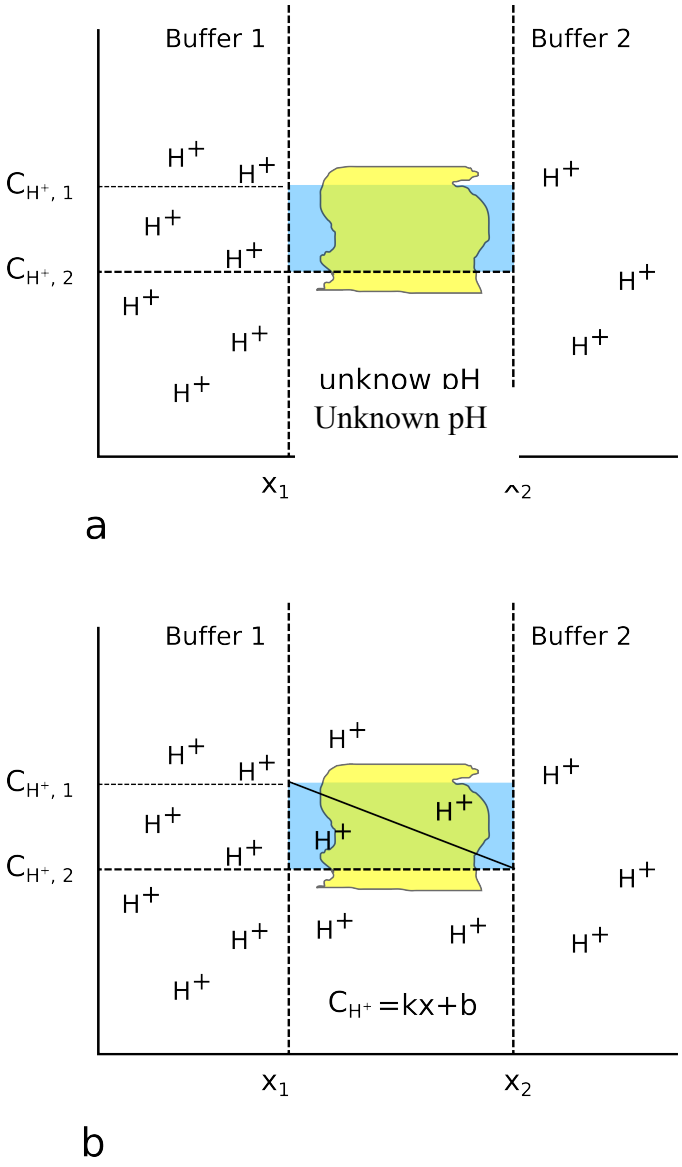

Figure 5.2 A schematic drawing of the proton concentration distribution at the opening and inside the pores of a zeolite single crystal. In a) it is assumed that the dye molecules can not diffuse freely inside the pores and hence only the pore openings can be probed. The pH at the ends of the zeolite equals to that of the buffer solutions they are exposed to; and b) it is assumed that the dye molecules can diffuse all the way inside the zeolite pores. The concentration inside the pores is a linear distribution along the long axis described by Fick's law and the full length of the pores can be probed.

With the microfluidic design, it is possible that most of the molecules will diffuse into the crystal pores from the opening since the exterior surfaces are not accessible to the external dye solutions. Two scenarios are predicted when the interior surfaces are probed by the dye molecule: 1) only the pore openings can be accessible to the dye molecules and the concentration of the protons at the pore openings equals to the pH of the external buffer solutions in which they are exposed to; 2) the dye molecules can move all the way inside pores of zeolites, so that the full length of linear channels can be probed. The proton concentration will reach to a dynamic equilibrium inside the pores, the Fick's first law will be used to describe the proton concentration distribution inside linear structures. The proton concentration can be easily converted to pH scales at the pore openings or inside the pores. Figure 5.3 depicts the two scenarios.

5.2.4 Acidity measurements inside the zeolite channels

It can be seen from table 5.2 that, several dye molecules are responsive to pH of the environment and they have appropriate dimensions for the study. However, some of them need a UV light source to fluoresce. Since there are only blue and green lasers in Dr. Higgins's lab, p-Phenylenediamine and Resorufin are candidate dye molecules for the experiment. The responsive pH range of p-Phenylenediamine is 3.3 ~ 4.4 while that of resorufin is 4.4 ~ 6.4. In these pH ranges, the fluorescence transition will occur, providing a way to estimate the acidity of the environment. Table 5.3 shows the combination of the solutions of different pH values and the dye molecules that need to be examined in order to complete the calibration of the fluorescence responses of dye molecules to different acidities. Two types of solutions, either of the same type or different types can be checked on one individual single zeolite crystal.

Table 5.3 Experiment plan for microscope calibration

p-Phenylenediamine	resorufin
pH 1	pH 3
pH 3	pH 5
pH 5	pH 7

For the acidity measurement in zeolite porous structures, the dye solution will flow in the microfluidic channels in a similar manner as described for the fluorescence calibration. It is assumed that the acidic properties of the two ends of the zeolite fibers should be the same and the

data obtained from the two ends could be used to represent two independent data points on the same sample. Two types of the dye molecules will be used to stain the two ends of the zeolite and the dye molecule solution will flow in the microfluidic channel at the nanomolar or micromolar concentration.

A wide-field microscope will be used for fluorescence imaging. This system is built on an inverted epi-illumination microscope (Nikon TiE). Either a 473 nm or 488 nm laser will be used depending on the excitation and emission spectra of the dye molecules (the fluorimeter will be used to study the spectra in bulk solutions). It is expected that fluorescence signals in the range of 570 ~ 590 nm will be detected since the dye molecules emit yellow or orange light when excited as is shown in Table 5.2. The fluorescence signals from the sample will be collected and separated from the incident laser light by several optical parts such as a beam splitter and a long pass filter An EM-CCD camera (Andor iXon DU-897) will be used to record the fluorescence dye molecules. The two ends of the zeolite crystals will be examined. If the pH of the environment falls in the fluorescence transition range of the dye molecule, yellow or orange fluorescence singles should be detected. If a UV laser source can be used, multiple dye molecules (listed in Table 5.2) can be used in a way similar to Hammett indicators to better estimate the acidities at the pores of the zeolites or inside the zeolite porous structures.

Either the bulk averaged or single molecule fluorescence signals could be expected, depending on the dye concentration in the external solutions for the fluorophores staining. It is reported[25,26] that 10^{-5} molar concentration did not give single molecule resolution and only averaged bulk signals could be detected, and hence it is necessary to lower the dye concentration in order to observe spatially separated individual molecules.

5.3 Preliminary Result and discussion

5.3.1 Zeolite fixation on the glass surface

With the procedure described above, the zeolite particles could be fixed onto the Zipcone^{TM} UA (or UE) modified surface properly and firmly by thermo cure. Figure 5.4 is an image of an individual $AlPO_4$-5 zeolite single crystal taken by a reflected light upright microscope (Olympus BX41) with a magnification of 400 ×. The problems are revealed in Figure 5.4. It can be seen that the zeolite particle cracked upon heating. This particle itself should be mechanically robust since it was calcined at a temperature around 500 ^{0}C. Currently,

there are two guesses to explain the cracking. The first guess is the fast volume expansion of air and water molecules absorbed on the interior surfaces of the zeolite pores and those molecules could not diffuse out of the zeolite pores before the expansion and destroyed the structure. If this is the reason for cracking, lowering the ramping rate might be a solution. The second guess is that there might be some organic residues inside the pores of the solids, which should have been removed during the calcination. The second guess is based on the observation that the zeolite particle turns out to be black (and it was optically clear before heating). This might be the color of tar, which could be formed from the organic residues left by the incomplete calcination. If the organics are the causes of the cracking, the synthesis procedure as well as the post-synthesis treatments needs to be optimized.

Table 5.4 An individual zeolite single crystal imbedded firmly onto the zipcone™ UA treated glass surface. The cracking of the particle can be observed and the experimental procedures need to be optimized.

5.3.2 Stability of the microfluidic channel

Figure 5.5 shows an example of the microfluidic device. The colored solutions are concentrated dye molecules to make the flow path of the fluid obvious. The stability of the structure is defined by the flexibility and the hydrophobicity, which are related to the composition of the photoresist polymer mixture, the curing time, the cleaning procedure of the substrate and the PDMS slab and the design pattern of the photo mask. Several recipes have been tested and the one described in the experimental section is very repeatable. The channel depth was measured by a profilometer and the typical values were between 60 ~ 70 μm. The width othe channel was decided by the pattern on the photo mask which was 300 μm. The flow rate of the solutions was between 0.1 ~ 0.5 ml/hour and the system can run 40 ml continuously without any leakage.

The test for a microfluidic device with zeolite particles was attempted. However, the refractive index of the zeolite fiber and that of the photoresist mixture are very similar and the crystal was lost track during photolithography and an appropriate pattern over the solid could not be formed. Even though there is no immediate solution for this issue right now, some marking techniques (such as a marker pen or scratches on the glass surface) might be useful since the particle size of the $AlPO_4$-5 and SAPOS zeolites is large enough to be resolved by naked eyes or by a compound microscope with better resolution.

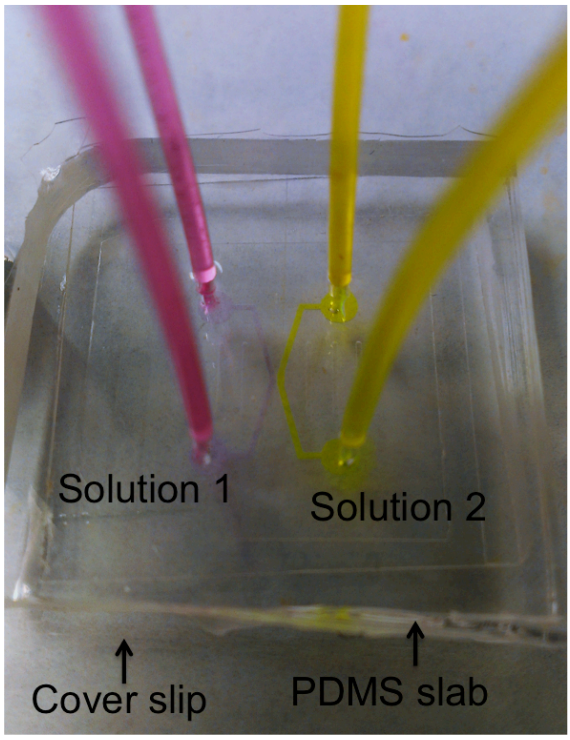

Figure 5.5 Image of a microfluidic device. The solutions were doped with high concentration of dye molecules in order to visualize the flow pattern inside the microfluidic channels. The center was supposed to be the zeolite bed, however, the crystal becomes invisible when covered with the photoresist mixture with similar refractive index. However, when the uncured photoresist was removed, the particle would be visible again on the cured surface, proving that the zeolite particle can be fixed onto the cover lip by thermo curing of a dilute ZipconeTM UA (or UE) solution in isopropanol.

5.4 Future work

It is hoped to synthesis $AlPO_4$-5 and SAPOS zeolites single crystals in Dr. Hohn's lab. Every step of the synthesis and post-synthesis treatment procedures needs to be closely monitored since every one of them is directly or indirectly related to the properties of the solids and the performance of the microfluidic device. The $AlPO_4$-5 and SAPOS synthesis methods are listed in Appendix D and Appendix E. The methods are from literatures and detailed operations need to be optimized specifically for fluorescence microscopic experiments. As for the problem of similar refractive indexes of the photoresist and the zeolite particles, instead of working on only one, multiple particles could be fixed onto the substrate at the same time in one microfluidic

device and there will be a better chance that one or several of them will be in the right position of the microfluidic device.

Reference

(1) Bein, T. Host-guest interactions in zeolites and periodic mesoporous materials. *Studies in Surface Science and Catalysis.* **2007**.

(2) Corma, A. From Microporous to Mesoporous Molecular Sieve Materials and Their Use in Catalysis. *Chemical reviews.* **1997**, *97*, 2373–2420.

(3) Sen, T.; Tiddy, G. One‐Pot Synthesis of Hierarchically Ordered Porous‐Silica Materials with Three Orders of Length Scale. *Angewandte Chemie.* **2003**.

(4) Aracil, J.; Martinez, M.; Corma, A. Formation of a jojoba oil analog by esterification of oleic acid using zeolites as catalyst. *Zeolites.* **1992**.

(5) Wilson, S.; Lok, B. Aluminophosphate molecular sieves: a new class of microporous crystalline inorganic solids. *Journal of the American Chemical Society.* **1982**.

(6) Flanigen, E.; Bekkum, H. van; Jansen, J. *Introduction to Zeolite Science and Practice*; 1991.

(7) Davis, M. Ordered porous materials for emerging applications. *Nature.* **2002**.

(8) Corma, A. Application of Zeolites in Fluid Catalytic Cracking and Related Processes. *Studies in surface science and catalysis.* **1989**.

(9) Davis, M.; Saldarriaga, C.; Montes, C. A molecular sieve with eighteen-membered rings. *Nature.* **1988**.

(10) A synthetic gallophosphate molecular sieve with a 20-tetrahedral-atom pore opening. *Nature*. **1991**.

(11) MeurigáThomas, J. Synthesis and characterization of a novel extra large ring of aluminophosphate JDF-20. *Journal of the Chemical Society, Chemical Communication.* **1992**.

(12) Lobo, R.; Tsapatsis, M. Characterization of the extra-large-pore zeolite UTD-1. *Journal of the American Chemical Society.* **1997**.

(13) Dessau, R.; Schlenker, J.; Higgins, J. Framework topology of $ALPO^{-8}_4$: the first 14-ring molecular sieve. *Zeolites* **1990**.

(14) Vogt, E.; Jr, J. R. The reversible transition of the molecular sieve VPI-5 into $ALPO^{-8}_4$ and the structure of $ALPO^{-8}_4$. *Journal of Solid State Chemistry* **1990**.

(15) Loiseau, T.; Férey, G. Synthesis and crystal structure of ULM-16, a new open framework fluorinated gallium phosphate with 16-ring channels. *MRS Proceedings.* **1996**.

(16) Zhou, Y.; Zhu, H.; Chen, Z.; Chen, M. A Large 24-Membered-Ring Germanate Zeolite-Type Open-Framework Structure with Three-Dimensional Intersecting Channels. *Angewandte Chemie.* **2001**.

(17) Finger, G.; Kornatowski, J. Growth of large crystals of silicoaluminophosphate molecular sieve SAPO-5. *Zeolites.* **1990**.

(18) Hedge, S. G.; Ratnasamy, P.; Kustov, L. M.; Kazansky, V. B. Acidity and catalytic activity of SAPO-5 and AlPO-5 molecular sieves. *Zeolites.* **1988**, *8*, 137–141.

(19) Lok, B.; Messina, C.; Patton, R. Silicoaluminophosphate molecular sieves: another new class of microporous crystalline inorganic solids. *Journal of the American Chemical Analysis.* **1984**.

(20) Martens, J.; Mertens, M. Synthesis and characterisation of silicon-rich SAPO-5. *Studies in Surface Science and Catalysis.* **1988**.

(21) Demuth, D.; Stucky, G.; Unger, K.; Schüth, F. Synthesis of large optically clear silicoaluminophosphate crystals with AFI structure. *Microporous Materials.* **1995**.

(22) Chen, J.; Wright, P.; Natarajan, S.; Thomas, J. Understanding The Brønsted Acidity of Sapo-5, Sapo-17, Sapo-18 and SAPO-34 and Their Catalytic Performance for Methanol Conversion to Hydrocarbons. *Science and Catalysis.* **1994**.

(23) Elangovan, S. SAPO-5 and SAPO-11: Synthesis, characterization and camphene isomerization activity. *Reaction Kinetics and Catalysis Letters.* **1995**.

(24) Qi, J.; Zhao, T.; Xu, X.; Li, F.; Sun, G. High activity in catalytic cracking of large molecules over micro-mesoporous silicoaluminophosphate with controlled morphology. *Science China Chemistry* **2010**.

(25) Roeffaers, M. B. J.; Ameloot, R.; Baruah, M.; Uji-I, H.; Bulut, M.; De Cremer, G.; Müller, U.; Jacobs, P. a; Hofkens, J.; Sels, B. F.; De Vos, D. E. Morphology of large ZSM-5 crystals unraveled by fluorescence microscopy. *Journal of the American Chemical Society* **2008**, *130*, 5763–72.

(26) Seebacher, C.; Rau, J.; Deeg, F. Visualization of mesostructures and organic guest inclusion in molecular sieves with confocal microscopy. *Advanced Materials.* **2001**.

(27) Vietze, U.; Krauss, O.; Laeri, F.; Ihlein, G. Zeolite-dye microlasers. *Physical review Letters.* **1998**.

(28) Madou, M. *Fundamentals of microfabrication: the science of miniaturization*; 2002.

(29) Pai, J.; Wang, Y.; Salazar, G. Photoresist with low fluorescence for bioanalytical applications. *Analytical Chemistry.* **2007**.

(30) Cundy, C.; Cox, P. The hydrothermal synthesis of zeolites: history and development from the earliest days to the present time. *Chemical Reviews* **2003**.

Chapter 6 - Conclusion and future work

Conclusion

This project investigated the application of single molecule fluorescence microscopic methods to study solid acid materials. The aim is to provide valuable information that could not be obtained by conventional characterization methods, which only provide averaged ensemble property information. A dual emission pH-sensitive dye molecule, C-SNARF-1 was examined in bulk solutions with pH ranging from 1 ~ 7. The intensity ratios (*R*) of two dominant bands at 580 nm and 640 nm wavelengths were used to obtain information about the acidity of the dye's environment. Two sensitivity regions of C-SNARF-1 were observed: one is at around 4 - 5 and the other one is around 7. These results provided the basis of the behavior of dye molecules.

Pure silica thin films treated with phosphate solutions of different pH values were probed by C-SNARF-1. Histograms of *R* values from individual dye molecules that were doped onto the thin films were obtained and fitted to Gaussian functions. A similar trend of the intensity ratio as a function of pH was acquired by analysis of the peak positions. The peak positions represented the most common local acidity in the samples, which was different from the average acidity. The ability to easily obtain such information is a distinct advantage of SM methods over most ensemble experiments. The width obtained from each histogram also provided interesting information about the behavior of C-SNARF-1 and the silica framework. Two sensitive regions were observed, in agreement with the bulk solution studies. Surface silanol groups with pKas around 7.5 were also observed, which gave unexpectedly narrow peaks at pH 7.

Silica-alumina thin films with different Si/Al ratios were characterized with C-SNARF-1. It was found that pure silica (0% Al) contained the least acidic microenvironments in this study. The introduction of tetrahedral Al atoms into the films produced more acidic sites, as indicated by spectra of C-SANRF-1 with small *R* values. Violamine R is another molecule selected to probe the acidic properties in the silica-alumina network and confirmed with the observation in the C-SNARF-1 studies.

The results from this work are important because they provide information on the distribution of acidity in solid acid materials that can not be obtained by conventional techniques such as IR, NMR and gas absorption/desorption. This research demonstrates that the single

molecule fluorescence microscopic method can be used to characterize the heterogeneity of solid acid catalysts.

In order to use the SM method for more realistic acidic catalyst systems, a microfluidic device were designed. The purpose of this device is to block the exterior surface of a single zeolite particle and only probe the interior surface in the pores of the particle. The fabrication of the device was tested and the syntheses of AlPO4-5 particles were attempted. The final fabrication and the zeolite recipes still need to be optimized.

Future work

Conventional characterization methods can be used to characterize the silica-alumina samples, such as FTIR, gas ab/desorption and titration methods. The synthesis procedures and treatments should be very close to that of the thin film samples. This requires a method to evaporate the solvents very quickly under room temperatures.

In situ characterization with single molecule fluorescence microscopic methods can be designed by using acid catalyzed fluorogenic reactions, such the polymerization/oligomerization of thiophenes. *In situ* characterization chambers need to be constructed to design experiments under elevated temperatures.

The idea of the microfluidic device needs to be supported by working with a large quantity of zeolite single particles. The synthesis of $AlPO_4$-5 and SAPOs may be explored to collect large crystal sizes, which allow easy manipulation of the particles. Several pH responsive dye molecules can be used in a similar way as Hammett indicators to quantitatively probe the Brønsted acidity in the pores of zeolites or a single dual emission dye molecule may be applied. It will be very promising if a UV laser source could be used as the excitation light for the SM studies since there are several pH responsive fluorophores that need to be excited by light beams with shorter wavelength that the green or blue laser used in this study.

Appendix A - Structures of the dye molecules

The dye molecules listed in Table A.1 are candidates for the single molecule fluorescence studies of the interior surfaces inside the pores. These molecules were also edited in Avogadro™ to measure the dimensions that were possible for the dye molecules to diffusion into the pores of zeolites. The structures were schemed by MarvinSketch™, a chemical editor for drawing chemical structures and reactions.

Figure A.1 Fluorescent pH indicators with appropriate dimensions for single molecule fluorescence studied of interior surfaces of zeolites.

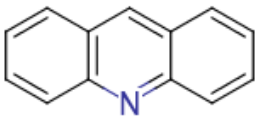

Acridine

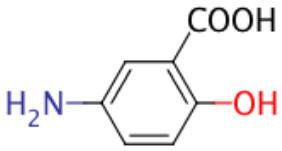

5-Aminosalicylic acid

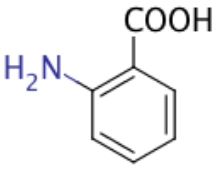

Anthranilic acid

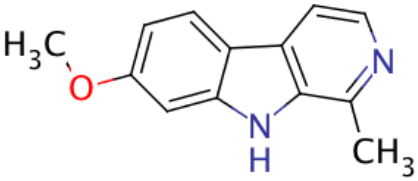

Harmine

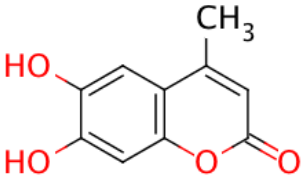

4-Methylescelutin

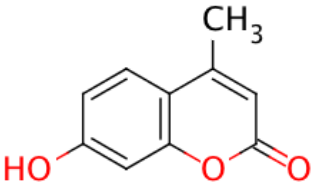

4-Methylumbelliferone

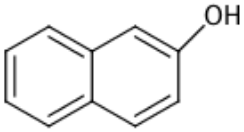

β -Naphthol

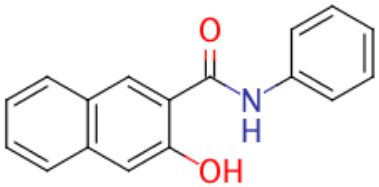

Naphthol AS

Table A.1 (Continued).

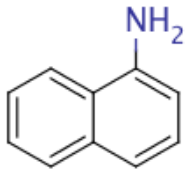

α-Naphthylamine

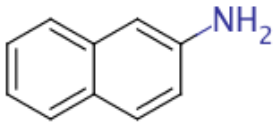

β-Naphthylamine

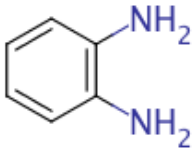

o-Phenylenediamine

p-Phenylenediamine

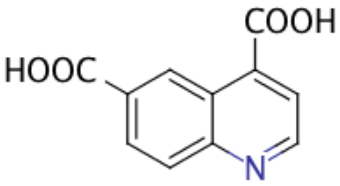

Quininic acid

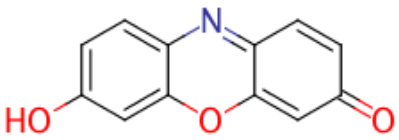

Resorufin

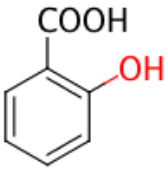

Salicylic acid

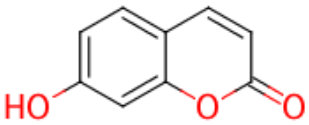

Umbelliferone

Appendix B - Fabrication of the microfluidic device

The procedure and design of the micro-channel device is schemed in Figure B.1. The cover slip was plasma-cleaned for 3 ~ 5 mins before a layer of 30% Zipcone UA in isopropanol was deposited by spin casting at a rate of 5000 rpm for 30 seconds. A grain of zeolite particle was positioned on the coated surface. The particle was fixed on the cover slip while the photoresist was thermo cured on a hot plate at around 80 ~ 120 ^{o}C, as shown in Figure B.1a. Another layer of photoresist mixture (60% Zipcone UA (or UE) and 40% NOA 74) was spread on the cured surface. A photo mask, printed with the microfluidic channel pattern on a 3M^{TM} transparent paper was put on top of the liquid photoresist with a zeolite fiber. A UV light source was used to initiate the reaction of the UV cure.

In Figure B.1b, the micro-channel was formed after the UV cure. A piece of thick PDMS slab drilled with holes was used to cover and seal the microfluidic channel. The holes on the slab were on top of the microfluidic channels on the cured photoresist and hence only the ends of the zeolite crystals were exposed to the channels and most of the exterior surfaces were blocked with the cured photoresist mixture.

A completed microfluidic device is shown in Figure B.1c. Two solutions (either with the same or different concentrations) doped with dye molecules will flow in the two microfluidic channels and two syringe pumps will be used to flow solutions at a rate of 0.1 ~ 0.5 ml/h. The interior surfaces or the pore openings of the zeolite particle will be stained. To create a proton concentration around the pore openings of the zeolite or a gradient inside the linear pore structures, two buffer solutions of different pH values will be flowing in the microchannels as is shown in Figure B.1c. Bulk fluorescence acidity studies could be conducted at high dye doping while single molecule studies could be done at nanomolar concentrations.

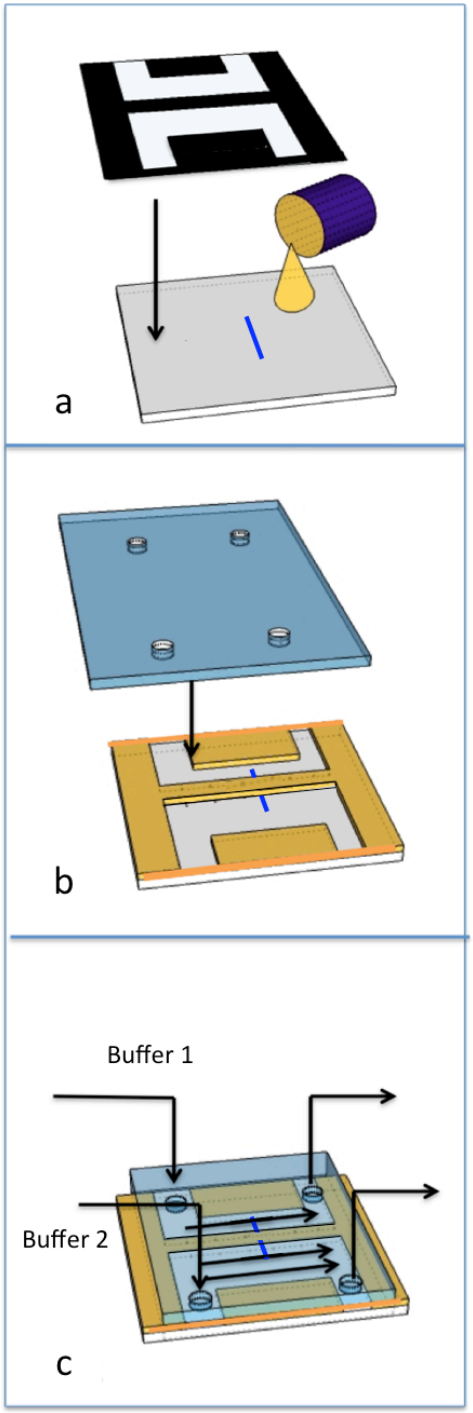

Figure B.1 Fabrication procedures of the microfluidic device. The blue bar represents a single zeolite crystal.

Appendix C - PDMS slab preparation

PDMS preparation is done using the SYLGARD® 184 SILICONE ELASTOMER KIT. The chemicals were all from Dow Corning Company. The procedure for making the thick PDMS slab is described as below.

a. The elastomer and hardener were mixed at a 10 parts to 1 part ratio (10:1) in a weighing bowl.

b. The mixture was then stirred vigorously with a plastic pipette to make sure the hardener was well distributed in the elastomer.

c. The mixture was poured on top of a clean glass board with removable mold. The mold was a simple thick plastic frame and it was clenched on to the glass board with two.

d. The mixture was then placed in a desiccator at room temperature, which was vacuumed to remove the air bubbles in the viscous liquid. This step took for about 30 ~ 40 mins.

e. Once almost all the bubbles were cleared, the PDMS mixture was put into an oven for 100 ~ 120 mins at 60 ^{o}C to get cured.

f. When the mixture had hardened, it was cut into the desired dimensions (2.5 cm × 2.5 cm) with a razor blade, matching the size of the cover slip. It was then peeled off from the glass surface.

g. The cut-off PDMS slab was then punctured with a drill, which was made from a hypodermic needle.

h. The PDMS slab was immediately used on top of the microfluidic channels since the exposure in air will introduce dust and other particles, which would cause the slab to be non-sticky.

Appendix D - $AlPO_4$-5 synthesis

For the proposed synthesis of AlPO4-5, hydrofluoric acid will be involved in the synthesis in order to obtain large single crystal sizes. The procedure is based on literature which shows that hydrothermal synthesis yields large crystals. Synthesis in the presence of F- is one of the strategies that has been widely used to effectively obtain zeolite crystals with large sizes.[1,2]

Qiu et al.[3] reported that large single crystals of aluminophosphate could be obtained by adding fluoride to the reaction mixtures. It was believed that AF_3^- and PF_6^- existed in the starting gel and then were hydrolyzed to release the Al and P species during the crystallization. Different composition of the raw material and the addition of other atoms lead to other type of zeolite crystals.

The crystals synthesis will be started from a molecular gel composition of xAl2O3 : P2O5 :yTPA : 500H2O : zHF. The source reagents were tri-isopropylate aluminum, orthophosphoric acid (85%, wt%), tripropylamine (TPA), hydro-fluoric acid (HF, 40wt%) and deionized water. The typical synthesis procedure is as follows:[1,4]

a. Preparing a tri-isopropylate aluminum solution by dissolving tri-isopropylate aluminum in deionized water;

b. Stirring the mixture for 12 h;

c. Adding diluted orthophosphoric acid dropwise into the aluminum solution and stirring for 2 h;

d. Adding the organic template, TPA, into the mixed gel solution and stirring for 2 h;

e. Adding diluted HF solution into the mixed solution and further stirring for 2 h;

f. Filling a Teflon-lined stainless-steel autoclave with the prepared gel solution, and aging for a period of time;

g. Putting the autoclave into an oven and setting the temperature to 180^{o}C. Let the gel react for 5–36 h;

h. Quenching the autoclave in tap water and separating the product by decantation;

i. Washing the crystals with deionized water;

i. Drying the crystals at at 80 ^{o}C overnight.

The starting composition that will be tested is listed in Table D.1. These compositions were reported to have good morphology and optical transparency.[1,5] The dimensions of the resulting crystals were also reported to be related to the molar gel composition of the starting gel.

x	y	z	The predicted maximum particle size length × width (μm)
1.2	1.5	3.0	680 × 210
1.2	1.4	3.0	530 × 180
1.2	1.5	3.5	700 × 350

Figure D.1 The molar ratios of the starting gel that will be examined to produce large single crystals of high yields with good morphology (no or limited crystal intergrowth) and optical transparency.

The quality of the zeolite crystals was also reported to be a function of the reaction temperature and reaction time. Temperatures of around 175 ~ 180 ^{o}C will be attempted first. Long reaction times of longer than 30 h will be used.

Appendix E - SAPO-5 synthesis

Silicoaluminophosphates (SAPOs) are of considerable scientific interest among the family of phosphate based zeolite crystals for their potential for industrial application.] SAPOs can be used for several acid-catalyzed reactions such as isomerisation of xylenes, transalkylation between toluene and trimethylbenzenes, alkylation of benzene with methanol, isomerisation of 1-pentene, isopropylation of benzene, methanol to hydrocarbons reaction and propylene oligomerization.[6–10] SAPOs also have an AFI-type structure with pore diameter of up to 0.73 nm. The first synthesis procedures were reported by Lok et al.[1112] They are believed to possess Brønsted acid sites since Si^{4+} replace P^{5+} ions and generate negative framework charge that needs to be compensate by protons.

The crystal size of SAPOs can be synthesized to above 100 μm^4a. A procedure that will be tested and optimized is as follows;

a. Al_2O_3 source preparation. It is going to be prepared by adding 54 ml of iced cold NH_3 solution (32%) to 0.2 m of $AlCl_3 \bullet 6H_2O$. It can also be prepared by dissolving 0.1 mol of $Al_2(SO_4)_3 \bullet 18H_2O$ in 200 ml water. The mixture should be stirred vigorously at room temperature for 1 h. The final precipitate can be filtered out and washed by water.

b. Solution A is made by adding triethylamine (TEA) to ice-cold diluted H_3PO_4 (containing about 20% water). At the end of the reaction, the pH of the mixture should be around 2.5.

c. Pyrogenic silicas (fumed silicas) is used as the SiO_2 source. Aerosil^{TM} 200 can be purchased online. It is a hydrophilic fumed silica with a specific surface area of 200m^2/g. The detailed information can be found at the supplier's website:

https://www.aerosil.com/lpa-productfinder/page/productsbytext/detail.html?pid=1855

d. The solution B is prepared by the treatment of the SiO_2 source with Al_2O_3 Source in about 60% water content. The mixture is under vigorous stirring for 2 hr. Then final pH of solution B should be 6 - 7.

e. Solution A is added to solution B dropwisely, followed by stirring for 15 – 60 mins. The pH of the final reation should be 3.0 – 3.5.

f. The gel is then directly transferred into a PTFE-lined stainless-steel autoclave. The autoclave is then put into a preheated oven at a temperature between 190 ~ 210 ^oC for 70 h.

g. After the crystallization, the autoclave is quenched in tab water. The crystals are then decanted, washed and dried at 120 ^{o}C overnight.

Similar to the synthesis of $AlPO_4$-5, the above procedures needs to be optimized in order to obtain crystals with good morphology, optical transparence and large sizes. The staring molar compositions can be $1Al_2O_3 : 1.03P_2O_5 : 0.15SiO_2 : 1.55$TEA : 750H2O. A reaction temperature of 210 ^{o}C could be attempted for 70 h. This procedure is predicted to yield clear rod-like crystals with average particle sizes of 99 ± 48 μm. Particle sizes of 130 ± 20 μm can be collected at considerable amount. A few of crystals of up to 250 μm can be obtained.[5]

Reference

(1) Jiang, F. Y.; Zhai, J. P.; Ye, J. T.; Han, J. R.; Tang, Z. K. Synthesis of large optically clear AlPO 4 -5 single crystals. 2005, *283*, 108–114.

(2) Vietze, U.; Krauss, O.; Laeri, F.; Ihlein, G. Zeolite-dye microlasers. *Physical review Letters.* 1998.

(3) Qiu, S.; Pang, W.; Kessler, H.; Guth, J. Synthesis and structure of the $[AlPO_4]_{12}Pr_4NFNF$ molecular sieve with AFI structure. *Zeolites* 1989.

(4) Ihlein, B. G.; Schüth, F.; Krauû, O.; Vietze, U. Alignment of a Laser Dye in the Channels of the $AlPO_4$ -5 Molecular Sieve. 1998, 1117–1119.

(5) Demuth, D.; Stucky, G.; Unger, K.; Schüth, F. Synthesis of large optically clear silicoaluminophosphate crystals with AFI structure. *Microporous Materials.* 1995.

(6) Masukawa, T.; Komatsu, T.; Yashima, T. Strong acid sites generated in aluminosilicate region of SAPO-5. *Zeolites.* 1997.

(7) Montoya-Urbina, M.; Cardoso, D. Characterization and catalytic evaluation of SAPO-5 synthesized in aqueous and two-liquid phase medium in presence of a cationic surfactant. *Journal of Catalysis* 1998.

(8) Hedge, S. G.; Ratnasamy, P.; Kustov, L. M.; Kazansky, V. B. Acidity and catalytic activity of SAPO-5 and AlPO-5 molecular sieves. *Zeolites.* 1988, *8*, 137–141.

(9) Hedge, S.; Ratnasamy, P.; Kustov, L.; Kazansky, V. Acidity and catalytic activity of SAPO-5 and AlPO-5 molecular sieves. *Zeolites.* 1988.

(10) V. Hulea, N. Bilba, M. Lupascu, E. Dumitriu, D. Nibou, Sl Lebaili, Hl Kessler; Study of the transalkylation of aromatic hydrocarbons over SAPO-5 catalysts. *Microporous Materials.* 1997.

(11) Wilson, S.; Lok, B. Aluminophosphate molecular sieves: a new class of microporous crystalline inorganic solids. *Journal of the Amierican Chemical Society.* 1982.

(12) Lok, B.; Messina, C.; Patton, R. Silicoaluminophosphate molecular sieves: another new class of microporous crystalline inorganic solids. *Journal of the Amierican Chemical Society.* 1984.